REPORT

ACT4storage - Acoustic and Chemical Technologies for environmental monitoring of geological carbon storage

CONTROLLED CO_2 RELEASE EXPERIMENT, 2019

DOC.NO. 20180127-03-R
REV.NO. 2 / 2021-02-01

NORWEGIAN GEOTECHNICAL INSTITUTE
NGI.NO

Project

Project title:	ACT4storage - Acoustic and Chemical Technologies for environmental monitoring of geological carbon storage
Document title:	D3 - Nearshore evaluation report 2019
Document no.:	20180127-03-R
Date:	2019-11-26
Revision no. /rev. date:	2 / 2021-02-01

Client

Client:	Gassnova
Client contact person:	Kari-Lise Rørvik
Contract reference:	

for NGI

Project manager:	Ann E. A. Blomberg
Prepared by:	Ann E. A. Blomberg, Ivar-Kristian Waarum, Espen Eek, Christian Totland, Geir Pedersen (NORCE), Ole Lorentzen (FFI), Scott Loranger
Reviewed by:	Ivar-Kristian Waarum

NORWEGIAN GEOTECHNICAL INSTITUTE
NGI.NO

Main office
PO Box 3930 Ullevaal St.
NO-0806 Oslo
Norway

Trondheim office
PO Box 5687 Torgarden
NO-7485 Trondheim
Norway

T 22 02 30 00
F 22 23 04 48
NGI@ngi.no

BIC NO. DNBANOKK
IBAN NO26 5096 05 01281
ORGANISATION NO.
958 254 318MVA

ISO 9001/14001
CERTIFIED BY BSI
FS 32989/EMS 612006

Summary

This report is the second delivery of the CLIMIT demonstration project ACT4storage (Acoustic and Chemical Technologies for environmental monitoring of geological carbon storage). The ACT4storage project is funded by Gassnova and Industry Partners. During this project, we have conducted a series of controlled CO_2 release experiments to assess the performance of different sensor technologies in different environments. In 2018 we conducted laboratory tests over several weeks to evaluate the capabilities of relevant chemical sensors in a controlled environment. In the fall of 2018 we conducted an 8-week long field trial in a sheltered area of the Oslo fjord to further study the capabilities and limitations of chemical as well as acoustic sensors in a more realistic environment. This report describes the second and final round of nearshore controlled release experiments conducted in the spring of 2019, also in the Oslo fjord but in deeper water and ocean conditions similar to the North Sea environment.

While the 2018 nearshore tests were carried out in sheltered waters in Horten inner harbour with water depths of < 20m and anoxic conditions, the 2019 nearshore tests were conducted in more representative ocean conditions. The water depth at the new location was 60 m, and the carbonate system was similar to what can be expected in the North Sea. This controlled release experiment was carried out in a similar way as in 2018, but with some technical modifications and more mobile sensor platforms. The response to the controlled leak was measured using two seabed templates equipped with active and passive acoustic sensors, chemical sensors and an ocean current profiler. A subsea video camera was used to document the release. In addition to the fixed seabed templates, we had significant focus on the use of mobile platforms. We used the Simrad Echo research vessel equipped with state-of-the-art acoustic sensors to map the bubble plume and study bubble rise heights. The HUGIN AUV was also used with CO_2, O_2, pH, and CH4 sensors integrated, to study the response from chemical as well as high resolution active acoustic sensors when moving through the CO_2 plume. Finally, a SeaExplorer glider equipped with a CO_2 and an O_2 sensor was used for one week when we conducted several releases of dissolved CO_2.

We observe that the correlation between CO_2 and O_2 is a powerful tool for distinguishing between normal variations in the carbonate system and a leak-related anomaly. When response times are relevant, such as when using an AUV, a pH sensor can act as a proxy for a membrane-based CO_2 sensor which has a longer response time. State-of-the-art echo sounders mounted on a surface vessel allow acoustic observation of CO_2 bubbles reaching as high as 30-50 m above the seafloor. Finally, a high-resolution synthetic aperture sonar (HISAS 1030) mounted on the HUGIN AUV offers high-quality imagery of the seabed including features potentially related to a leak. We also demonstrate the HISAS' ability to detect CO_2 bubble plumes and discuss the importance of the angle of observation for plume detection.

Contents

Appendix

Review and reference page

1 Background

Several large-scale carbon capture and storage (CCS) projects are in the planning stage worldwide[1, 2], in addition to a few dozen small-scale projects which already have been successfully executed, storing from a few hundred to ~1 million tons of CO_2 per year[2, 3]. An important step in the planning of geological carbon storage (GCS) projects is to identify solutions for monitoring of the reservoir and surrounding environment. For offshore environments, this includes monitoring of the reservoir, overburden and seabed/water column. Monitoring of the reservoir and overburden is mainly performed using 3- and 4D seismic techniques.[2, 4, 5] The ACT4storage project addresses marine environmental monitoring, targeting the seabed and the water column. [6-8] Key monitoring technologies include active and passive acoustics to map and characterize CO_2 bubbles in the water column, and chemical sensors to monitor natural water chemistry and identify anomalies associated with dissolved CO_2. While acoustic sensors are able to detect the presence of CO_2 in gas phase, chemical sensors can be used to detect either the level of dissolved CO_2 in the water column directly, or measure other parameters related to CO_2 such as pH and O_2. Several previous studies on leakage detection in the water column focus on the elevated CO_2 levels and/or reduced pH levels associated with a CO_2 enriched plume[8-10], while others indicate that the relationship between O_2 and CO_2 is key to anomaly detection[11, 12]. Through the ACT4storage nearshore controlled release experiments we study the chemical and acoustic response of a simulated CO_2 leak, and evaluate the suitability of different monitoring technologies. Special focus is on determining which technologies are best suited for different platforms (stationary, AUV, glider, surface vessel).

The water column, seabed and atmosphere are all part of an open system that is affected by a vast number of natural processes. Monitoring the water column therefore poses the considerable challenge of separating natural variability from anomalies related to unintended leakage from the reservoir.[13] Natural variability in CO_2 concentration is considerable, [7, 11, 12, 14] with consequent variability in all parameters affected by the ocean carbonate system, including the level of dissolved oxygen (DO), which is fundamentally connected with the level of CO_2. To avoid or reduce false alarms, the co-variability of multiple chemical parameters should be monitored. For many sea areas, biogenic processes are the cause of variation in both pCO_2 and DO. These include photosynthesis (reduces pCO_2 and increases DO), respiration and decomposition (increases pCO_2 and reduced DO). Therefore, pCO_2 normally correlates inversely with DO.[11, 12] Uchimoto et al. (2017&2018) argued that a constant pCO_2 threshold value will result in too many false positives or negatives, and suggested that the threshold should be adjusted with respect to the DO% in the specific marine environment.[7, 12] The basic idea is that waters with lower DO% require a higher pCO_2 threshold value compared to water with high DO%, hence a covariance threshold was proposed. Atamantchuk et al. (2015) deployed several sensors during a controlled release nearshore environment, and noted that the external source of CO_2 caused a deviation from the natural correlation between pCO_2 and oxygen.[10] However, there is limited data on the pCO_2 and DO covariance during offshore simulated leakage experiments.

In this report, we describe the nearshore controlled CO_2 release experiments carried out in 2019 as part of the ACT4storage project. Artificial leakage of CO_2 was simulated by releasing CO_2 either in gas phase (as bubbles), dissolved in seawater, or a combination of gaseous and dissolved CO_2. The response was measured and characterized using active and passive sensors mounted on seabed templates, as well as on a research vessel equipped with state-of-the-art acoustic sensors, a HUGIN AUV equipped with advanced chemical and acoustic sensors, and a SeaExplorer glider equipped with a pCO_2 and an O_2 sensor.

2 Objectives and expected outcome

The main objective of this nearshore controlled release experiment was to further evaluate the capabilities and limitations of relevant technologies for environmental GCS monitoring. The 2019 tests complement the tests performed in 2018, with some adjustments to increase the learning outcome. Most importantly, the test site was moved to a more representative ocean environment with deeper water (60 m water depth) and representative geochemical conditions. Based on the work done so far, including the results presented in the report, we will provide a set of recommended guidelines for technology selection and use for environmental GCS monitoring.

3 Test site and baseline conditions

3.1 Test site

The test site for the 2019 nearshore tests was on the north side of Østøya, as indicated in Figure 3-1. This test site was selected based on several factors. The water depth in the area is approximately 60 m, gradually sloping but relatively flat. This is water depth is comparable to relevant offshore sites including the Sleipner region with water depths of ~70-90 m.

The geochemical composition in this region is more representative of North Sea conditions. Along with the increased water depth, this was the main reason for moving from the 2018 test site in Horten inner harbour. In particular, the anoxic conditions from the inner harbour were avoided. This turned out to be very important since the correlation between O_2 and CO_2 in the water column has proven to be a useful tool for anomaly detection. At the Østøya test site we had access to power, and a cabin with desk space and a dry and protected place to set up the computers and data acquisition system (DAQ).

Figure 3-1 Test locations for the 2018 and 2019 nearshore tests, respectively. The 2018 tests were carried out in a protected environment with 16-18 m water depth and anoxic conditions. The 2019 tests were moved to more representative conditions with oxic conditions and 60 m water depth.

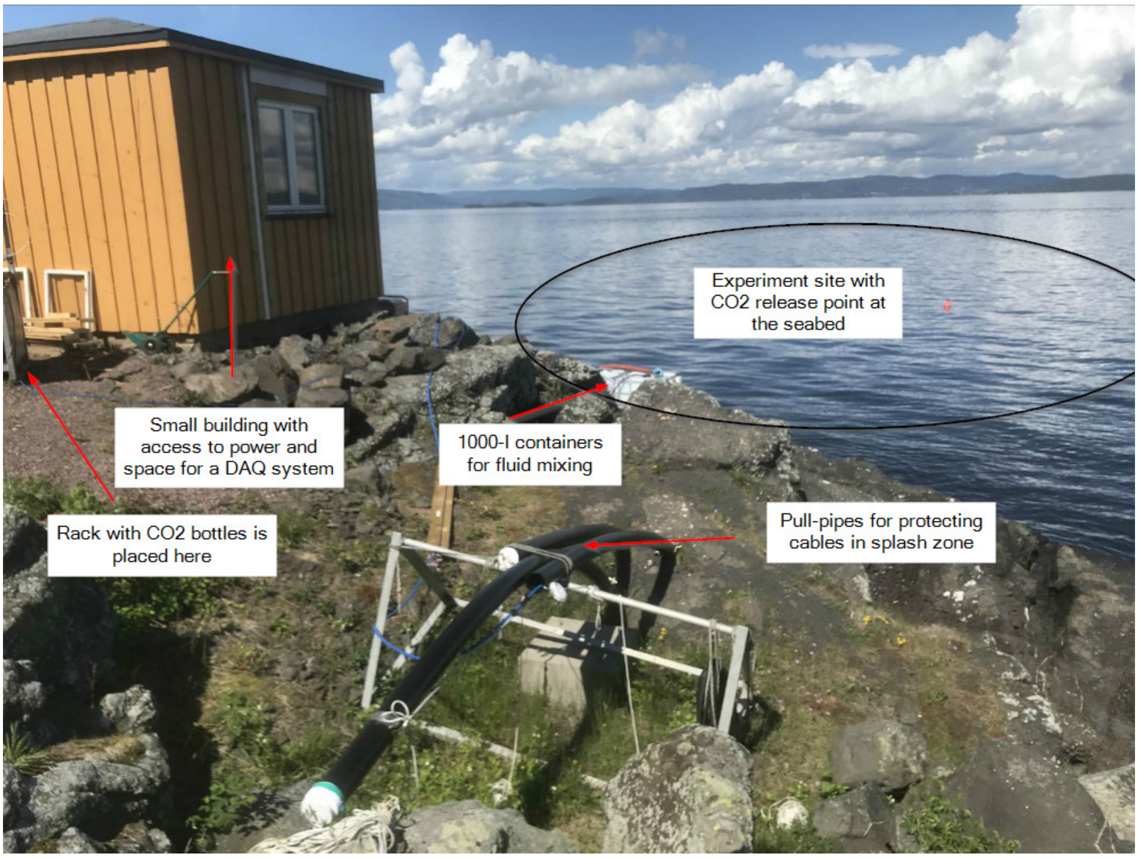

Figure 3-2 The data acquisition system, consisting of power supplies and computers, was placed inside the yellow building. Cables for data communication and power were guided through the splash zone out to sea through the black pipes to the right.

3.2 Baseline conditions

This region is part of the Oslo Fjord. Ocean currents are limited and were recorded in the water column from ~2 m above the seafloor up to 40 m above the seafloor (~20 m below the surface) during the nearshore controlled release period (May 2019). The seawater temperature in this period was below 8°C with a subsurface minimum of 6°C at around 20m depth. The salinity profile is affected by freshwater entering the fjord from the Drammen river (Drammenselva). Minimum salinity (< 25) was found near the surface, *i.e.* in the upper 5-10 of the water column. Below, the salinity sharply increases to reach 34.6-34.7 at 50m depth. As a result of the temperature and salinity vertical distribution, the density gradient is very strong. Density values range from 1005 kg m^{-3} near the surface to 1027 kg m^{-3} at depth resulting in a low-salinity/low-density layer in the upper 5-10 m of the water column. This change in density was not problematic for most of the tests. It did, however, cause difficulties for the glider operation.

Vertical O2 profiles show that surface waters are well oxygenated. An O_2 minimum is found at about 20-30 m below the surface, just below a strong thermocline and is likely to be associated with O_2 consumption through respiration processes. Below this O_2

minimum, values slightly increase with depth, reaching around 440 µmol/l at 30m depth and up to 460 µmol/l at 60m depth.

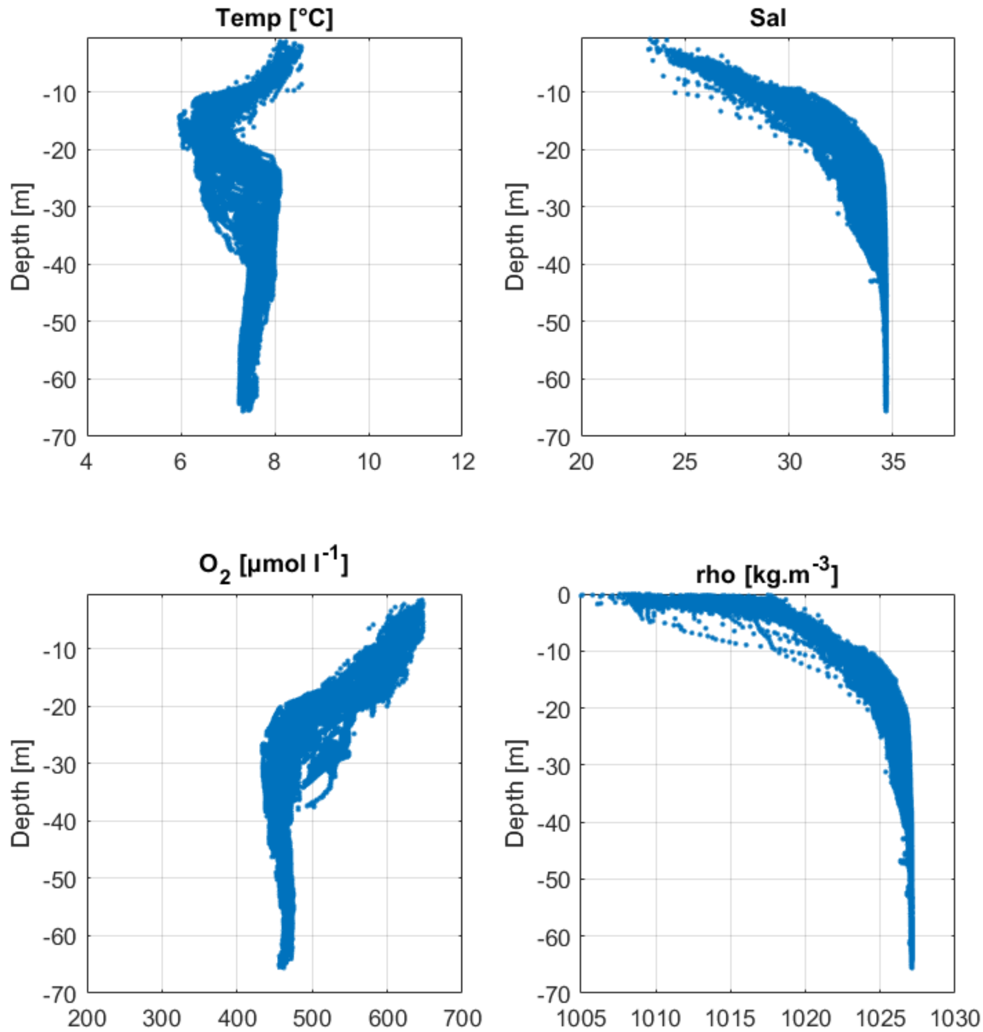

Figure 3-3: The upper plots show salinity and temperature profiles obtained using the SeaExplorer glider on May 14th, 2019. The lower plots shows measured O2 profiles and calculated density. The upper 5-10 m of water are influenced by freshwater from the Drammen River, resulting in a significant density gradient.

We measured baseline CO_2 values in the range ~520 to 560 µatm. The salinity and temperature measured at the stationary sensor frame over the course of the nearshore controlled release experiments reveal that different water masses occasionally entered the test site. However, the correlation between CO_2 and O_2 persisted for all days without controlled release activity.

The estuarine circulation in the Oslo fjord is predominantly limited to the upper 20 m, and replenishment of the deeper waters mainly occurs during Winter.[15] This is consistent with currents/absence of currents measured at the site, with little or no currents present most days near the bottom, and a few days with an eastbound current direction (the chemical sensor frame (Template A) is located northeast of the leakage frame). The days with an eastbound current direction likely represent the entering of new water masses to the site, as indicated by Figure 3-4, showing temperature versus salinity measured at Template A during different time spans without any controlled CO_2 release.

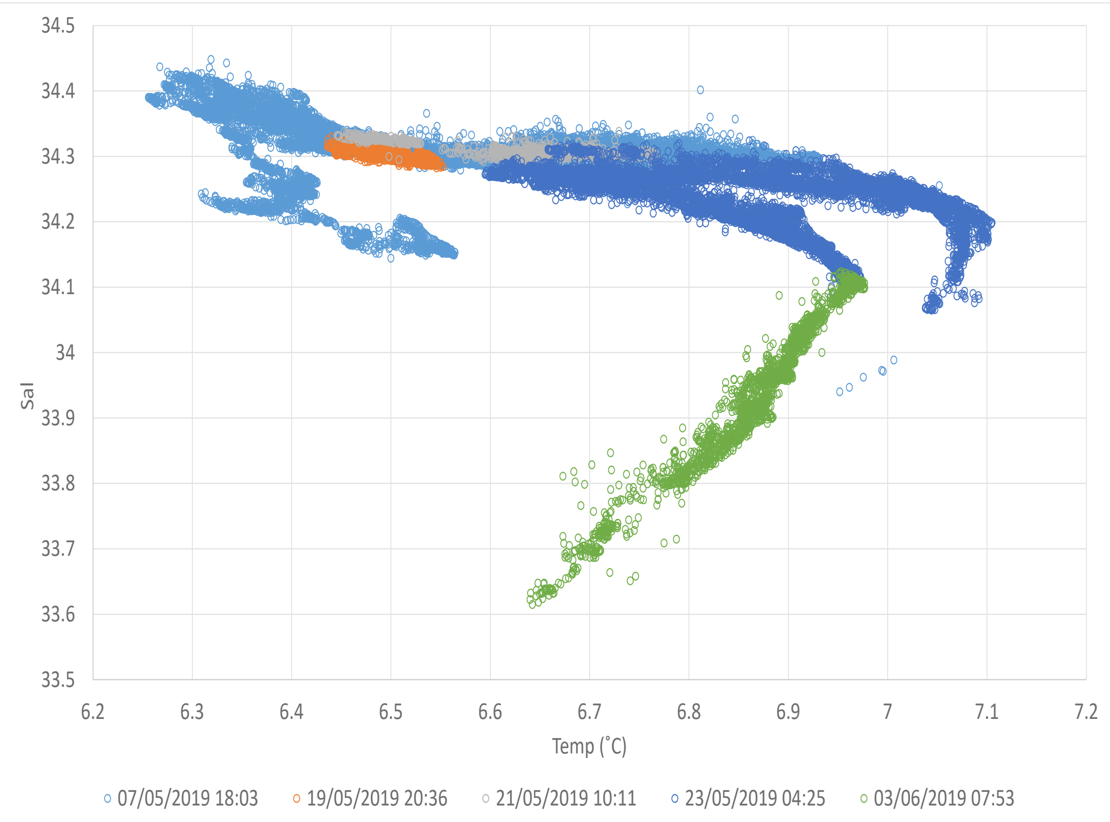

Figure 3-4 Measurements of temperature versus salinity for five different time spans (only start time is indicated in the plot). The colour coding (green, orange, grey, light- and dark blue) represents different water masses entering the site and reaching our sensor frame (Template A).

4 Controlled release system

The system designed by NGI for the 2018 nearshore tests was re-used with minor improvements. The system enables release of air or CO_2 in gas phase as well as CO_2 dissolved in seawater. The reasoning behind this design is that depending on the leak scenario, CO_2 may enter the water column in gas or dissolved form, and in some cases both. In addition, in the event of CO_2 entering the water in gas phase (bubbles), this CO_2

quickly dissolves into the surrounding water, causing an increase in the level of dissolved CO_2.

Figure 4-1 Leak frame developed by NGI for controlled release of air, CO_2 bubbles, and seawater saturated with CO_2. The fluid- and gas flow was controlled and documented from shore, and a subsea video camera was placed on the frame to verify the simulated leak.

The release point was located at the seabed approximately 100 m from shore, where the water depth is 60 m (Figure 4-2 and Figure 4-3). The CO_2 containers were located on land for ease of operation (Figure 4-4). CO_2 in gas phase was transported directly from the containers to the leak point through a hose, using the pressure inside the CO_2 containers as the driving force.

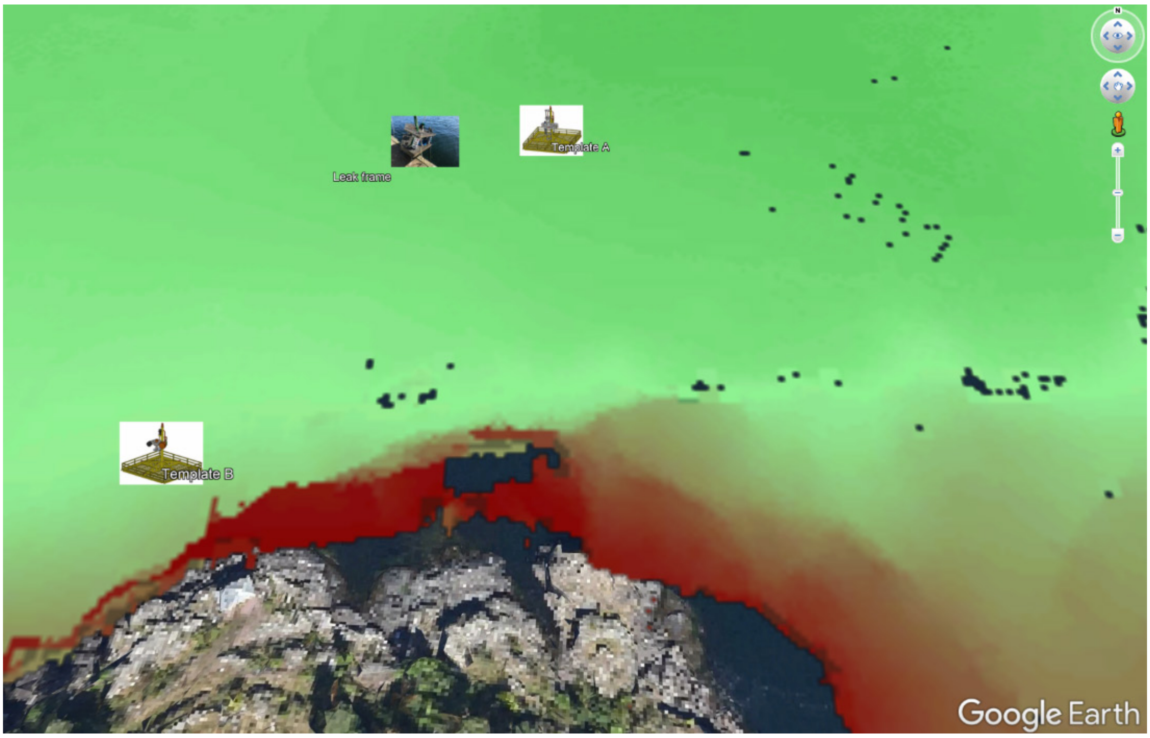

Figure 4-2 Position of leak frame and stationary templates A and B. Template A was equipped with a passive hydrophone, chemical sensors and a current meter. It was placed 22 m North-East of the leak frame at the start of the deployment, and later moved to 10 m from the leak frame. Template B was placed 65 m from the leak frame and equipped with active acoustic sensors.

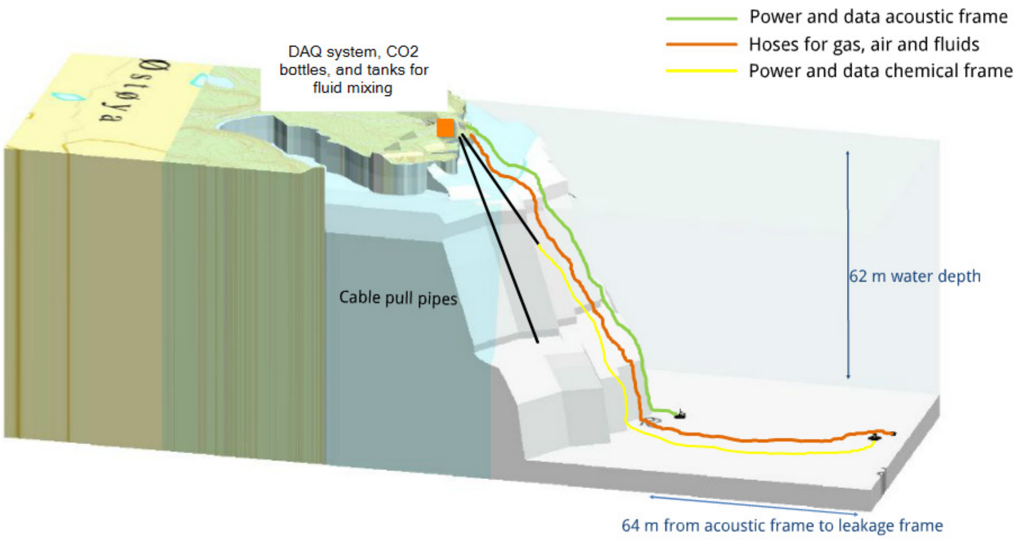

Figure 4-3 3D illustration showing Østøya and the steep transition to 60 m water depth. Approximate locations of the leak frame and the seabed templates are indicated.

Figure 4-4 *CO_2 containers used during the controlled release experiments. CO_2 was either released directly in gas phase (via flow meters to control and document the flow) or dissolved in seawater to mimic CO_2-enriched fluids entering the water column.*

Seawater with higher levels of CO_2 than the background was prepared in 1000-litre tanks by using seawater from 4-5 m below the surface (limited by the length of the hoses to the hydraulic pumps for water intake) and manipulating the levels of dissolved CO_2 and salinity until target values were reached (Figure 4-5). The manipulated seawater was then released through a hose, using a pump as the driving force. We used three 1000-litre tanks so that two tanks could be prepared while a third was being released, ensuring near-continuous controlled release.

Figure 4-5 *CO_2-enriched pore fluids were simulated by adding appropriate amounts of CO_2 into seawater in three 1000-litre tanks. The contents were then released in a controlled way using a pump and a hose placed at the seabed. The release point is located 100 m from shore, to the left of the red buoy. AlSeamar's SeaExplorer glider was deployed from the small boat in the upper right corner of this image.*

We used three separate hoses; one for CO_2 dissolved in seawater, one for gas bubbles released through holes with 3 mm orifice diameter, and one for gas bubbles released through holes with 5 mm diameter (Figure 4-6). The different orifice sizes were used to manipulate the bubble size distributions. The hoses could be used simultaneously or one at a time. We also released air to evaluate and compare bubble rise heights. The pressure of the gas release was controlled using a valve on the CO_2 bottles, and a mechanical flow meter to control the flow rate and ensure repeatability in the measurements. In addition, digital flow meters were used to continuously log the flow rates (Figure 4-8). A video camera was placed at the leakage point to verify and document the leak. Figure 4-7 shows example images of CO_2 gas release rates of 1.3 litre/min and ~25 litre/min.

Figure 4-6 Three hoses were used to facilitate release of seawater with elevated CO_2 levels, and CO_2 or air in gas form (bubbles) with different orifice sizes and spatial distribution. The hose to the left was used for seawater, with a single 10 mm hole as release point. The middle and rightmost hoses were used for air and CO_2 in gas phase. The middle hose has 8 3-mm holes, and the rightmost hose has a single 5 mm hole. The orifice size was used to control the bubble size distribution. A video camera and external light source was used to document and verify the leak.

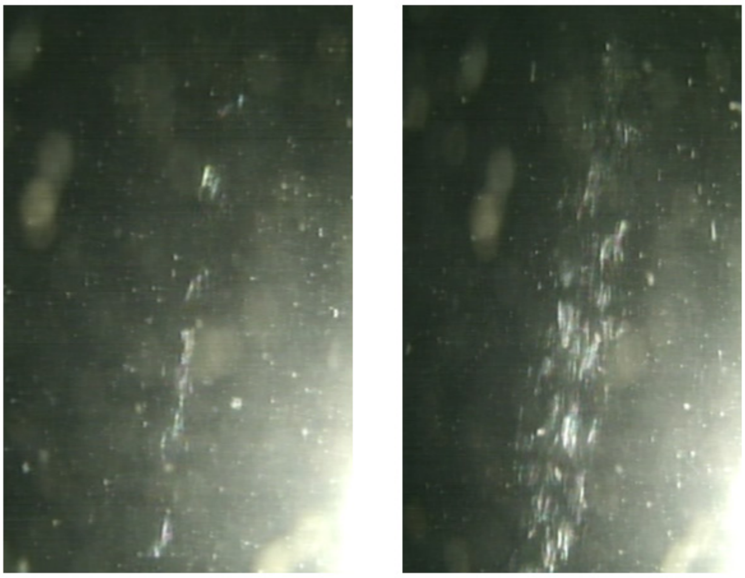

Figure 4-7 Camera image showing a controlled release of CO_2 at a rate of 1.3 l/min (left), and ~25 l/min (right)h

4.1 Measuring the flow rates and quantifying the release

Two different systems were used to document the flow rate (release rate) of CO_2 in gas phase as well as fluids (seawater saturated with CO_2). A manual flow meter (Figure 4-8) was used to control the flow of CO_2 in gas phase. The flow is shown as a percentage between 0 and 100%, with 100% corresponding to approximately 1.15 l/min. We used an empty water bottle submerged in water to calibrate and confirm this flow meter (determine the 100% value for CO_2). In addition, two digital flow meters were used; one for fluids and one for CO_2 in gas phase. The digital flow meters allowed us to continuously record the release rate (Figure 4-9). The digital flow meters have a measuring range up to 25 litre/min. Above 25 litre/min the release rate was estimated empirically.

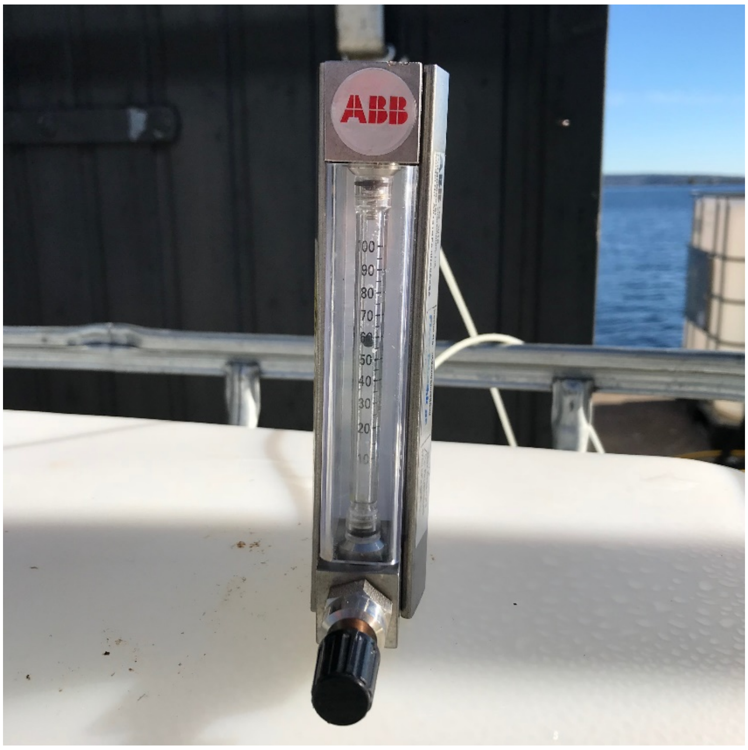

Figure 4-8 Flow meter used to accurately determine the flow rate of CO_2 in gas phase. Here, the black sphere is at 60 %, which corresponds to a leak rate of 0.75 l/min (100% corresponds to l/min).

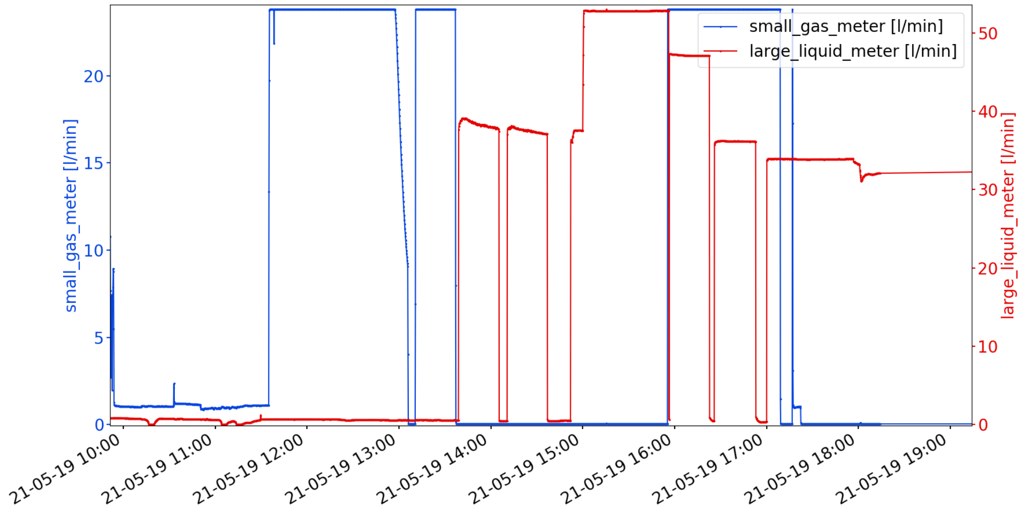

Figure 4-9 Examples of recorded release rates for CO_2 in gas phase (blue curve), and dissolved CO_2 in seawater (red curve), during a 10-hour period on 21st of May 2019.

5 Platforms and sensors

A dedicated marine monitoring program for GCS is likely to make use of several platforms, or sensor carriers. Stationary platforms are relevant for long-term monitoring of high-risk locations as well as background regions. Mobile platforms, including research vessels, AUVs and gliders are needed for large area coverage. In the 2019 nearshore tests we used both stationary templates, a HUGIN AUV equipped with a range of chemical and active acoustic sensors, a glider equipped with chemical sensors, and the Simrad Echo research vessel equipped with state-of-the-art echo sounders and sonars.

5.1 Stationary instrument templates

We used two stationary templates equipped with a range of chemical, acoustic and oceanographic sensors. These templates were placed at the seabed at a water depth of ~60 m, and both templates were in the water for 5 weeks. During this period, the chemical and oceanographic sensors were programmed to continuously record data at high resolution, which was stored on a PC on shore using a dedicated DAQ system. The active acoustic sensors were used for shorter time intervals during and in between release experiments.

5.1.1 Template A

Template A (Figure 5-1) was equipped with chemical and oceanographic sensors, in addition to a hydrophone. It was placed 22 m North-East from the leak frame, and halfway through the experiment (May 21st), it was moved closer and placed 10 m from the leak frame. The placement of template A relative to the leak frame was based on knowledge about the ocean currents, and the expected spatial extent of a released CO_2 plume. We were able to detect anomalies likely related to our release both at 10 m and 22 m distance from the release point. The following sensors were mounted on template A:

- icListen hydrophone
- CONTROS HydroC CO_2
- Franatech CO_2
- CONTROS HydroFlash O_2
- Idronaut multisensor including O_2 and pH sensors as well as sensors for salinity, temperature, and turbidity.

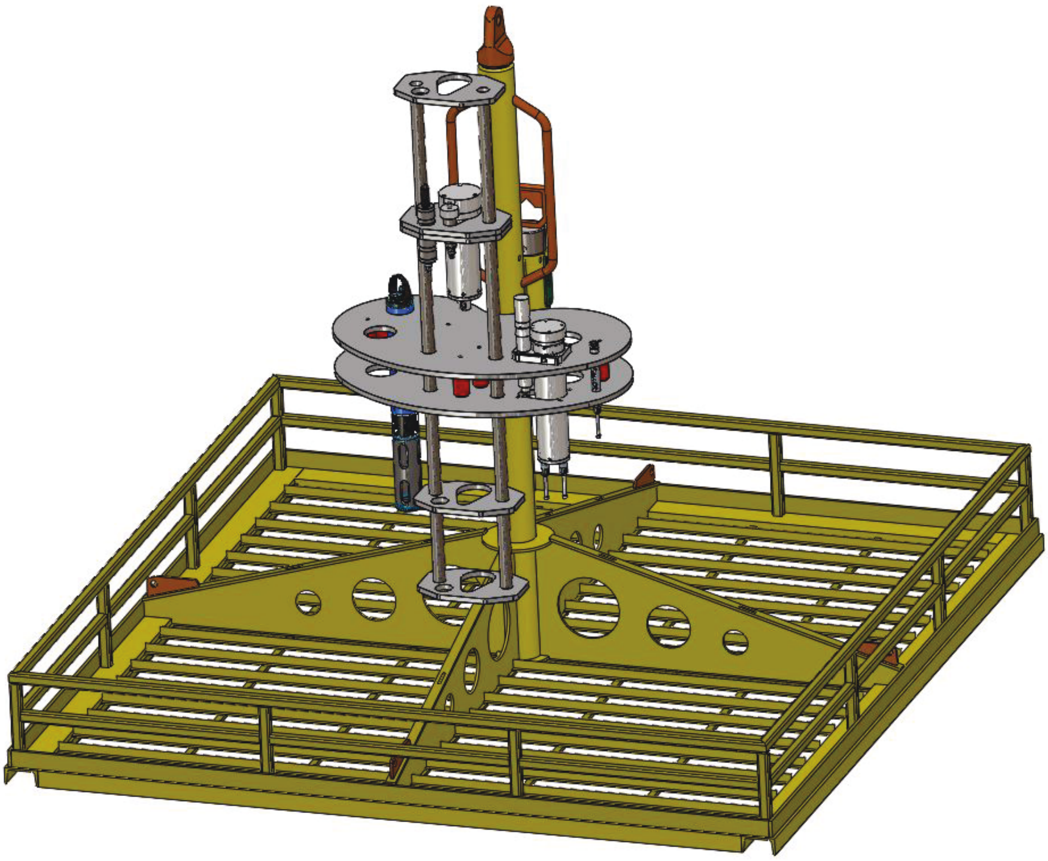

Figure 5-1 Template A, with chemical and oceanographic sensors (measuring CO_2, O_2, pH, salinity, and temperature) as well as a hydrophone for passive acoustic measurements.

The hydrophone placed on Template A was used to "listen" for bubbles escaping the seabed. Results from the 2018 nearshore tests indicated that a hydrophone is a low-power/low-cost sensor with the ability to detect relatively small bubble leaks (~1 l/min at 10 m distance).

The chemical sensors placed on Template A (CO_2, O_2, pH), in addition to salinity and temperature sensors, were used to monitor background variations in these parameters, and to measure the variations corresponding to a controlled CO_2 release. The Aquadopp current profiler allows us to document the direction and speed of ocean currents from the seabed up to 40 m above the sensor (20 m below the surface).

5.1.2 Template B

Template B (Figure 5-2) was placed 64 m from the release point (leak frame) and equipped with active acoustic sensors. The uppermost sensor is a high-resolution scanning sonar developed by Kongsberg Mesotech. It can mechanically scan 360 degrees and offers high image quality. We found that it is less sensitive than the other active acoustic sensors for detecting small amounts of CO_2 bubbles in the water column at this range (we were operating near the upper limits of this sensor's range and sensitivity). Ideally, this sensor should be placed within a few meters of an area of interest to detect the presence of bubbles.

In addition, the template holds an M3 multibeam sonar and a dedicated depth rated version of the EK80 broadband echo sounder (WBT Tube) with a 333 kHz and a 70 kHz transducer. These are mounted on a remotely operated pan/tilt unit in order to control the viewing angle and locate bubbles in the water column (Figure 5-3). Both the M3 and the EK80 were very useful for detecting and localizing bubbles in the water column.

The electronics needed for templates A and B, including power supply to each sensor and data communication hardware, were placed within a waterproof container secured at each of the templates (Figure 5-4).

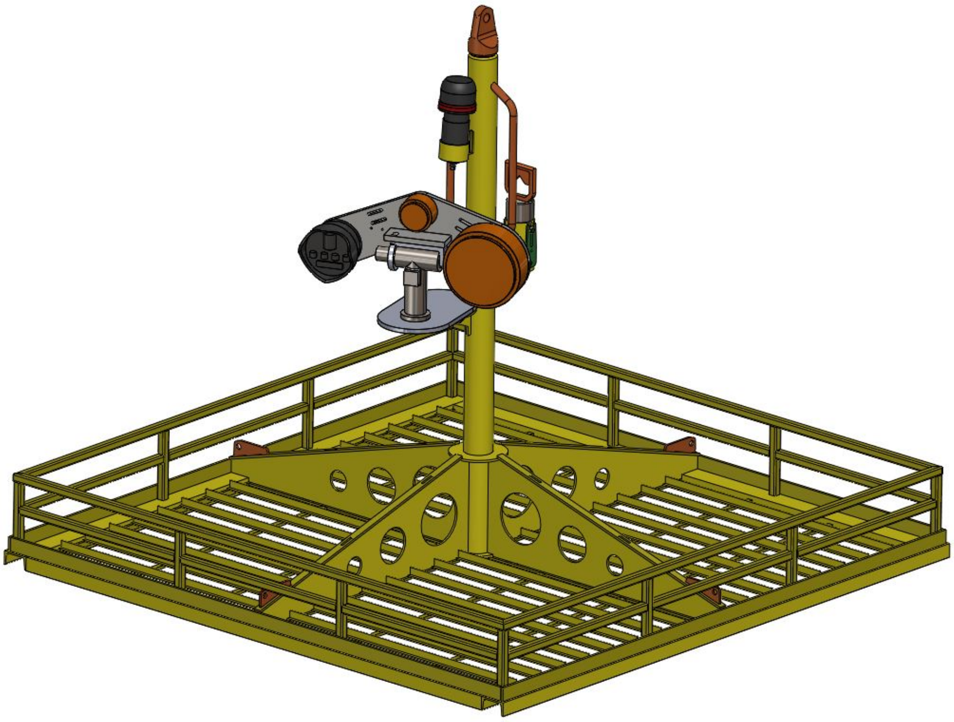

Figure 5-2 Template B, equipped with a single beam scanning sonar (on the top), an M3 sonar (black cylinder to the left) and an EK80 echo sounder (orange transducers). The M3 sonar and EK80 echo sounder are mounted on a remote-controlled pan/tilt unit such that the direction of the acoustic beam can be adjusted.

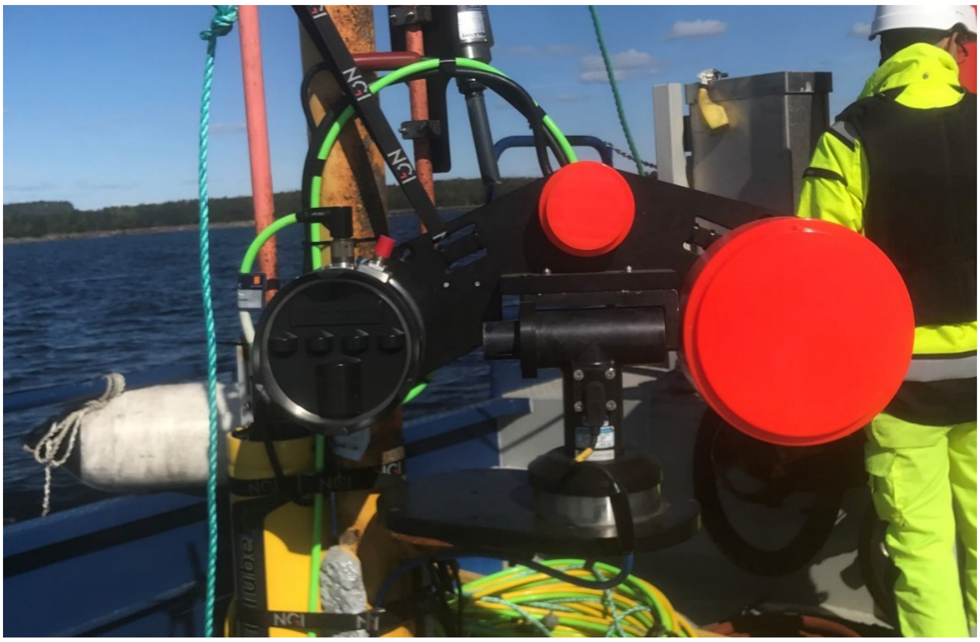

Figure 5-3 M3 multibeam sonar and EK80 echo sounder (WBT Tube with 333 kHz and 70 kHz transducers) mounted on template B. This picture was taken during deployment of the template.

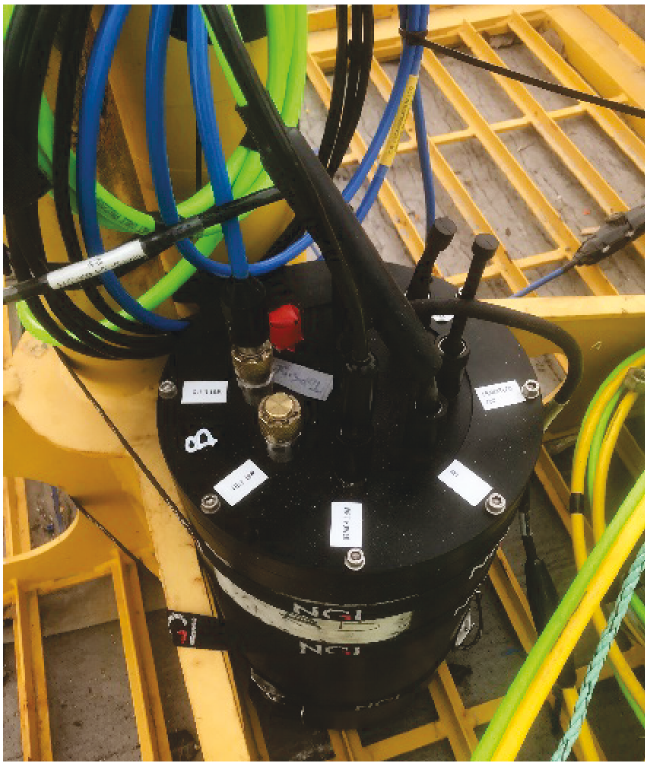

Figure 5-4 Subsea container designed and built at NGI, supplying sensors with adequate power and ensuring data communication

5.2 HUGIN AUV

An autonomous underwater vehicle (AUV) is designed for remote surveying of large areas subsea. The AUV can be equipped with a number of sensors including active and passive acoustic sensors, chemical, oceanographic and optical sensors. The motion of an AUV is controlled by a combination of buoyancy control and thrusters. There are a number of AUVs on the market, designed for different applications. In general, larger AUVs have limited operational times (12-48 hours) but can carry several sensors including those with high power consumption. Smaller AUV's are less expensive and can have longer operational times but cannot carry the same sensor payloads.

During the 2019 nearshore control release experiments we used the HUGIN AUV which can be considered a large AUV. The HUGIN AUV is modular and the sensor payload can be adapted to the monitoring needs. In this project, the following sensors were integrated, in addition to the sensors used for navigation and communication:

- CONTROS HydroC CO_2
- CONTROS HydroFlash O_2
- CONTROS HydroC CH_4
- Franatech CO_2
- Franatech CH_4
- Ocean Seven Idronaut pH
- High resolution synthetic aperture sonar (HISAS)

Integration work including hardware and software was carried out as part of the ACT4storage project, as a joint effort between FFI, NGI, and Kongsberg Maritime. The HUGIN AUV was deployed from the Kongsberg vessel Sølvkrona during the nearshore test (Figure 5-5).

Figure 5-5 HUGIN AUV during deployment from the vessel Sølvkrona. The sensor payload was updated to suit this experiment, including CONTROS HydroC CO_2 and CONTROS HydroFlash O_2, CONTROS HydroC CH4, Franatech CO_2, Franatech CH4, Idronaut pH, and HISAS synthetic aperture sonar.

Sensor placement within the platform should always be considered, since this may have an impact on the sensor's performance. During this deployment, the pH and the O_2 sensors were mounted with the sensing part of the probe protruding into the water for continuous water measurements. The CO_2 and CH4 sensors were supplied with water using a dedicated system of hoses and pumps transporting the water through the HUGIN to the sensor, using one pump for each sensor. It should be noted that this causes a slight delay in the measurements (~4 seconds) and may also impact the sensor response times.

5.3 SeaExplorer glider

A glider is an AUV designed to collect data over large areas and can be equipped with a range of chemical and oceanographic sensors. Recent developments also include active acoustic sensors such as a wide band echo sounder (https://cyprus-subsea.com/press-release-deepecho-module-successfully-integrated-on-a-seaglider-first-scientific-wide-band-echosounder-on-an-ocean-glider-tested-in-the-mediterranean-sea/).

The motion of a glider is normally controlled by variation of buoyancy, and not by thrusters (Figure 5-7). This allows the vehicle to operate for long periods, typically several months, without the need for an accompanying vessel. The cost of acquisition is thus low, making the glider suitable for long-term monitoring of chemical and oceanographic parameters over large areas. In the 2019 nearshore tests, AlSeamar's SeaExplorer was used for 6 days of calibration and data acquisition. The glider was equipped with the following sensors:

- Por Oceanus Mini CO_2 sensor
- SeaOwl liquid hydrocarbon sensor
- METS CH4 sensor from Franatech
- SeaBird CTD and O_2 sensor

The SeaExplorer glider was deployed and recovered using a small boat (Figure 5-6).

Figure 5-6 AlSeamar personnel preparing to deploy the SeaExplorer glider during the controlled release experiments

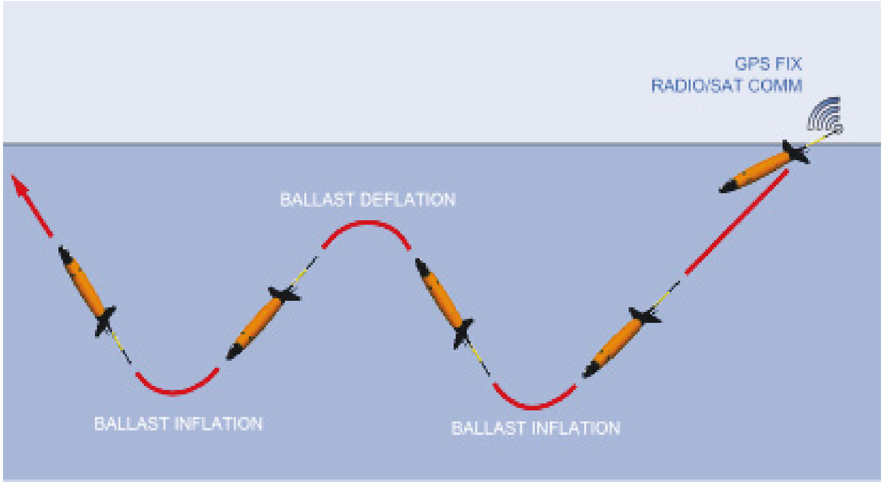

Figure 5-7 Typical travel path of a glider, using buoyancy control to move up and down in the water column

5.4 Simrad Echo Research Vessel

A surface vessel such as a research vessel or a seismic acquisition vessel can carry a range of acoustic sensors relevant for detecting CO_2 in gas phase. An efficient approach for GCS would be to install relevant sensors on a seismic vessel to acquire water column data simultaneous with the seismic measurements, both during a baseline study and subsequent periodic monitoring surveys. Whether or not surface vessel mounted acoustic sensors are efficient tools for detecting CO_2 plumes depends largely on the rise heights of these bubbles.

Figure 5-8 Simrad Echo R/V at the end of day 1 of data acquisition

During the 2019 nearshore tests we used the Simrad Echo research vessel owned by Kongsberg Maritime. Simrad Echo is very well equipped with state-of-the-art acoustic sensors. We acquired data for two full days, studying the acoustic response of a controlled leak using a range of single- and multibeam echo sounders including the EK80, SN90, EM712, ME70, and EM2040.

6 Release experiments

The controlled release system (including monitoring templates) was installed at the seabed on May 7th and recovered on June 3rd. During these 27 days, we had 12 days of controlled release experiments. We often had several types of experiments during a single day, varying from very small gas bubble releases to evaluate the active acoustic response, to large, continuous releases of CO_2 in gaseous and/or dissolved phase.

The sensors on the stationary templates were programmed to continuously record throughout the period, and we only experienced short interruptions due to loss of power. In addition to the stationary templates, the Simrad Echo R/V was used for 2 days, the HUGIN AUV for 1 day, and the SeaExplorer glider for 4 days. Table 6.1 offers an overview of the days with controlled CO_2 release, and specifies the phase of the released CO_2 (gas phase, dissolved phase or both) and the monitoring platforms used to record data. A range of leakage scenarios were simulated to evaluate the ability of the various monitoring platforms to detect the leakage and to consider the effects of

- The amount and rate of released CO_2
- Position of the sensors relative to the release point
- The CO_2 plume density (controlled by varying the salinity of the released fluids)
- CO_2 phase (gas or dissolved).

Table 6.1 Overview of release experiments and monitoring platform used

Date	Controlled release type	Monitoring platform
9.5.	Dissolved CO_2, Gas phase CO_2	Stationary templates, Simrad Echo R/V
10.5.	Dissolved CO_2, Gas phase CO_2 and air bubbles	Stationary templates, Simrad Echo R/V
13.5.	Dissolved CO_2, Gas phase CO_2 and air bubbles	Stationary templates, SeaExplorer
14.5.	Gas phase CO_2 and air bubbles	Stationary templates, SeaExplorer
15.5.	Dissolved and gas phase CO_2	Stationary templates, SeaExplorer
16.5.	Gas phase CO_2	Stationary templates, SeaExplorer
21.5.	Dissolved and Gas phase CO_2	Stationary templates, HUGIN AUV
22.5.	Gas phase CO_2	Stationary templates
27.5.	Gas phase CO_2	Stationary templates
28.5.	Dissolved and gas phase CO_2	Stationary templates
29.5.	Dissolved and gas phase CO_2	Stationary templates
3.6.	Gas phase CO_2	Stationary templates

6.1.1 Releasing CO_2 in gas phase

CO_2 in gas phase was released using the system described in Section 4, and the flow was controlled and documented using a mechanical and a digital flow meter. All flow rates were measured above sea level. A better solution would have been to have the flow meter installed subsea at the release point to document more accurately the release rate at the seabed. Table 6.2 lists the different days with release of CO_2 in gas phase, with an average release rate and estimated total amount of CO_2 released. The chemical sensors do not measure the CO_2 bubbles directly but measure an increase in the level of dissolved CO_2 in the water column. Dissolution of CO_2 will cause a slight increase in water density, which in turn can have consequences for the mobility and location of a plume in the water column.[16]

Table 6.2 Estimated total release of CO_2 in gas phase for the different days of the experiment, measured in l/min

Date	Short description	Average release rate [litres/min]	Estimated total release of CO_2 [litres]
9.5.	Small releases (0.5 l/,min and 1l/min)	0.75	270
10.5.	Small releases (0.5 l/,min and 1l/min)	0.75	270
13.5.	Moderate release over 5 hours	8	
14.5.	Significant release over 6 hours	16	5720
15.5.	Significant release over 6 hours	16	5760
16.5.	Significant release over 2 hours	16	1920
21.5.	Varying release over 8 hours	12	5760
22.5.	Small release of CO_2 gas over 4 hours	0.5	120
27.5.	Varying release over 8 hours	4	1920
28.5.	Varying release over 8 hours	2	960
29.5.	Significant release over 2 hours	25	3000
3.6.	Moderate release over 2 hours	2	240

6.1.2 Releasing CO_2 in dissolved phase

A scenario where the leakage consists of CO_2-enriched seawater, rather than gas phase CO_2, can occur if the CO_2 plume migrates upwards through geological formations and pushes pore water towards the seabed[17]. Such a leakage scenario may in principle persist for an extended period prior to the occurrence of bubbles. Due to the potentially different chemistry of pore water, such as varying salinity, this can result in different chemical signatures than the release of CO_2 gas only. In this study, the salinity of the released artificial pore water is varied, which influences its density, and thereby its movement and location in the water column.

Table 6.3 summarizes the release experiments involving dissolved CO_2. Table 6.3 has more entries than Table 6.1 because multiple tanks of water were released for each day of experiments. We classify the experiment as releasing water with very low density, low density, medium density, and high density, where 'medium density' is close to the ambient water density, and 'high density' indicates a density higher than the ambient density, etc. The density of these fluids affects the plume behaviour. We expect a plume with high density to sink to the seabed, potentially reaching (and passing) the sensors on Template A due to diffusivity processes. On the contrary, we expect a plume with low density to rise quickly towards the surface, while a plume with medium density may find its equilibrium somewhere in between. The motivation for varying the density of the CO_2 plume was to control the plume behaviour according to the monitoring platform used. The plume dynamics are complicated and affected by mixing with the surrounding waters, making it difficult to predict exactly where the plume is located.

Table 6.3 Overview of fluid release experiments, where seawater with varying levels of CO_2 and salt content were released. The salinity affects the density, and thus also the plume behaviour and buoyancy. The ambient salinity and density at 60 m depths was about 34 psu and 1027 kg/m3, respectively. Densities written in red indicates higher values than ambient conditions. The flow rate was typically around 33 L/min.

Date	Release start – stop (local time)	Salinity (psu)	Density (kg/m^3)*	mM CO_2**	Comment
13.5.	15:19-15:41	17.3	1014.9	81	Very low density
13.5.	16:01-16:26	23.3	1019.3	59	Very low density
14.5.	10:27-10:52	23.8	1021.0	78	Low density
14.5.	10:56-11:22	23.6	1019.5	53	Low density
14.5.	11:54-12:19	23.7	1019.7	62	Low density
14.5.	14:47-15:14	29.8	1024.4	59	Medium density
14.5.	15:50-16:16	29.9	1024.5	53	Medium density
14.5.	14:10-14:35	29.6	1024.3	58	Medium density
15.5.	10:41-11:09	23.6	1019.5	55	Low density
15.5.	11:12-11:36	23.6	1019.5	53	Low density
15.5.	14:24-14:50	23.1	1019.5	91	Low density
15.5.	14:52-15:16	24.5	1020.4	76	Low density
15.5.	15:18-15:42	23.1	1019.4	82	Low density
15.5.	15:47-16:12	35.3	1028.7	59	High density
15.5.	16:15-16:40	23.0	1019.1	56	Low density
21.5.	13:41-14:08	33.5	1028.2	126	High density
21.5.	14:12-14:39	32.4	1027.1	110	Medium density
21.5.	14:54-15:21	32.1	1026.9	105	Medium density
29.5.	10:14-10:38	19	1016.3	89	Very low density
29.5.	11:09-11:36	23	1020.2	144	Low density
29.5.	12:38-12:33	27	1023.6	166	Medium density
29.5.	13:09-13:37	33	1028.5	182	High density
29.5.	14:10-14:37	38	1031.4	100	High density
29.5.	15:07-15:34	44	1036.4	120	High density

*The density is calculated based on the concentration of CO_2, salinity and pressure at 60 m depth (6.9 bar)

**Calculated based on pH, using the software Aqion.

7 Response to controlled release experiments – stationary templates

The stationary templates were equipped with chemical, oceanographic and acoustic sensors. Here, we present measurements from these sensors during selected time intervals, representing both baseline conditions and leakage scenarios.

7.1 Chemical sensors

In this section we present results from the CONTROS HydroC (CO_2), CONTROS HydroFlash (O_2), and Idronaut sonde with an Ocean Seven pH sensor. We also had two Franatech CO_2 sensors mounted on Template A, but unfortunately there was an issue with these, likely related to water ingress, resulting in low performance and loss of data.

The temporal resolution for the CONTROS HydroC sensor is determined by the sample rate which is selectable using a proprietary software (DETECT). We used the default sample rate of 1 Hz for a duration of 27 days. Consecutive recorded samples over a period of 5 seconds (i.e., 5 samples) were averaged in order to reduce noise. In the results presented below we have also applied a simple filter which removes spikes in the data, including periodic sensor zeroings used for postprocessing. The HydroFlash was set to a sample rate of once every minute. The Ocean Seven pH sensor was selected due to its high accuracy (0.01 pH), and output data at a sampling rate of 12 Hz.

7.1.1 Observed relationship between CO_2 and O_2

The ability to detect an anomaly related to a controlled CO_2 release using CO_2 sensors placed on stationary templates was demonstrated during the 2018 nearshore experiments. The aim of the 2019 experiments with the same sensors was to confirm these results in deeper water (60 m instead of 18 m) and in a more open environment with geochemical conditions that are more representative of the North Sea. An important objective during these experiments was to study the relationship between CO_2 and O_2 during different leakage scenarios and investigate if this can be used for more robust anomaly detection (including avoiding false alarms caused by naturally elevated levels of CO_2). This relationship has been documented by others[7, 10, 12], but with limited experimental data at realistic water depths. Because of natural biogenic processes such as photosynthesis (reduces pCO_2 and increases DO), respiration and decomposition (increases CO_2 and reduces DO), the level of O_2 in the sea is normally inversely proportional to the level of CO_2. The data acquired during this project confirms this expected inverse correlation during periods without any controlled release experiment. A deviation from this correlation indicates that an additional source of CO_2, such as leakage, is present.

Figure 7-1 shows the measured CO_2 and O_2 levels during baseline conditions, i.e. periods without any CO_2 release. Each plot shows a 12-hour period, with the plots to the left covering one day (8 AM to 8 PM), and the plots to the right covering one night (8 PM to 8 AM). The inverse correlation between these parameters during "normal" conditions can be seen as a "mirroring effect" between the blue curve (CO_2) and the red curve (O_2). The sensors used in this example (CONTROS HydroC and CONTROS HydroFlash) demonstrate that this effect can be measured very accurately and that very small changes in one parameter is immediately reflected in the other.

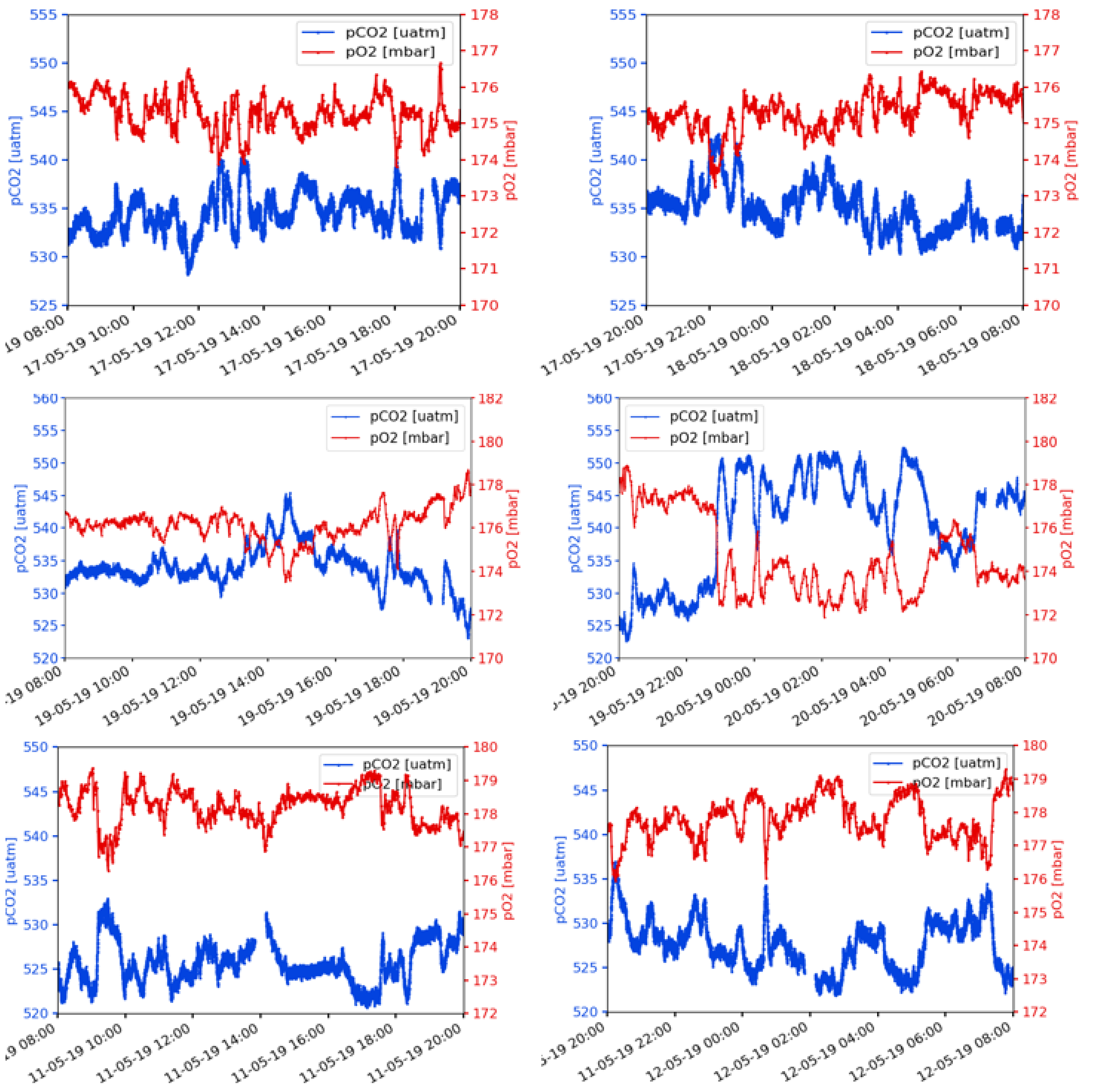

Figure 7-1 Baseline conditions: observed inverse correlation between CO_2 and O_2 for three days and three nights without controlled CO_2 release

The degree of CO_2/O_2 correlation can be verified be plotting the ratios between these parameters (Figure 7-2). We observe that the measurements appear to follow a linear relationship, indicating normal conditions.

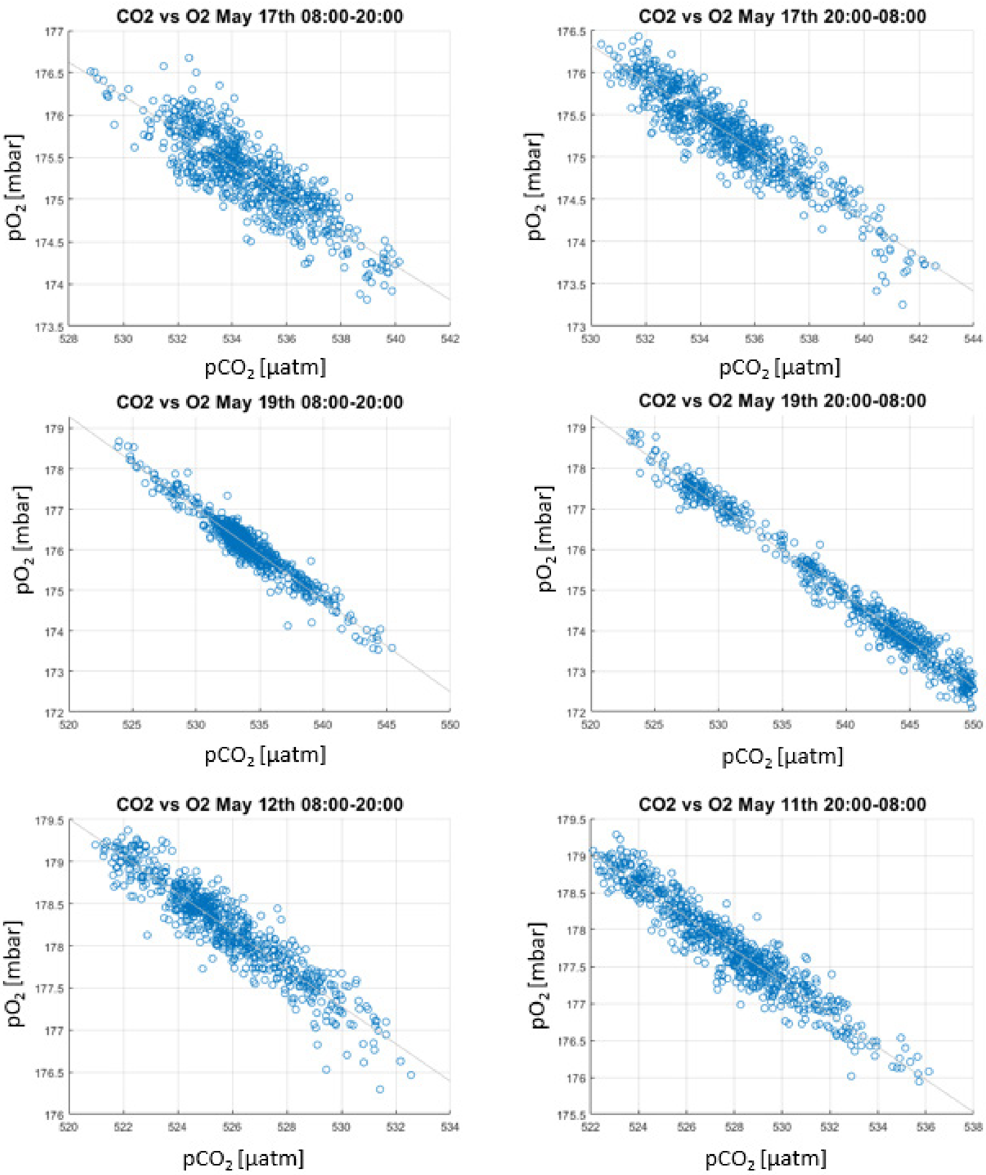

Figure 7-2 Baseline conditions: scatter plots of pCO_2 and pO_2 for the same time periods as in Figure 7-1 indicating the linear relationship during baseline conditions

7.1.2 Anomaly detection based on CO_2/pH-O_2 correlation

When a secondary source of CO_2 is present, the relationship between CO_2 and O_2 is affected. This can be observed as a deviation from the expected correlation pattern. Figure 7-3 (left) shows the measured CO_2 and O_2 levels during which a controlled CO_2 release was performed. The orange ellipses indicate observations where the normal inverse correlation pattern is lacking. The scatter plots (right) show that while most of the measurements represent normal conditions, some data samples clearly deviate from this pattern, in this case indicating that a secondary CO_2 source is present.

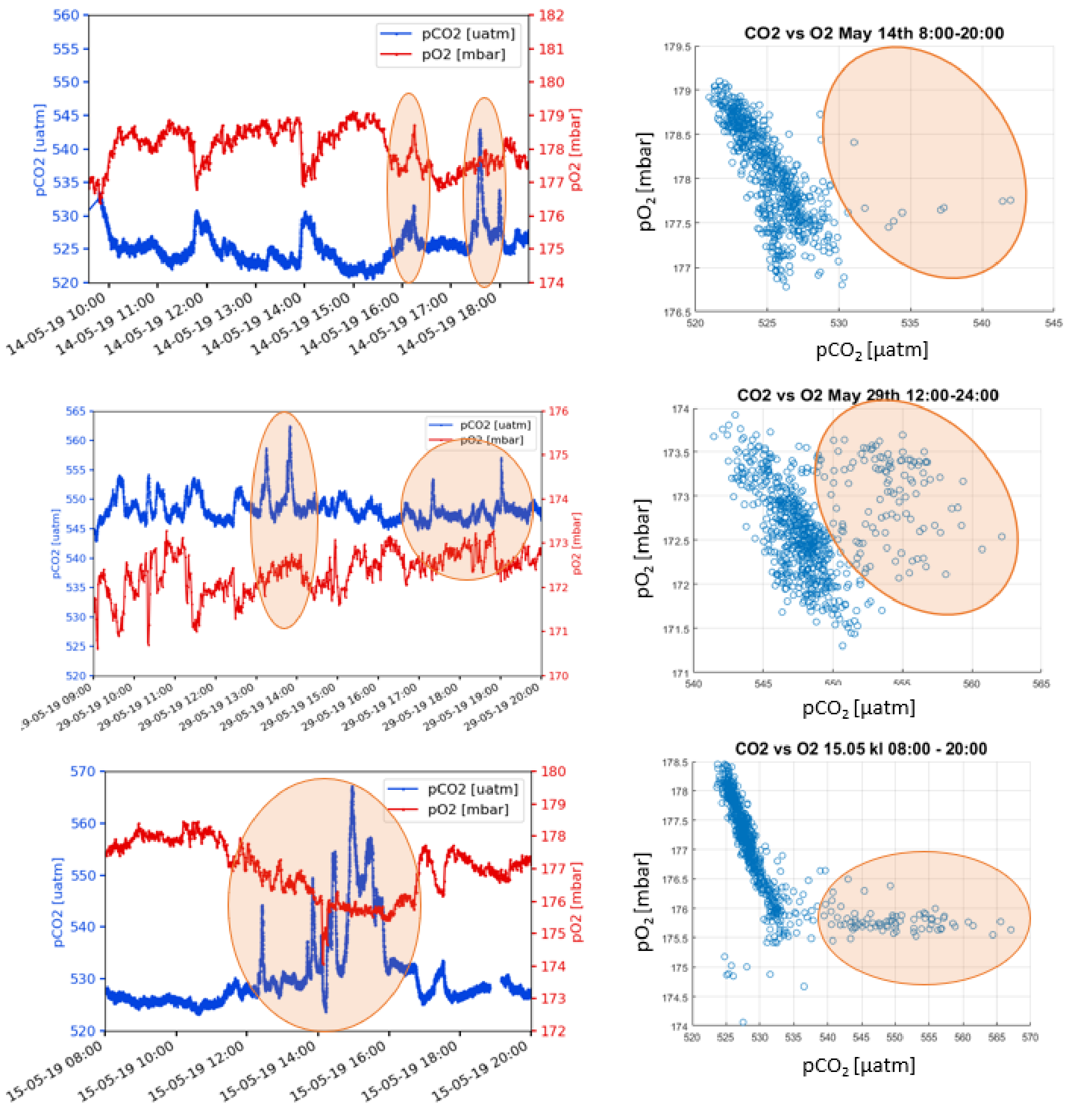

Figure 7-3 Measured CO_2 and O_2 during periods with a controlled CO_2 release (left), and the corresponding scatter plots with deviations from a linear correlation (right)

Another approach to identifying anomalies is to invert and scale the axis of one of the parameters (O_2 or CO_2), and visually or statistically identify regions where these curves differ substantially. Figure 7-4 shows CO_2 versus O_2 with an inverted y-axis during a 12-hour period without controlled CO_2 release. We observe that the red and blue curves follow each other nicely. Figure 7-5 and Figure 7-6 show corresponding curves for two days when we performed controlled CO_2 release experiments. The regions where the red and blue curves do not follow each other are likely to represent time spans during which a CO_2 plume passes Template A, affecting the signals recorded by the chemical sensors placed there. The same regions result in a deviation from the correlation curve as in Figure 7-3.

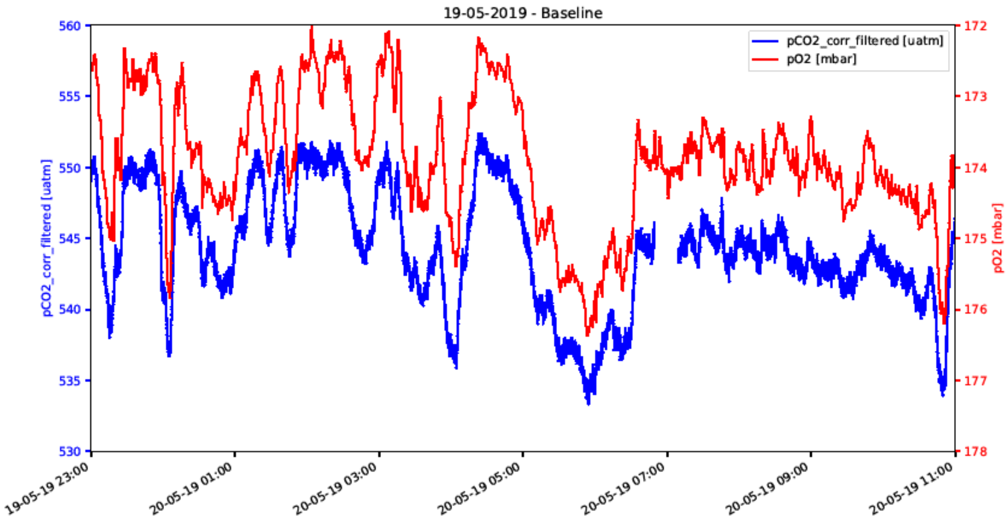

Figure 7-4 Baseline - an example of the measured CO_2 and O_2 concentrations over a 12-hour period (from 11 PM to 11 AM on May 19th). The y-axis for O_2 has been inverted to emphasize the correlation between these parameters during baseline conditions

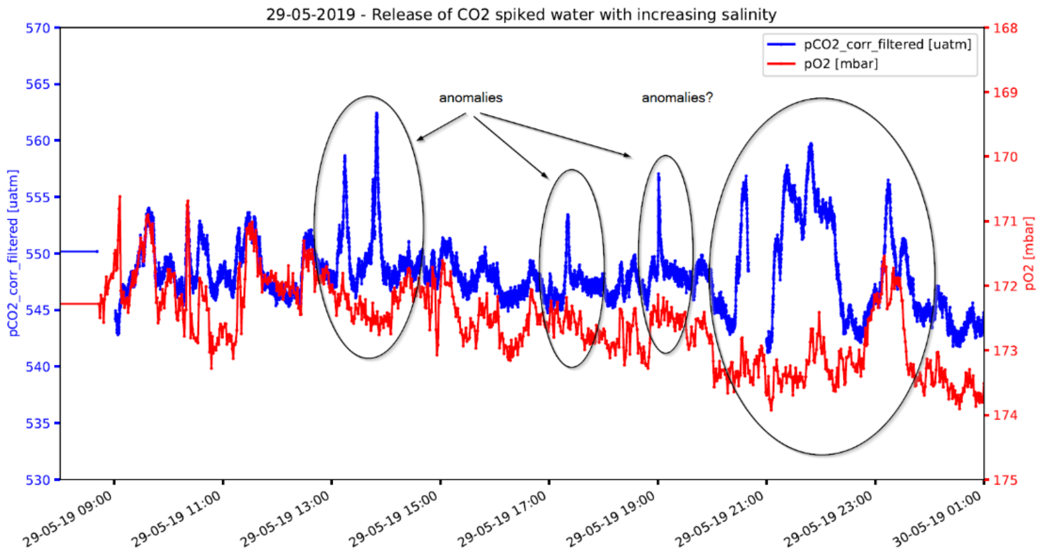

Figure 7-5 *CO_2 and O_2 (with inverted y-axis) measurements during a 10-hour period over which we had a systematic controlled release of CO_2 in both gas phase and dissolved in seawater (Figure 7-7). Systematic releases of dissolved CO_2 were followed by a considerable gas release which started at 16:10 and lasted until the bottle was empty (~2 hours). At this time, the sensors were placed 10 m from the leak frame.*

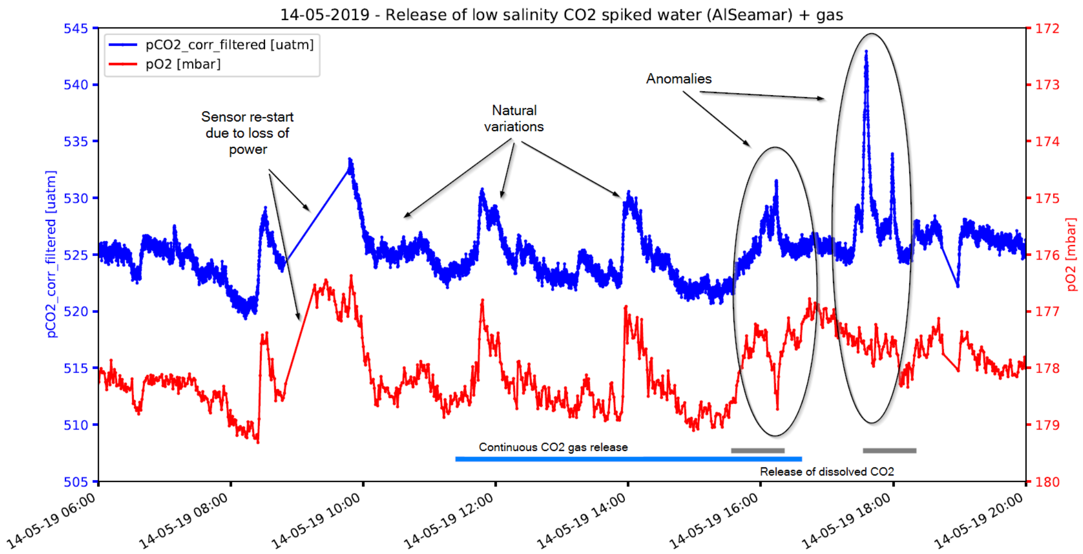

Figure 7-6 *CO_2 and O_2 (with inverted y-axis) during a day with controlled CO_2 release. Anomalies are identified visually as regions where the red and blue curves do not follow each other. The same regions appear as regions with low CO_2/O_2 correlation indicating a secondary source of CO_2.*

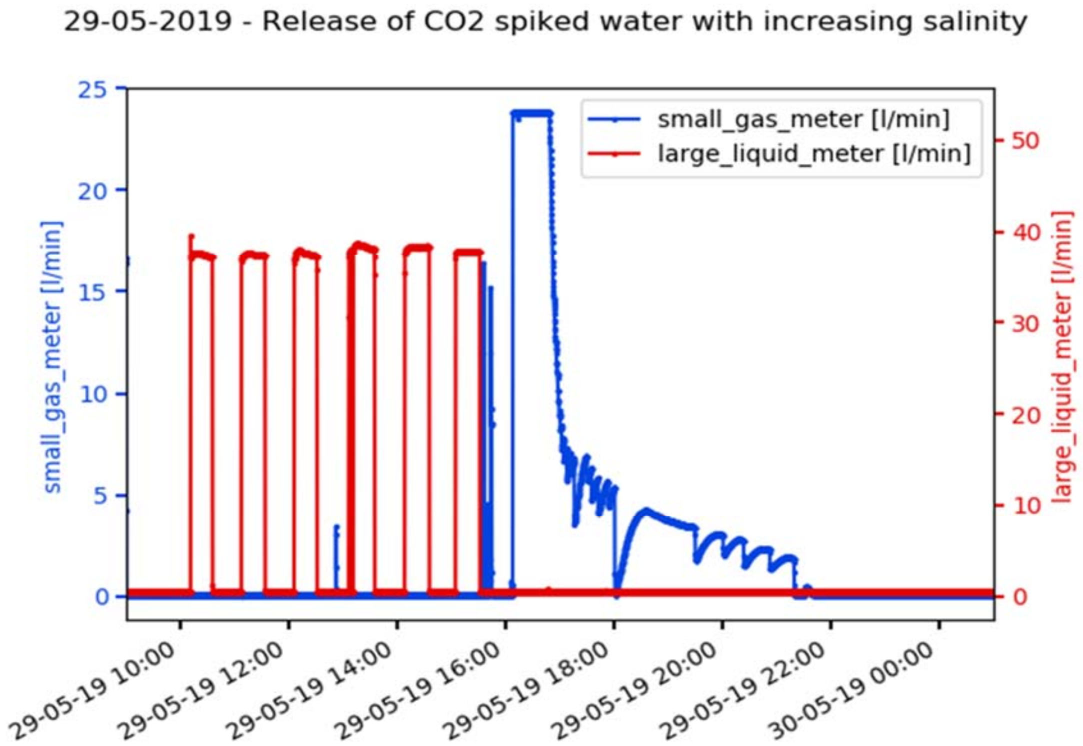

Figure 7-7 Release of dissolved CO_2 (red curve), and CO_2 bubbles (blue curve), over the same period as the measurements shown in Figure 7-5

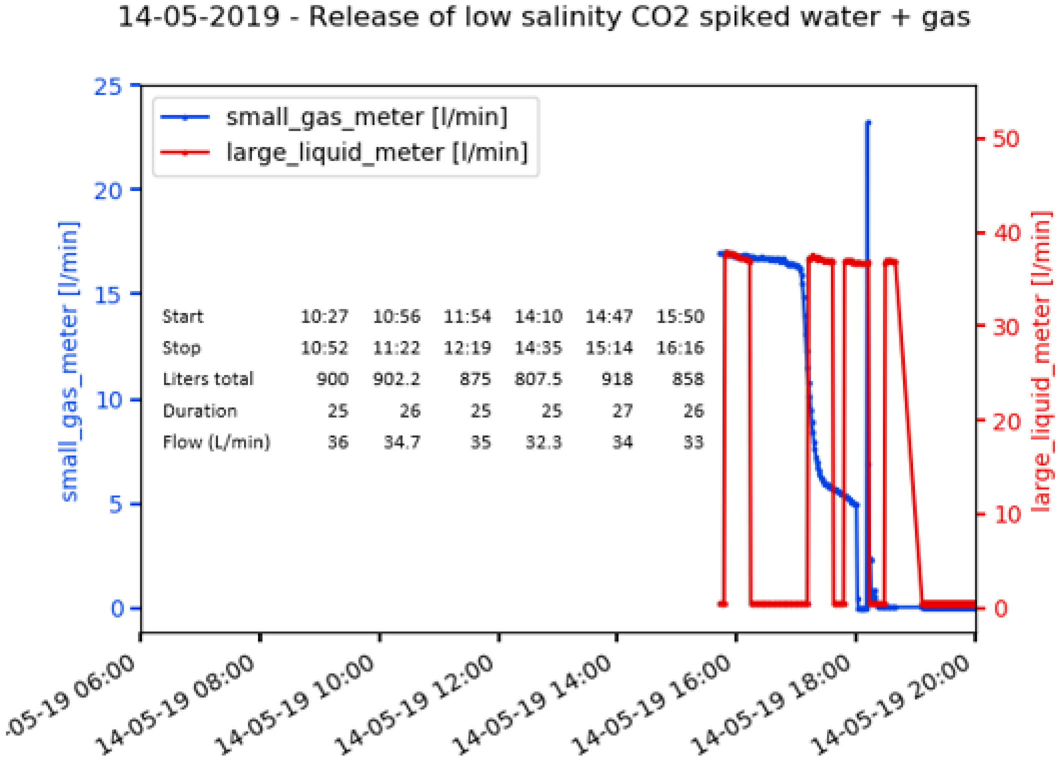

Figure 7-8 Release of dissolved CO_2 (red curve) and CO_2 bubbles (blue curve), over the same period as shown in Figure 7-6. The digital flow meters were mounted just before 16:00. See inlined table for earlier releases of dissolved CO_2.

A more detailed discussion of the CO_2-O_2 relationship during baseline conditions and during three different controlled release scenarios (Figure 7-9) is offered below. Figure 7-9 (A) shows the observed CO_2 (blue line) and O_2 (red line) concentration in the water at 60 m depth over a period of 48 hours, measured using the CONTROS HydroC and HydroFlash sensors. As explained in Section 3.2, biogenic processes control the variation of both pCO_2 and DO, which lead to an inverse correlation between these parameters under normal conditions (i.e., no external source of CO_2). We observe this correlation throughout the data set, when no CO_2 is being released.

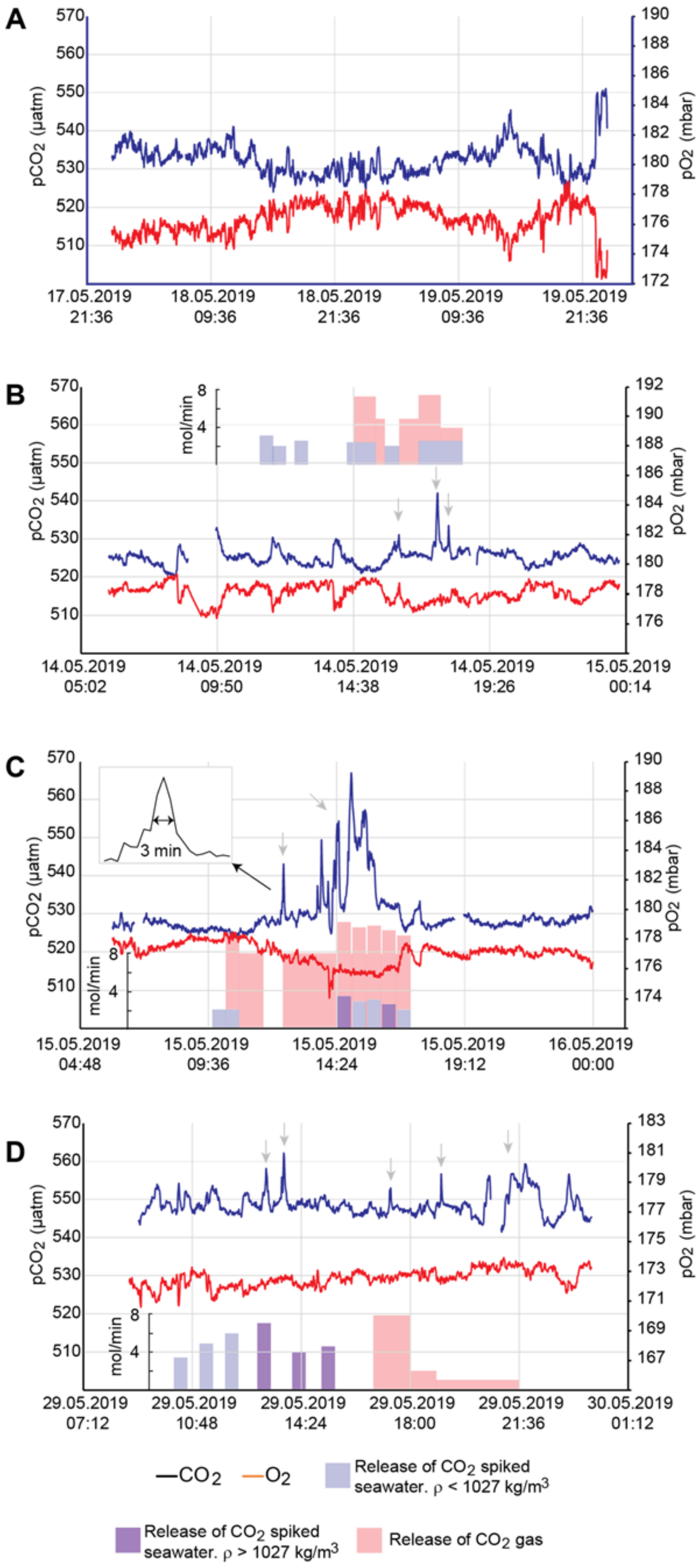

Figure 7-9 Observed pCO_2 (blue line) and pO_2 (red line) measured using stationary sensors on Template A during baseline conditions (A), and during controlled CO_2 release experiments (B, C, D). Plots A, B and C show the response from sensors located at a 25 m distance from the release point, whereas plot D illustrates the response when Template A has been moved to a new location 10 m from the release point. Plot A exemplifies the baseline conditions with a clear biogenic correlation of pCO_2 and pO_2. The amount of CO_2 released during the experiments (B – D) is calculated and indicated in the plots (mole CO_2/min), as well as the type of medium used, i.e. CO_2 gas and/or CO_2-spiked high-density/salinity or lower-density/salinity seawater

Figure 7-9 (B, C, D) illustrates the correlation between CO_2 and O_2 for three days where considerable amounts of CO_2 were released, both as gas and dissolved in seawater (indicated in the figure by red and blue bars). In these cases, we observe the predicted correlation for most of the day, interrupted by shorter time periods during which this correlation is lacking. We refer to this lack of correlation as an anomaly, most likely related to our controlled release of CO_2. Anomalies are observed in the CO_2-O_2 correlation during all three days with controlled CO_2 release shown in Figure 7-9 (B, C, D). These are indicated by arrows.

Prior to 21st of May (Figure 7-9 A, B, C), the sensors were located 25 m from the leak point, after which the sensors were moved to a 10 m distance (Figure 7-9 D).

Figure 7-9 B shows measurements from the sensors (CONTROS HydroC and CONTROS HydroFlash) during a period (14th of May) over which we had a release of CO_2 both in gas phase and in dissolved phase. In total, about 1 500 moles of CO_2 were released during this period. In this case we observe modest anomalies in the CO_2 measurements which are well within the range of natural variations (±5-20 µatm). However, the lack of correlation with O_2 increases the likelihood that these anomalies are caused by a secondary source of CO_2 not naturally present, i.e., that they are caused by our controlled release of CO_2. At this time the sensors were located 25 m from the leak point. The distance was accurately mapped using the Kongsberg Mesotech M3 multibeam sonar (see Section 7.3).

Figure 7-9 C shows a larger anomaly the following day (15th of May). This difference in response is likely connected to the larger amount of CO_2 released on May 15th. On May 15th we released significant amounts of CO_2 in gas phase throughout the day, along with multiple 1 000 L tanks of seawater with a high CO_2 content and varying salinity. In total, more than 3 500 moles of CO_2 were released this day. The integral/area of the CO_2 response this day is in the order of 50 000 µatm, whereas on the 14th of May (Figure 7-9 B) the response integral is 8 500 µatm. However, the estimate of the total amount of released CO_2 is conservative since the gas release on May 15th exceeded the maximum range of the digital flow meter. Consequently, the response may correlate better to the amount of released CO_2.

The ocean current conditions during May 14th and May 15th were very similar (Figure 7-10), with very slow currents, and no dominating current direction. This was also visually observable from a camera mounted on the release frame, where particles in the water moved slowly back and forth, rather than in a specific direction.

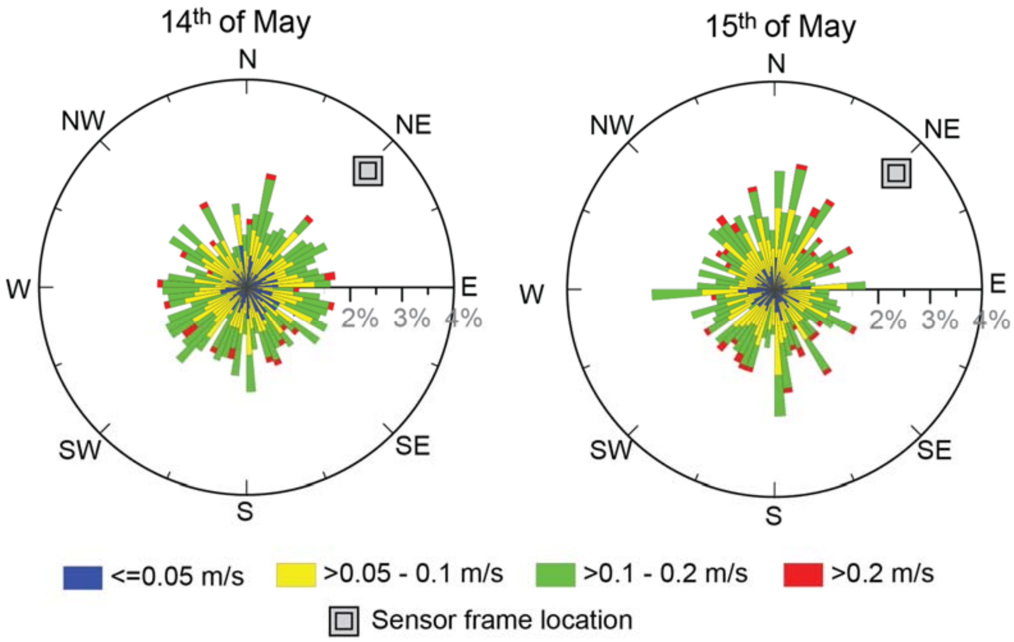

Figure 7-10 Current conditions on the 14th and 15th of May, from the start time of release experiments to the final observation of responses. The location of the stationary sensor template (A) relative to the leak frame is indicated by a grey rectangle.

Figure 7-9 D shows a similar situation during another day with controlled release experiments. At this time the sensor frame (Template A) had been moved closer to the leak frame such that the new distance was 10 m. Again, we observe anomalies recognized as elevated levels of CO_2 along with a lack of correlation with O_2. On this day, the release experiments were conducted more systematically, where CO_2 was released dissolved in seawater with increasing salinity, and later as gas without simultaneous release of dissolved CO_2. Both dissolved CO_2 and CO_2 in gas phase give rise to anomalies in the CO_2-O_2 correlation. However, it is not possible to see any notable effect of increasing the salinity/density of the released CO_2-spiked seawater. It seems that the gas release gives rise to a broader response, which indicates that the variable density of the released CO_2-spiked sea water caused some plumes to miss the sensors. Since the sensors are located ~1 m above the seabed, it is possible that the denser plumes passed below the sensors. Conversely, the lighter plumes may pass higher up in the water column.

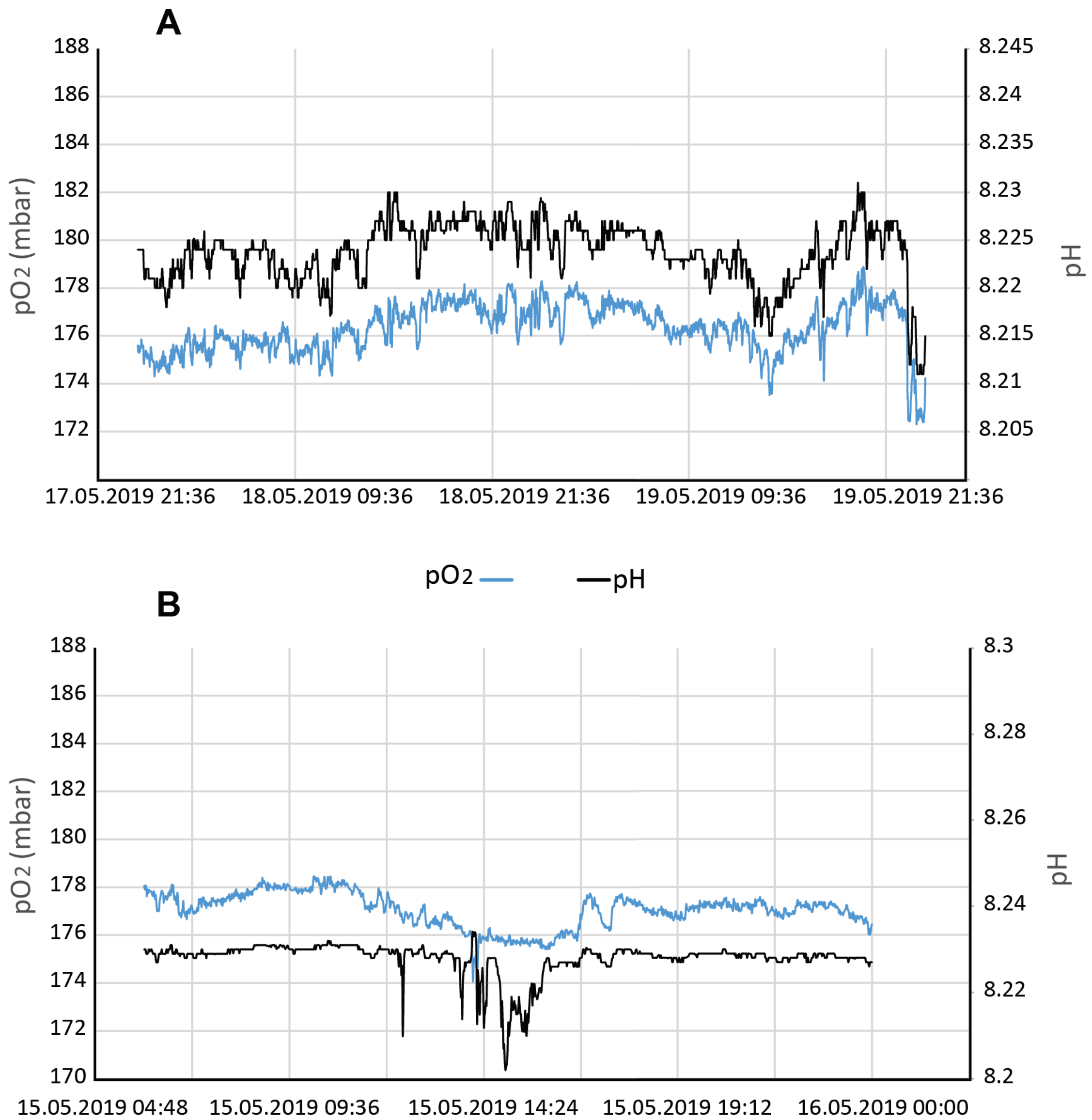

Figure 7-11 pH versus pO_2 measured at the stationary template A, during two days without any leakage experiments (A), and during one day of considerable CO_2 release (B)

pH will, similar to pO_2, be inversely proportional to CO_2. Hence, during natural variation, pH is expected to correlate with pO_2. Figure 7-11 shows that this indeed is the case, and that deviations from this correlation indicate leakage. However, the relative changes are smaller in pH compared to in pCO_2, and measurements of the pCO_2-pO_2 correlation may therefore be a more robust approach. Still, pH may be a supplement to pCO_2, and has the advantage of fast response times. As discussed further below, the fast response time of the pH sensor can be advantageous for mobile platforms.

These results indicate that CO_2 and O_2 sensors placed on a stationary template provides an effective and reliable way to identify anomalies and to differentiate between natural variations and a secondary source of CO_2 (for instance a CCS related leak). We also observe that a pH sensor can be used to supplement or replace a CO_2 sensor.

7.2 EK80 scientific echo sounder

CO_2 and air bubbles in water are easily visible using the EK80 echo sounder since these are strong acoustic scatterers. Key features of the EK80 echo sounder include:

- broadband capabilities
- acoustic leak quantification capabilities due to the split beam configuration and potential for accurate calibration
- high sensitivity - can detect small leaks including single bubbles depending on the distance
- large dynamic range
- flexible deployment options - hull-mounted on a R/V, stationary seabed template, AUV or glider

Using a pan/tilt unit to aim the echo sounder in the intended direction was key to getting good measurements. Without the possibility to adjust the acoustic beam direction, it is easy to "miss" a gas plume because of the 7 degree conically shaped beam of the echo sounder.
Figure 7-12 shows an example echogram acquired using the EK80 echo sounder during this experiment. In this case CO_2 bubbles were released at a flow rate of 1.3 l/min. The y-axis represents the distance from the echo sounder, and the x-axis represents time. The bubble plume is visible ~65 m from the echo sounder, corresponding to the distance between sensor template B and the leak frame. The white line in the middle indicates the location of the centre of the plume, determined from the maximum target strength for each time sample. We observe that the plume drifts slightly towards and away from the echo sounder over time. This is likely related to ocean currents.

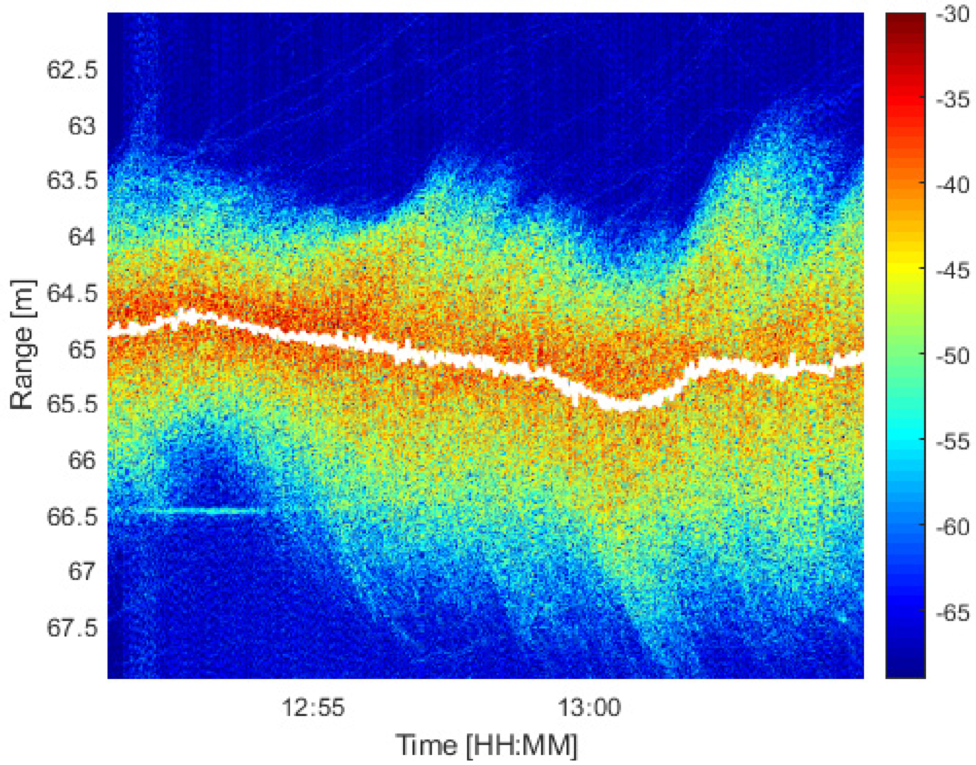

Figure 7-12 Echogram obtained from the EK80 during a controlled release of CO_2 bubbles. The y-axis shows range, or distance from the sensor, and the x-axis shows time. A gas plume is clearly visible at ~65 m range. The white line indicates the centre of mass of the plume, which seems to have a spatial extent (dispersion) of 2-3 m.

Quantitative measures of CO_2 plume properties can be extracted from the EK80 echogram and used as a component in a monitoring and warning system. Figure 7-13 shows relevant parameters extracted from the echogram in Figure 7-12, including the location of the plume (distance from echo sounder), density of the CO_2 plume, plume dispersion, plume width, mean target strength, and total target strength. An additional relevant parameter would be the estimated leak rate (flux), which is a topic we are currently studying.

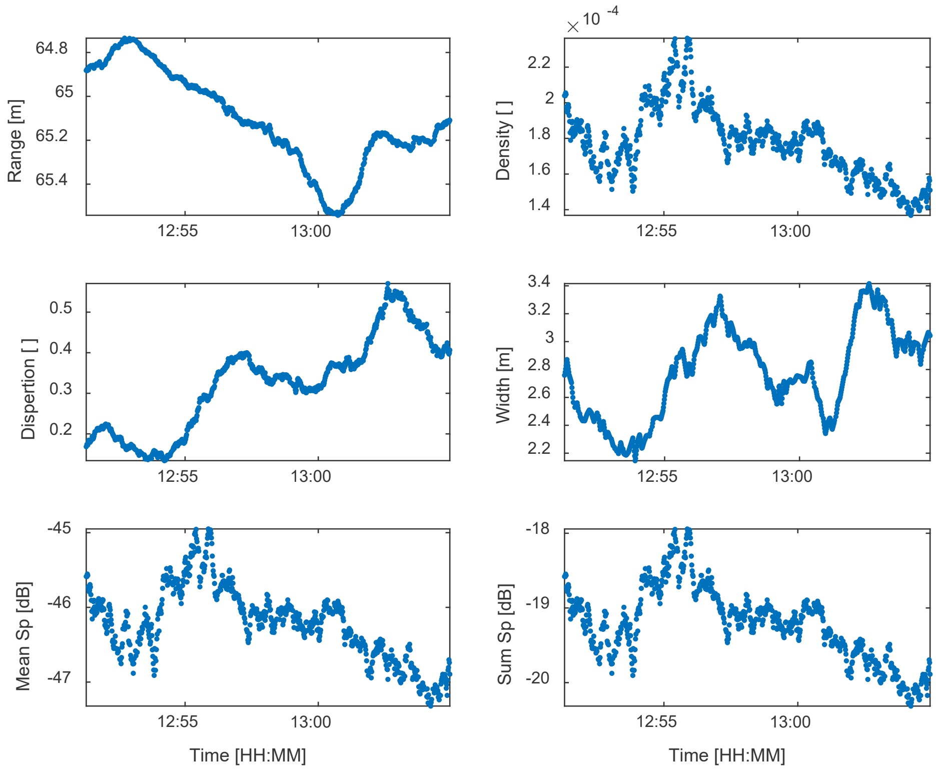

Figure 7-13 Plume characterization using the EK80 data. Based on the echogram, several quantitative measurements can be extracted. Here, the distance to the plume (range), dispersion, mean Sp (target strength), density, plume width, and total Sp have been computed. These parameters are helpful in quantifying the size of the plume, which again can be related to the amount of escaping CO_2.

7.3 M3 sonar

The Kongsberg Mesotech M3 multibeam sonar provides an overview of the seabed at the region of interest (Figure 7-14). The 140-degree opening angle makes it possible to map a large region and to detect multiple leaks as well as structures and features on the seabed which may be of interest. The placement of objects relative to one another can also be accurately determined. We used the M3 sonar images to determine the distance between the leak frame and the instrument templates. We also used it during a procedure where Template A was moved from one location to another, to interactively guide the operators and ensure that the template was correctly placed at the seabed.

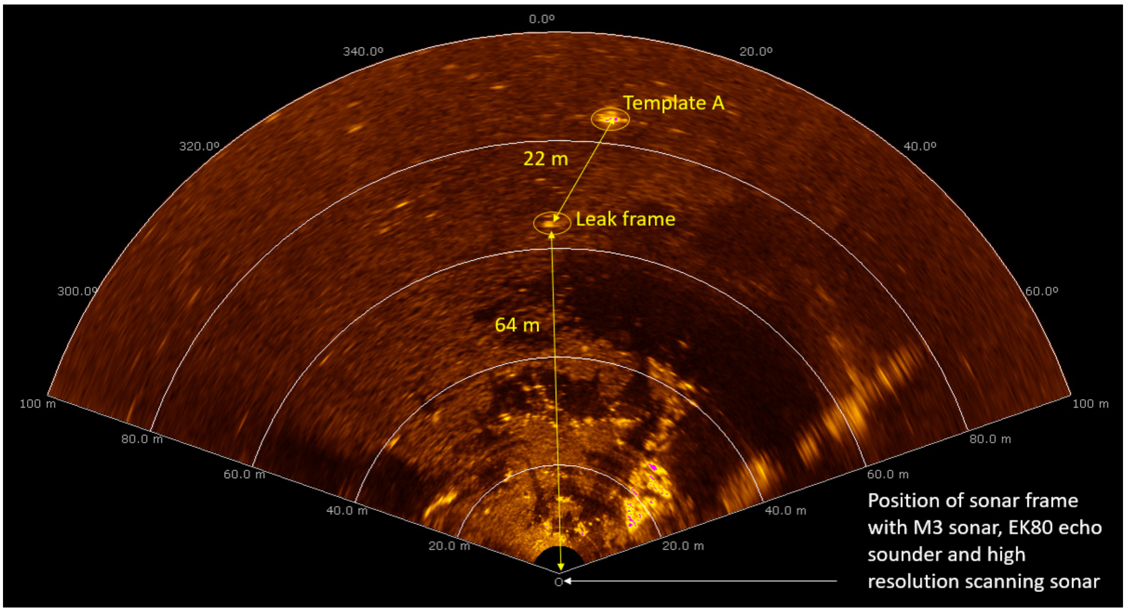

Figure 7-14 M3 sonar image showing the leak frame and Template A. No CO_2 leak is present. The distance between the sonar frame and the leak frame is 64 m, and the distance between the leak frame and Template A is 22 m.

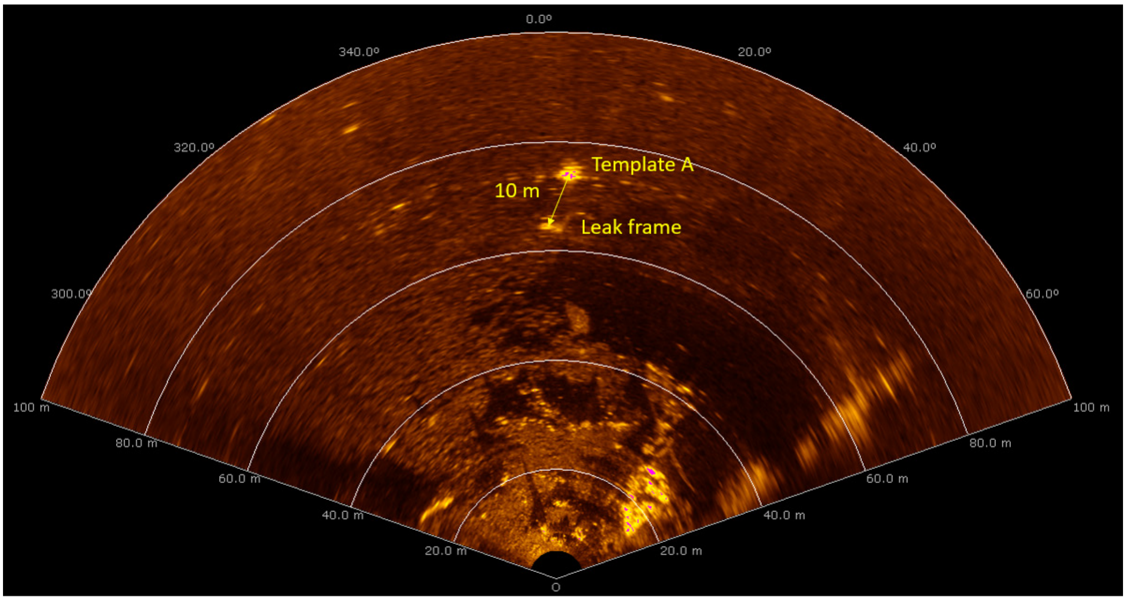

Figure 7-15 M3 sonar image after moving Template A to a new position closer to the leak frame. The M3 sonar was used during the moving procedure to guide the operators and verify correct positioning of Template A. Template A was moved using a vessel with a winch.

The M3 sonar and accompanying software includes several imaging modes. We used mainly the enhanced Image Quality (eIQ) Fine mode which results in the highest possible image quality. In this mode the angular resolution is 0.95 degrees. In applications with limited data storage or transfer capabilities, it is possible to select a different mode with a lower image resolution.

Further analysis is needed to determine the sensor's sensitivity and its ability to detect and quantify small leaks. Our experience is that small leaks are more easily detected using the EK80 echo sounder because of its high sensitivity and dynamic range, but also because of the imaging geometry and the relatively large vertical resolution cell of the M3 sonar (this can be tuned in software and has not been optimized in these examples).

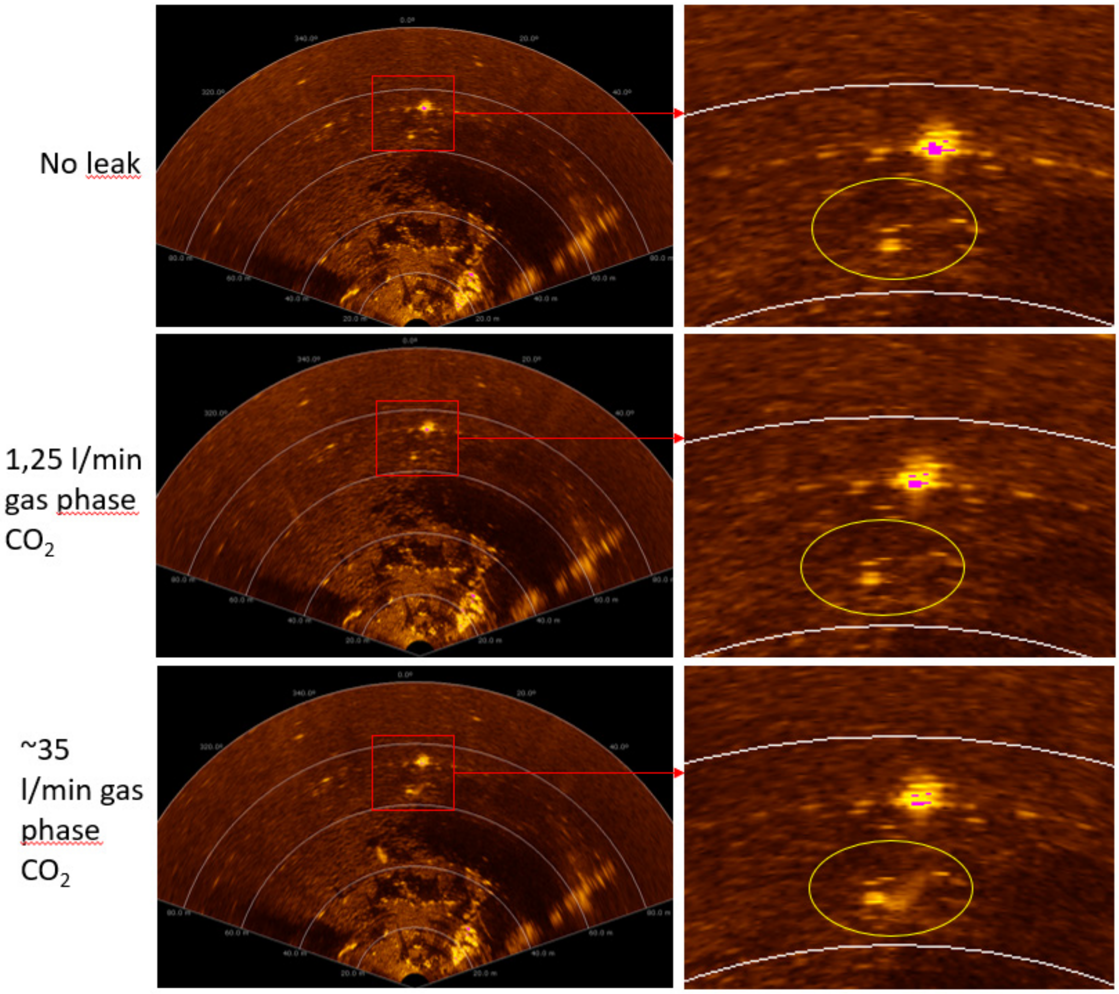

Figure 7-16 M3 sonar images showing a 140-degree scene (left). A region of interest including template A and the leak frame is indicated by the red rectangles and shown in a larger scale (right). The upper images show the situation with no CO_2 release. The middle images were acquired when a small leak (1.3 l/min) was being simulated, and the lower images were acquired during release of considerable amounts of CO_2 in gas phase (~35 l/min).

Figure 7-16 shows M3 sonar images of a 140-degree scene including the leak frame and template A. The distance between the sonar and the leak is 64 m. The images to the right show a larger scale image of the region of interest indicated by the red rectangles in the leftmost images. The upper images represent the case without a CO_2 leak, such that only reflections from the leak frame can be seen in the image. The middle images represent the case when 1.3 l/min CO_2 in gas phase is released, and the lower images were acquired during a ~35 l/min release of CO_2 in gas phase. We observe that without dedicated processing, relatively large leak rates are detected while smaller leaks are not directly observable at this distance.

7.3.1 Enhancing moving objects

One of the built-in functions in the M3 processing software is a moving average filter designed to enhance moving targets and suppress the stationary background. We found this useful when detecting small releases of CO_2 in gas phase. Figure 7-17 (upper image) shows the M3 sonar image acquired in eIQ mode, while Figure 7-17 (lower image) shows the same image but with the background removal filter applied. In addition to the CO_2 leak, other moving objects such as a shoal of fish is highlighted, while the stationary background including Template A is suppressed in the lower image.

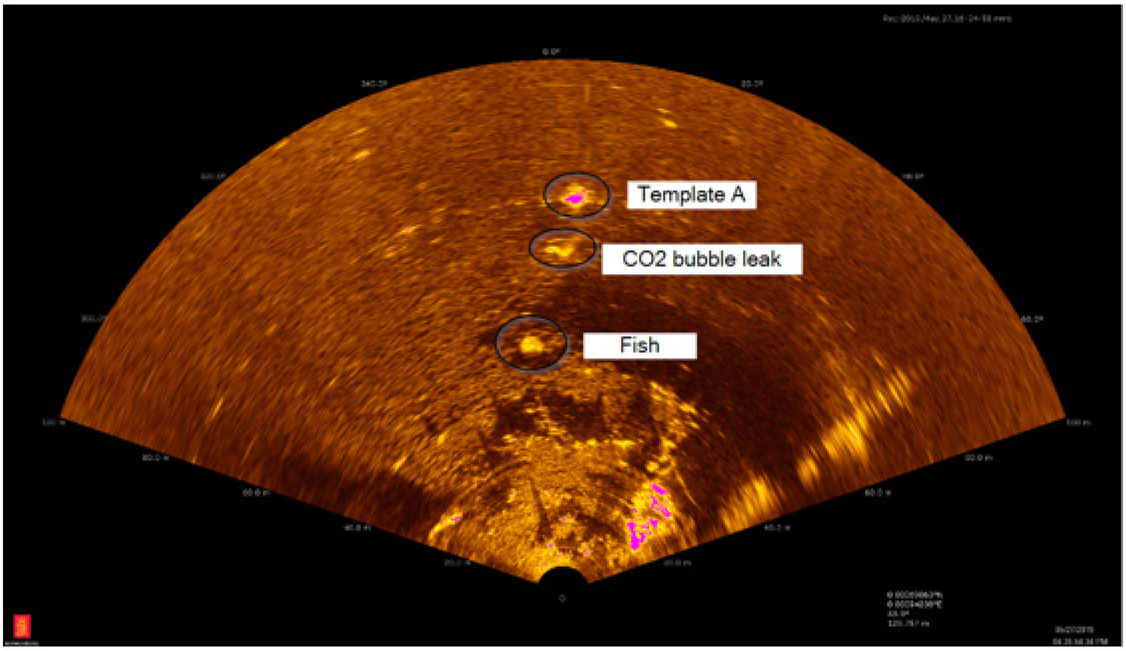

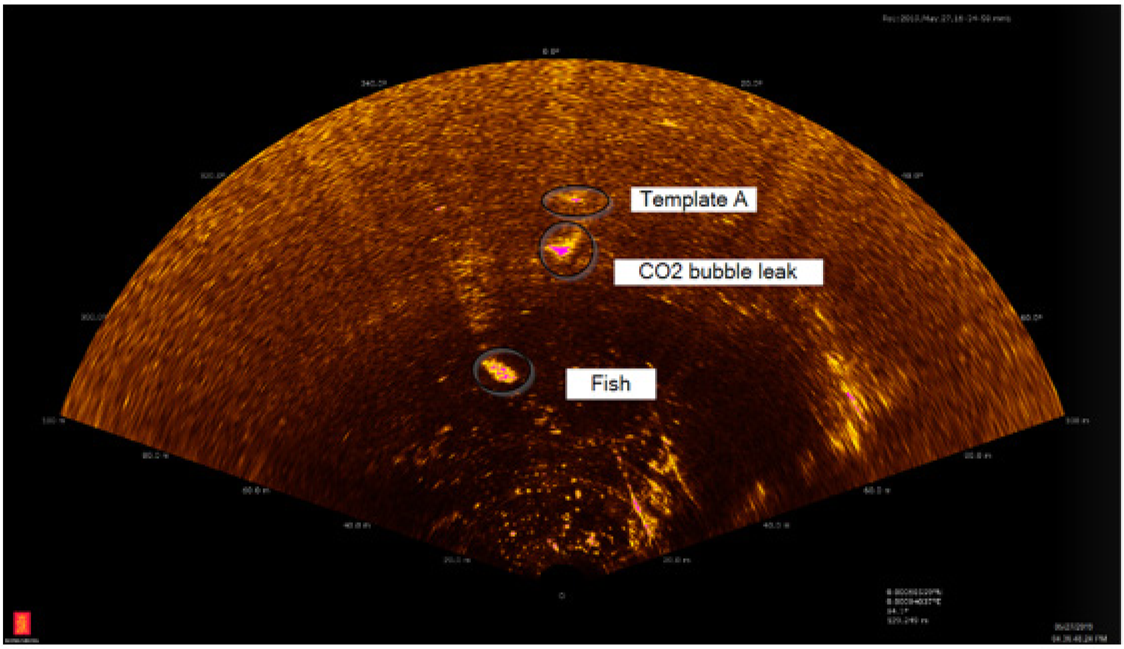

Figure 7-17 Upper plot: M3 sonar image obtained in imaging mode eIQ Fine. We clearly see template A, a metal structure with sensors mounted on it. We also see the CO_2 bubble plume when releasing ~35l/min of CO_2 in gas phase. A shoal of fish is visible as a highly reflecting region in the image. Lower plot: M3 sonar image obtained in imaging mode, eIQ Fine, with the background filter applied. This averages over 3 consecutive time samples to highlight moving objects. We found that this enhanced the presence of the CO_2 plume, since the bubbles are non-stationary over time. The non-stationary fish are also enhanced, while template A is suppressed.

7.3.2 Optimizing sensor viewing angle

The M3 sonar is offers a flexible vertical beamwidth, ranging from 3 degrees to 30 degrees. We found the 30-degree setting most useful since it captures a large part of the seabed as well as the leak. A 30-degree vertical beamwidth also captures a larger portion of a rising bubble train/plume than would be the case with a narrow beam. A narrower beam may be used to reduce or avoid reflections from the seafloor. While this can be an advantage when characterizing the acoustic reflections from only gas bubbles, the images are more challenging to interpret because of the loss of spatial context.

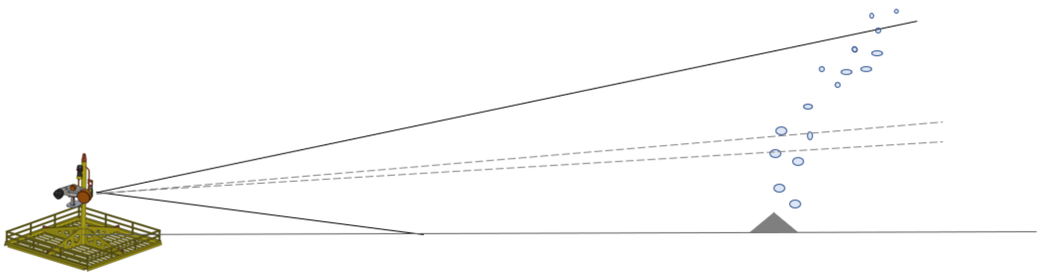

Figure 7-18 Schematic of the M3 imaging geometry. The vertical beamwidth is selectable between 3 (dashed lines) and 30 (solid lines) degrees.

During the 2019 nearshore controlled release experiments, the M3 sonar and EK80 echo sounder were mounted on the same remotely operated pan/tilt unit. This has advantages for data analysis and acoustic characterization of the plume, since both instruments have the same focal point within the bubble plume. However, the two systems do not necessarily have the same optimal viewing angle. We chose to optimize the viewing angle based on the EK80 echo sounder for most of the experiments, but also evaluated the effects of varying the M3 sonar tilt (Figure 7-19). We observe that a larger part of the plume was captured when tilting the sonar 20 degrees upwards, thus increasing the plume detectability. When tilting the sonar beyond 20 degrees, the images became severely distorted due to multipath reflections from the sea surface, and the plume was no longer visible.

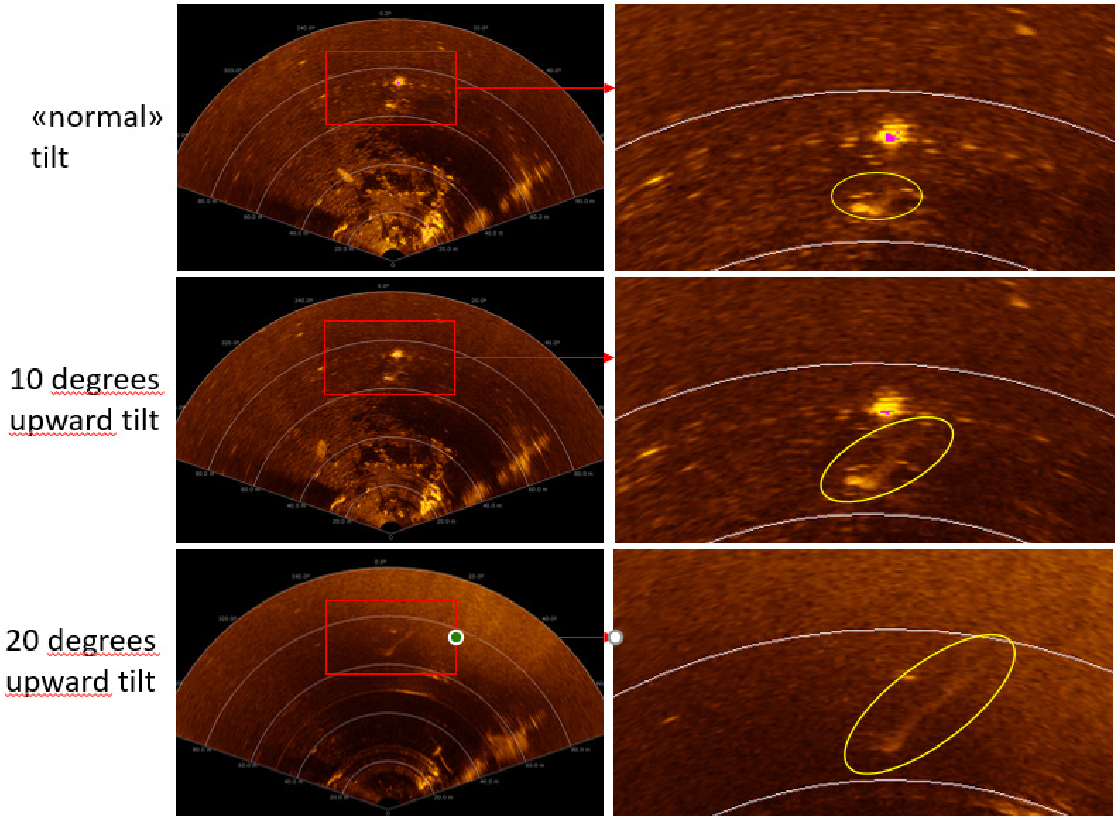

Figure 7-19 The ability to detect a gas leak can be improved by optimizing the sonar viewing angle. Here we see the effect of using the "normal" tilt, or the standard tilt used during most of the nearshore experiments in this project (upper plots), tilting the sonar 10 degrees upward (middle plots), and tilting the sonar 20 degrees upward (lower plots). We observe that a larger portion of the plume was captured when tilting the sonar upward. Tilting beyond 20 degrees resulted in poor images due to multipath from the sea surface.

7.4 Scanning sonar

The high-resolution scanning sonar we used is developed by Kongsberg Mesotech. It operates at high frequencies (325 kHz or 500 kHz, selectable). As opposed to the M3 multibeam sonar, the high-resolution scanning sonar is a single beam sonar. It transmits a single beam, waits for the return echo from each time sample (or distance), and then mechanically moves ~1 degree before transmitting the next ping. In this way it continuously scans a defined area of interest up to 360 degrees.

The high-resolution scanning sonar is designed for detailed imaging of objects at relatively close range (< 100m). In this controlled release experiment, we were not able to detect the controlled leak at 65 m range. This could be related to the way the sonar was positioned, or that the leak was located too far from the sonar. It should be noted that while the M3 sonar and the EK80 echo sounders were placed on a remotely controlled pan/tilt unit, the scanning sonar was not. As a result, the angle at which the sonar was directed was probably not optimal. Our experience suggests that for bubble detection, this sonar is well suited to monitor a relatively small area of interest (less than ~20 m range), but it has limited area coverage and dynamic range. The single beam transmission is an advantage in the presence of complex structures such as poles and lines, because there is little interference from off-axis directions. Dedicated processing may also be used to enhance suspected gas leaks in the image.

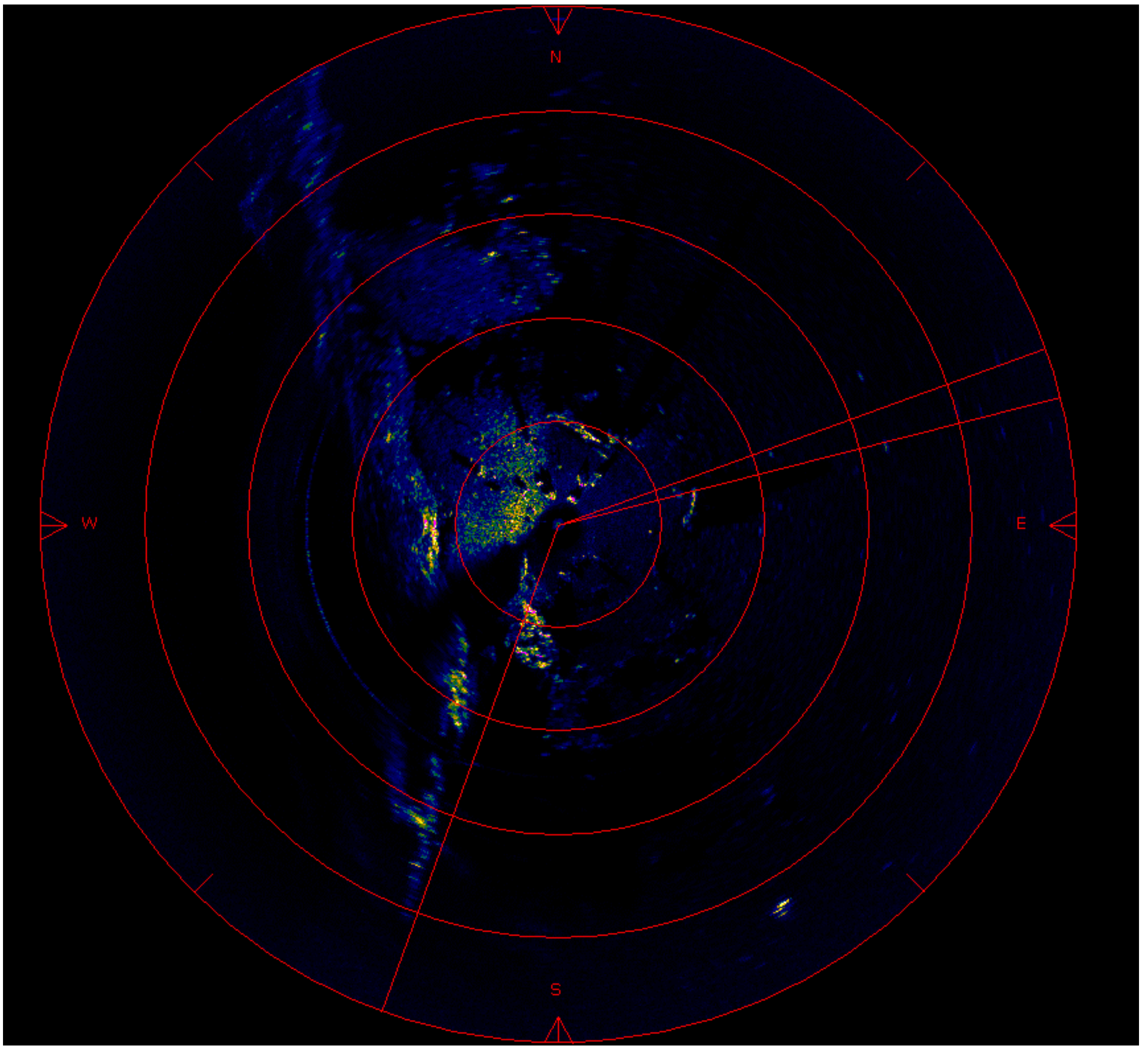

Figure 7-20 High resolution scanning sonar image showing a complete 360-degree scan of the area. Rocks and boulders are shown on the seabed. We were not able to detect a CO_2 leak using this instrument. It should be noted that the position and viewing angle of this sonar was not optimized since it was not placed on the pan/tilt unit. The limited sensitivity and dynamic range of this sonar makes it better suited for leak detection at closer range (< 20m).

8 Response to controlled release experiments – HUGIN AUV

The HUGIN AUV has a modular design and offers the possibility to integrate different sensors according to monitoring needs. The sensor payload was updated as part of this project to include the following sensors for the nearshore controlled release experiments:

- CONTROS HydroC CO_2
- CONTROS HydroFlash O_2
- CONTROS HydroC CH4
- Franatech CO_2 sensor
- Franatech METS CH4
- Ocean Seven pH
- HISAS 1030 synthetic aperture sonar

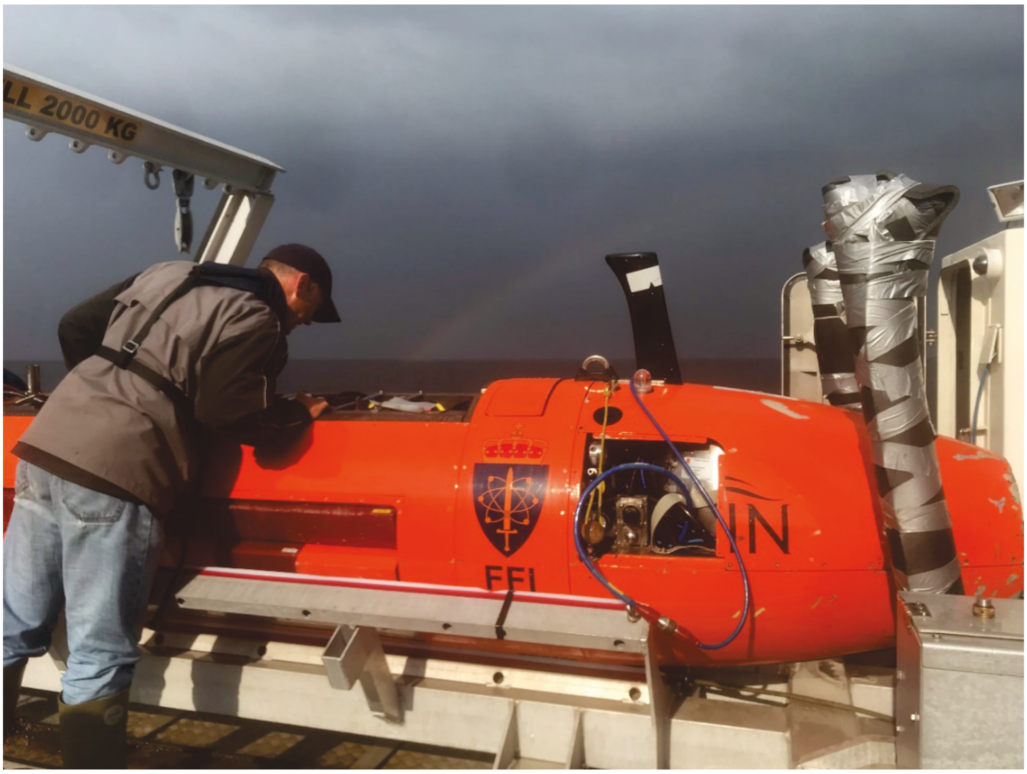

Figure 8-1 HUGIN operator checking that the chemical sensors are ready for deployment. The chemical sensors are integrated on the top, and the starboard side of the HISAS 1030 sonar is partially visible in dark red.

Figure 8-2 shows release rates during May 21st, when the HUGIN AUV was used for water column and seabed mapping. We varied between releasing CO_2 in gas phase in the morning, dissolved CO_2 in the early afternoon, and a combination of gas- and dissolved phase CO_2 in the late afternoon.

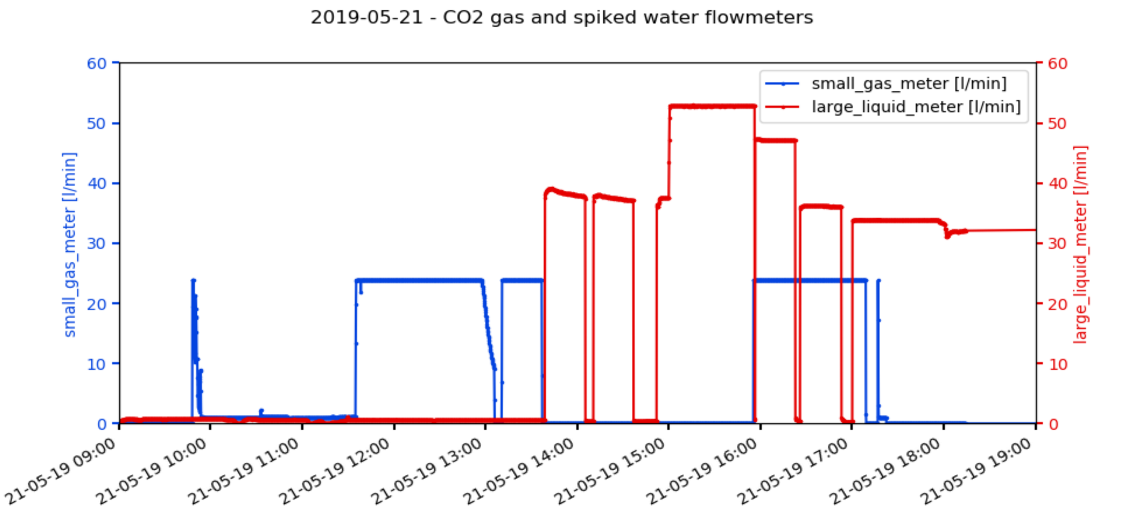

Figure 8-2 Relative release rates during the period when the HUGIN AUV was in the water. The blue curve shows release of CO_2 bubbles, and the red curve shows release of simulated pore fluids.

The HUGIN AUV was programmed to travel in a lawnmower pattern within the rectangle shown in Figure 8-3, with most of the lines acquired at varying depths close to the leak frame.

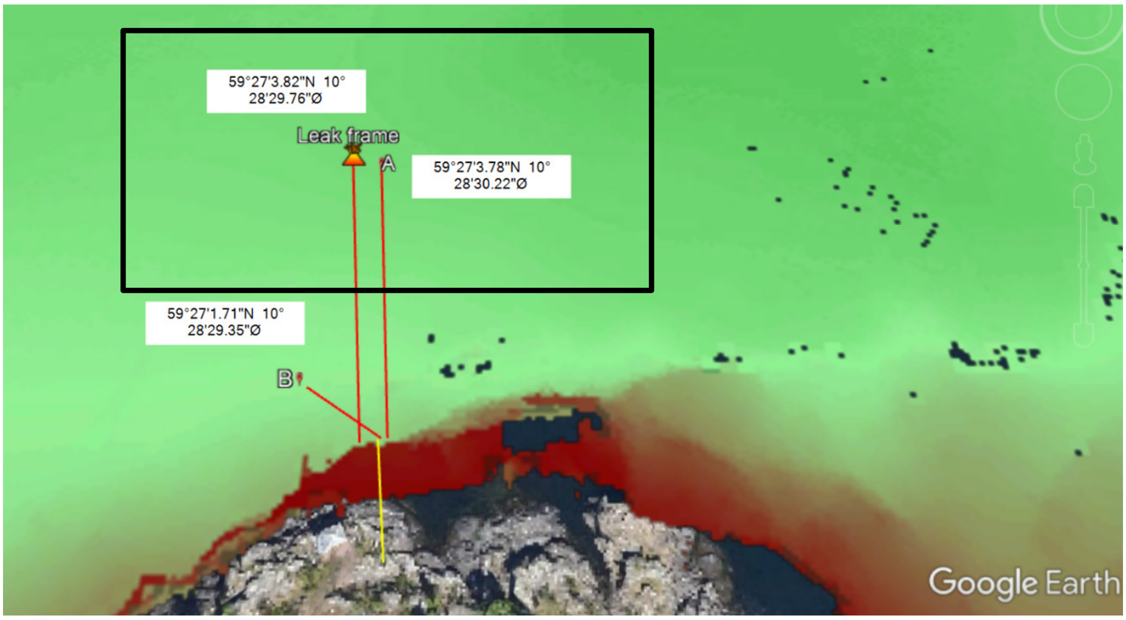

Figure 8-3 The black box indicates the area covered by the HUGIN AUV. Within this area, the AUV travelled in a lawnmower pattern at varying depths.

Figure 8-4 shows the actual travel path for the HUGIN AUV, extracted from navigation data. Figure 8-5 shows a close-up of the tight grid acquired near the leak frame. The aim was to sample the water column in three dimensions close to the simulated leak to detect anomalies using the chemical sensors as well as the HISAS sonar. The lines some distance from the leak frame are best suited for background measurements using the chemical sensors, and for acoustic imaging of the seabed and the CO_2 gas plume.

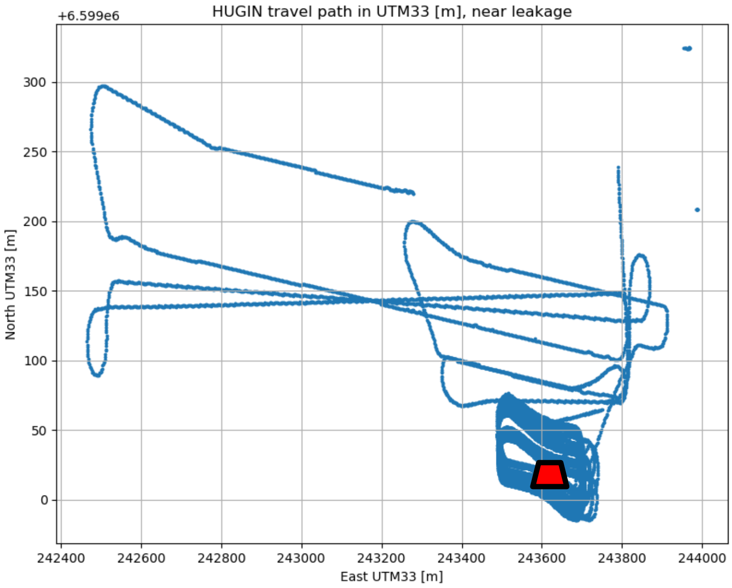

Figure 8-4 HUGIN travel path during the controlled release experiment. The position of the leak frame is indicated in red. The lines farthest from the leak are used to document the background situation.

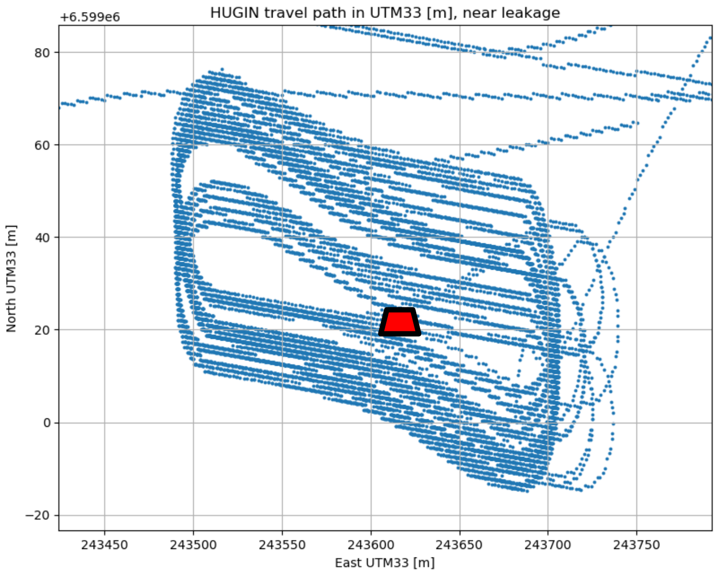

Figure 8-5 Close-up of HUGIN's travel path near the position of the controlled release point. These 2D lines were repeated at 5m depth intervals from 5 m above the seabed up to 10 m below the surface.

8.1 Chemical sensor response

Figure 8-6 shows the dissolved CO_2 concentration measured using the CONTROS HydroC sensor during the entire day of data acquisition. During the acquisition the sensor sample rate was 1 Hz, but a single output sample was an average of the 5 previous data samples. The blue line to the left in Figure 8-6 represents the first few minutes when the AUV was diving, and the CO_2 sensor has not had time to stabilize, resulting in unrealistically low CO_2 values. Similarly, the green line to the right show unrealistically high CO_2 concentration values. For the rest of the data, the trend is as expected with CO_2 concentrations increasing as a function of depth. A similar trend is measured using the Franatech CO_2 sensor (Figure 8-7).

Neither of the CO_2 sensors show any obvious anomalies related to the controlled CO_2 release. The response time of these sensors (as well as other membrane-based sensors) is affected by the time it takes the dissolved gas molecules to pass through the membrane, and is in the order of several minutes. This does not imply that these sensors are irrelevant for moving platforms, but it sets a lower limit to the size of a CO_2 plume which can be detected. Post processing techniques such as filtering and response time correction (RTC) may to a certain extent compensate for the long response time and increase the detectability of short-time events, as shown in Section 8.1.1.

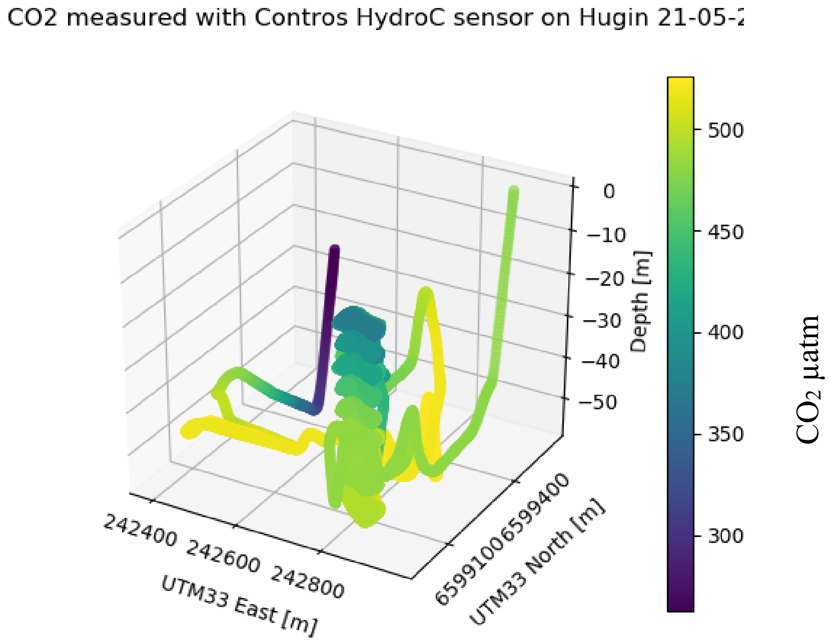

Figure 8-6 CO_2 partial pressure measured in µatm using the CONTROS HydroC sensor mounted on the HUGIN AUV. No obvious anomaly is visible in these data, and the trend is as expected with CO_2 concentrations increasing with depth.

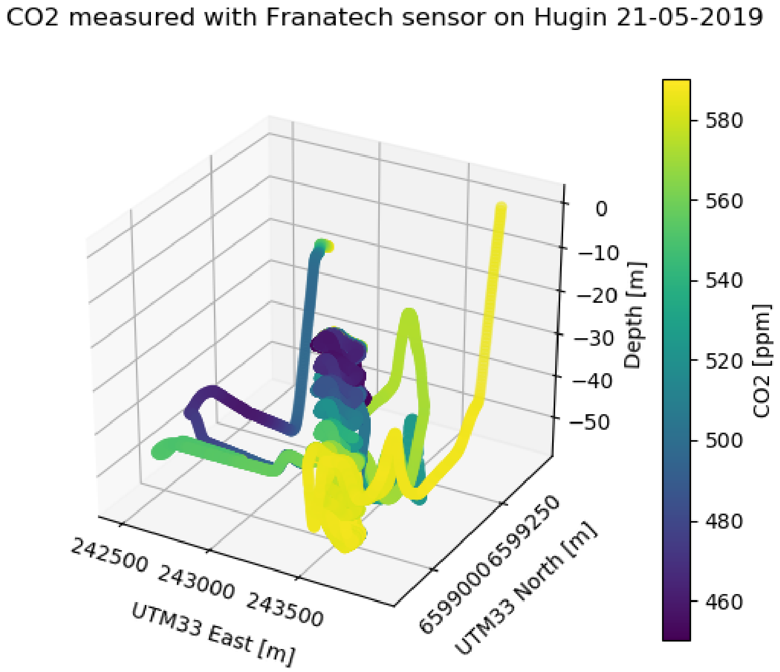

Figure 8-7 *CO_2 partial pressure measured using the Franatech CO_2 sensor mounted on the HUGIN AUV. The trend is similar to that measured using the CONTROS HydroC sensor. Note that the units are different – the CONTROS HydroC plot shows values in µatm, and the Franatech CO_2 sensor output is shown here in ppm.*

Because of the significant natural variations in CO_2 vertically in the water column, modest anomalies may easily be overlooked unless analyzing the data at discrete depth intervals. We closely analyzed the data for each depth that the HUGIN AUV had covered, without finding any indications of an anomaly prior to post processing. Figure 8-8 and Figure 8-9 show the CO_2 data for both sensors at a water depth of 50 m, in the afternoon after considerable release of CO_2.

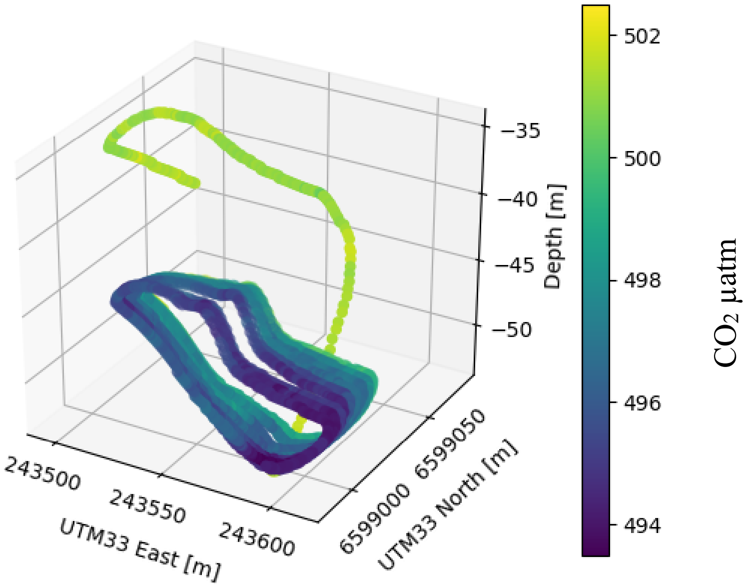

Figure 8-8 CO_2 measured using the CONTROS HydroC sensor at 50 meters water depth in the time interval 15:00 to 15:45, local time. No obvious anomalies can be observed.

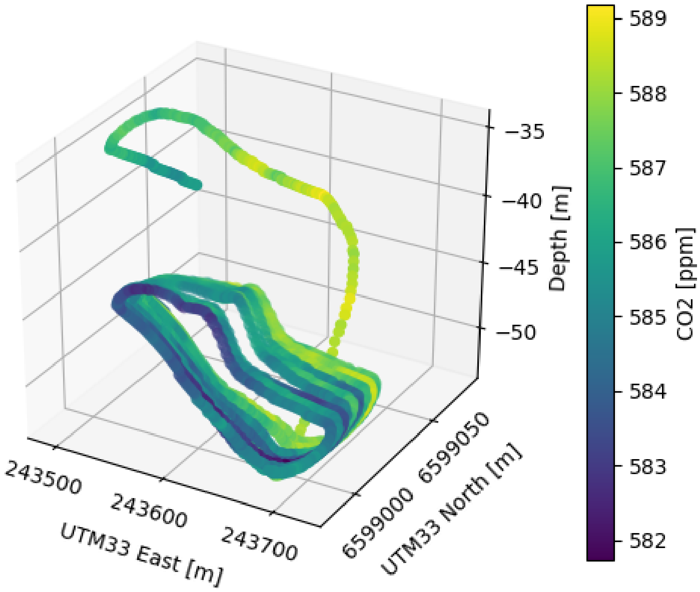

Figure 8-9 CO_2 measured using the Franatech sensor at a water depth of 50 meters, in the time interval 15:00 to 15:40, local time. No obvious anomalies can be seen.

The Ocean Seven Idronaut pH sensor and the CONTROS HydroFlash O_2 sensors are not based on headspace equilibration by means of a semi-permeable membrane, and display a faster response time than the CO_2 sensors. This is illustrated by Figure 8-12, which shows the sensor responses as the HUGIN AUV moved from 20 m depth to 30 m depth. This change in depth implies entering a different water mass with different water chemistry. In particular, we observe that the CO_2 content increases with water depth, while the O_2 content as well as the pH level decreases correpondingly. This is as expected, since the production of O_2 is higher near the surface. The O_2 and pH sensors respond almost instantaneously, while the CO_2 sensor takes some time (~10 minutes) to stabilize. A direct implication of this is that a pH sensor may be an efficient proxy or supplement for a CO_2 sensor when used on a moving platform.

The CO_2 response times for the Franatech CO_2 and CONTROS HydroC CO_2 sensors are in the order of minutes with the CONTROS sensor indicating a slightly faster response behavior (Figure 8-10 and Figure 8-11). This comparison is qualitative at this stage, and a dedicated laboratory experiment with known water chemistry would be needed in order to quantify this difference.

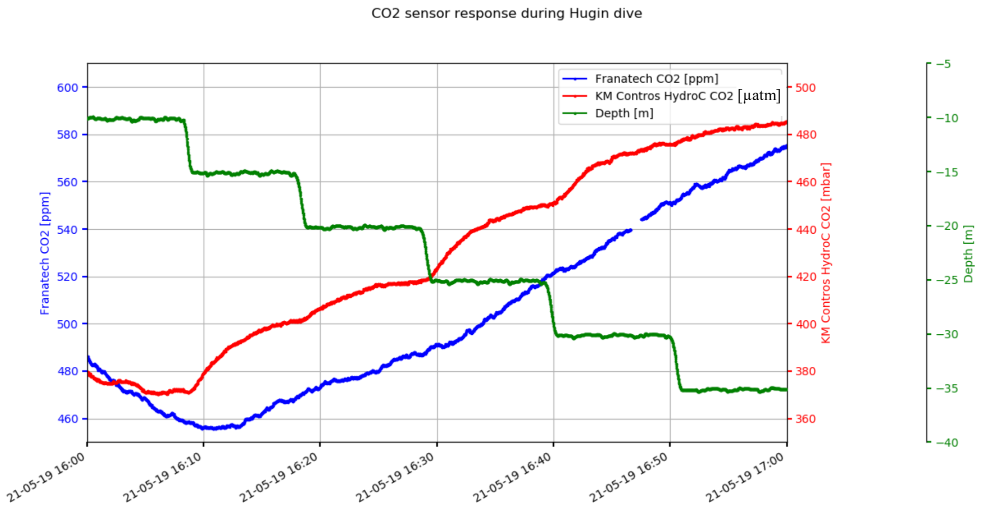

Figure 8-10 Sensor signals resulting from step changes in water depth for the Franatech CO_2 and CONTROS HydroC sensors. Both sensors respond in a similar manner, showing increased levels of CO_2 as water depth increases.

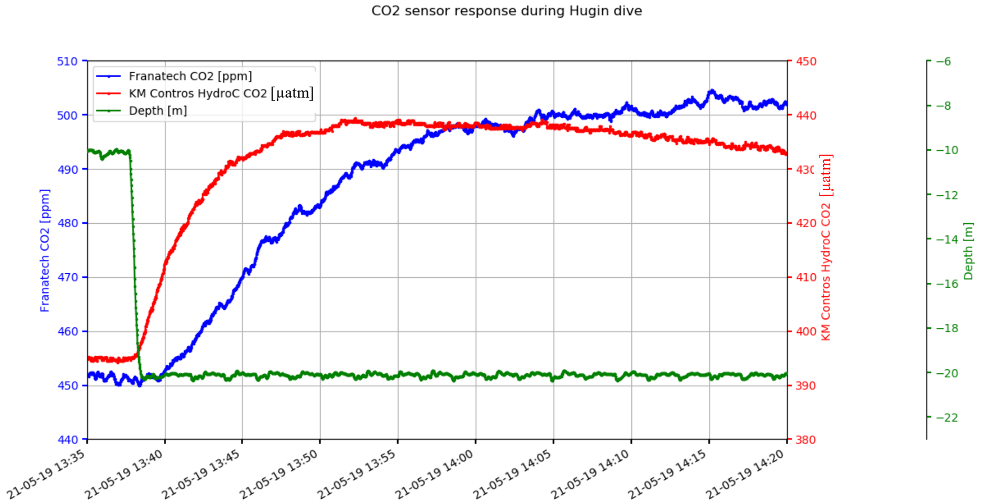

Figure 8-11 CO_2 sensor response for the CONTROS HydroC and Franatech CO_2 sensors, as the HUIGN AUV dives from 10 m water depth to 20 m water depth

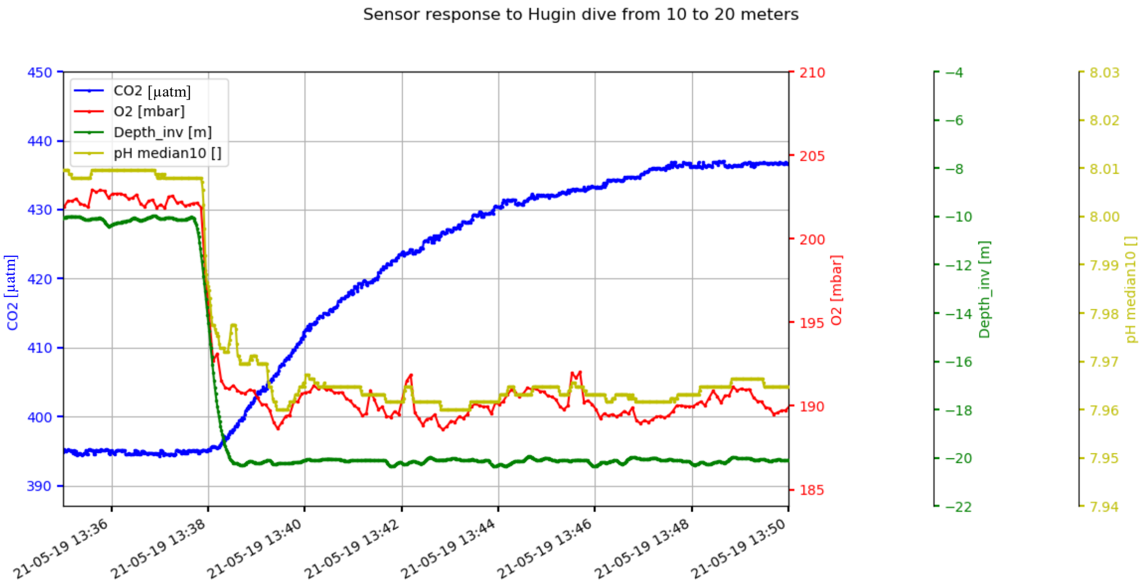

Figure 8-12 Sensor response times observed when the HUGIN AUV moved from 10 m below the surface to 20 m below the surface. The change in depth implies a change in the O_2, pH and CO_2 concentrations naturally present in the water. We observe that the O_2 and pH sensors respond nearly instantaneously to a change in water depth (green curve), while a membrane-based CO_2 sensor (here the CONTROS HydroC) requires some time to reach equilibrium.

Figure 8-13 shows the pH measured using the Idronaut Ocean seven sensor mounted on the HUGIN AUV. The trend matches what we observed using the CO_2 sensors, with a lower pH near the seabed as expected. No anomalies related to the controlled release of CO_2 can be immediately observed, but this is related to the fact that the natural vertical variations are much larger than the anomalies induced by our experiment.

By evaluating the pH data at discrete depth intervals it is possible to extract anomalies in each layer. While we did not observe any anomalies in the CO_2 data, we consistently observe a dip in the pH measurements each time the AUV passes close to the leak frame (Figure 8-14). This anomaly is only visible in the deep water (~50m depth), indicating that the CO_2 plume in this example was restricted to the deep water due to its high density. This anomaly was observed in the afternoon, after releasing significant amounts of CO_2 in gas phase as well as dissolved phase. Figure 8-15 shows the pH measured in the same place, but in the morning after only releasing gas phase CO_2. In this case no anomaly is observable. We hypothesize that this is because the gas phase CO_2 has not had time to dissolve into the water and form a plume of dissolved CO_2 which the sensors may detect.

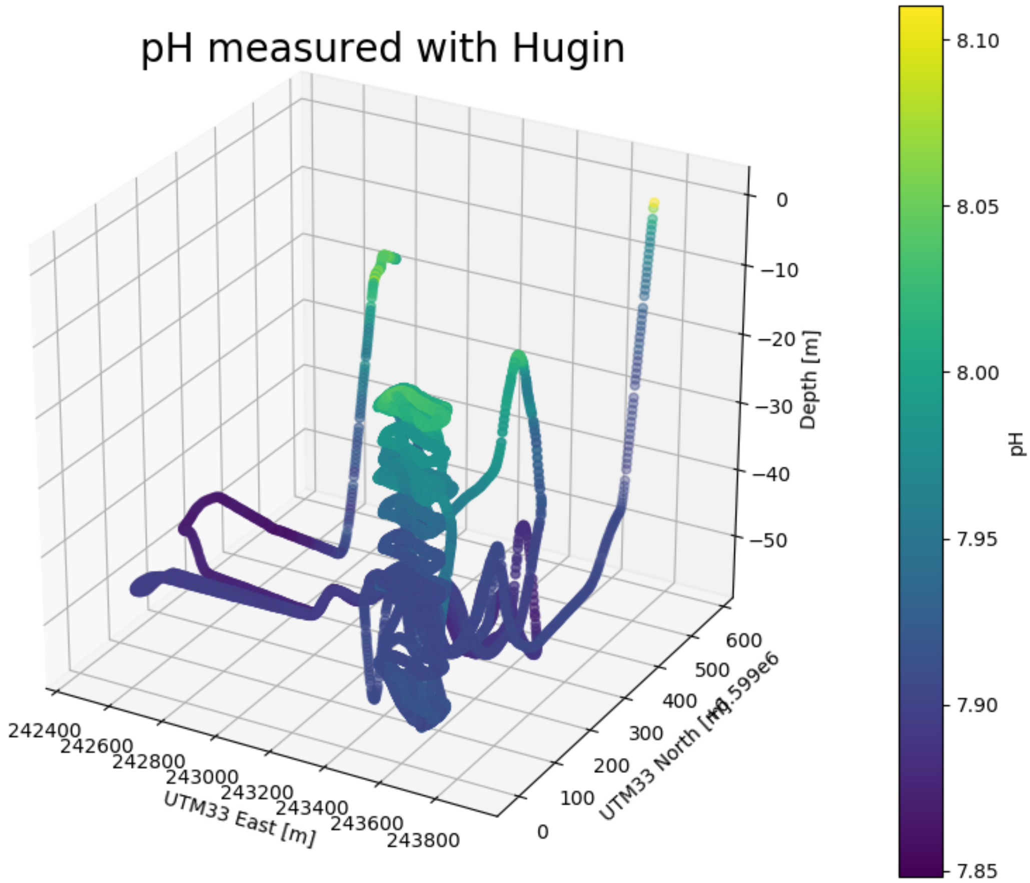

Figure 8-13 pH measured using the Idronaut Ocean Seven sensor mounted on the HUGIN AUV. A clear trend is that the pH decreases with increasing water depth, as expected. The relative differences in pH over this depth interval are larger than the expected variations introduced through our controlled release experiment, making it difficult to identify a CO_2 leak using the entire data set.

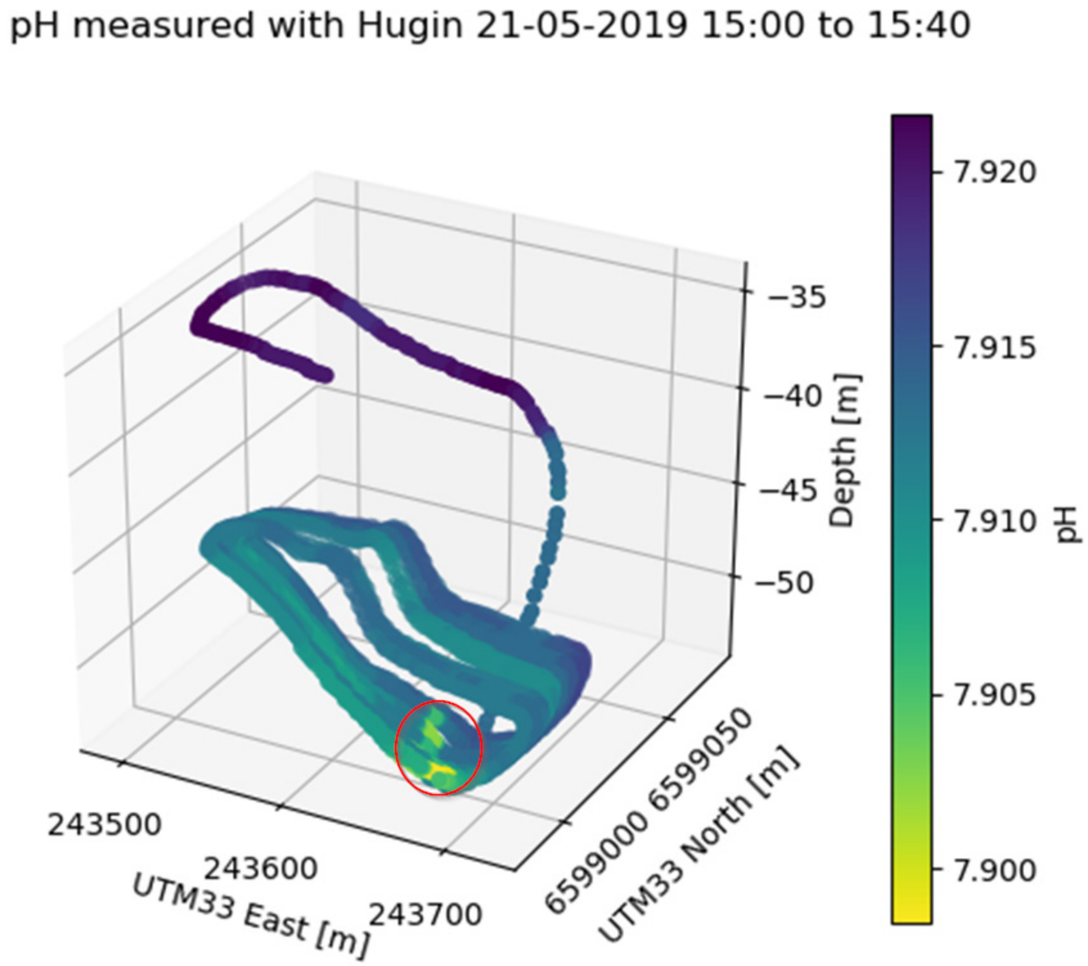

Figure 8-14 After an extended period (~3 hours) of controlled CO_2 release, a small but consistent decrease in measured pH is observed near the leak frame in the deeper water layers (~50m). The anomaly is indicated by the red ellipse. Since the decrease in pH is small relative to the natural variations vertically in the water column, this anomaly is only visible when isolating a single depth layer in the data and looking for variations within that layer.

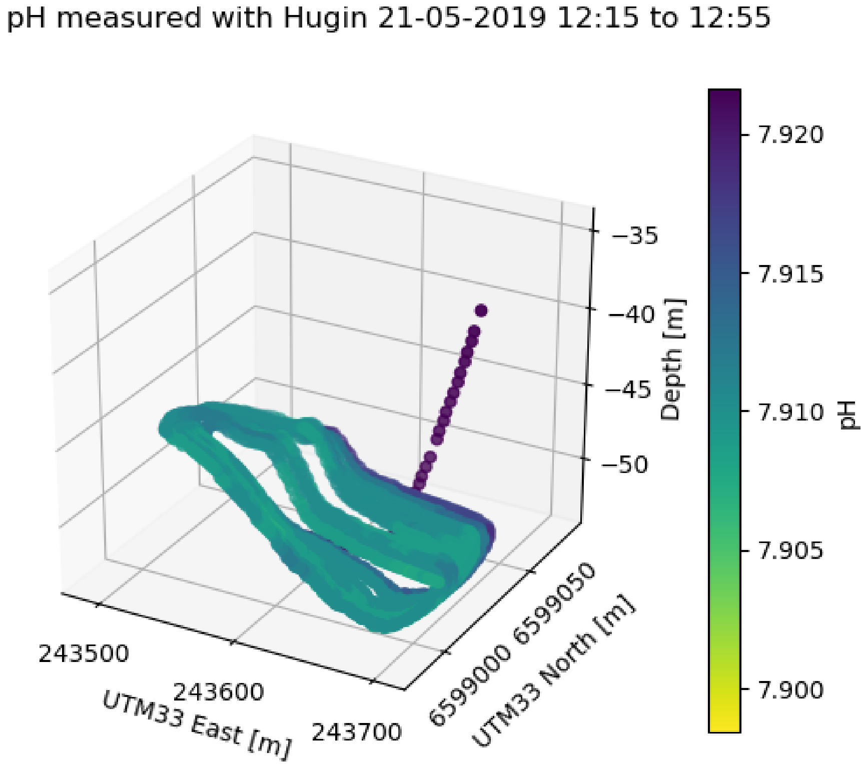

Figure 8-15 No anomaly was visible in the morning, releasing CO_2 in gas phase only

8.1.1 Potential post processing

In some cases, especially the pCO_2 data may benefit from dedicated post processing to increase the ability to detect short-term (or spatially limited) events. In particular, a response time correction (RTC) procedure has been proposed for detection of short-term signals using the CONTROS HydroC sensor[19]. As discussed above, we did not detect any anomalous CO_2 measurements in the raw CO_2 data from the HUGIN AUV. However, after dedicated RTC processing by the CONTROS team on the entire data set, we observe anomalies which align reasonably well with the observed dips in pH. Figure 8-16 shows a time-series plot of the measured pH (blue curve), pCO_2 (red curve), and RTC-corrected pCO_2 (green curve) over a 40-minute period during which the HUGIN AUV was circling above the leak frame at 50 m water depth. Each time the AUV passed directly above (or close to) the leak frame is indicated by a red arrow. While the pH sensor shows reduced pH at each of the 9 passes above the leak frame, the RTC corrected CO_2 data shows corresponding high values at 6-8 of the passes, and the non-corrected pCO_2 data is unable to register any leak events. The RTC-corrected CO_2 data appears slightly noisier after this processing step.

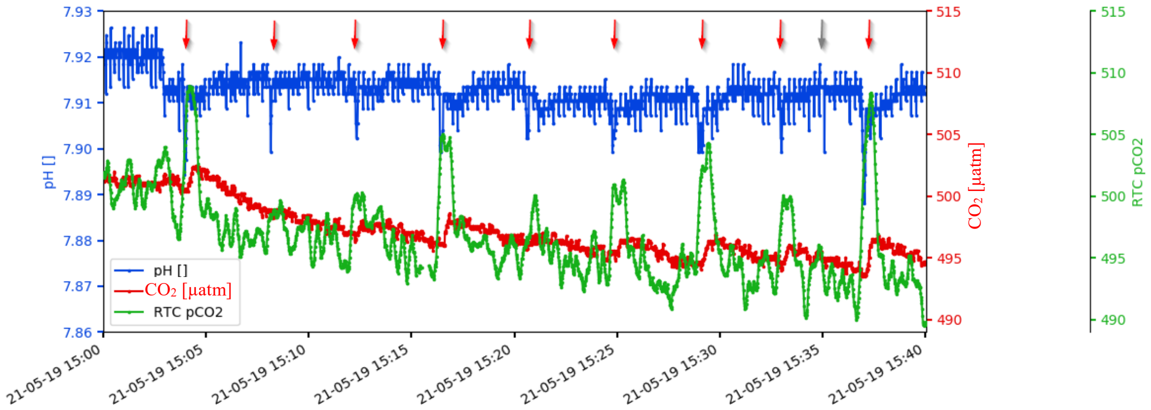

Figure 8-16: When traveling in a lawnmower pattern as in Figure 8-4, the AUV passes through the simulated CO_2 plume at regular intervals. This figure shows the measured pH (blue curve), pCO_2 measured using the CONTROS HydroC (red curve), and RTC corrected pCO_2 (green curve), over the same 40-minute period as in Figure 8-14. During this time, the AUV is at a constant depth of 50 m and passes the leak frame 9 times. Each pass above the leak frame is indicated by a red arrow. We observe a consistent dip in the pH measurements each time the AUV passes the CO_2 plume. The grey area represents a single sample in the pH measurements, potentially related to noise. The non-corrected pCO_2 measurements (red curve) do not register any leak events, while the RTC-corrected pCO_2 measurements show elevated pCO_2 levels during 6-8 of these passes.

8.2 Acoustic sensor response

While a range of acoustic sensors can be integrated on the HUGIN AUV, the chemical sensors required many of the available physical connectors on the AUV. Therefore, only one acoustic sensor was included during this experiment, the Kongsberg HISAS 1032 interferometric high-resolution synthetic aperture sonar. The HISAS is unique in that it offers high resolution imaging and bathymetric mapping of the seabed, at 4 cm resolution independent of range. Small-scale features on the seabed including bacterial mats related to fluid flow can be documented. This system has also been used previously to detect methane seepage from an abandoned well[20].

A synthetic aperture sonar (SAS) offers range-independent and significantly higher image resolution than a traditional side scan sonar, enabling detection and characterization of centimeter-scale features on the seabed. The basic imaging principle is illustrated by Figure 8-17. By combining multiple along-track pings, a very long receiver array is synthesized, resulting in significantly improved angular resolution [21]. This imaging technique requires accurate micro-navigation of the AUV at millimeter-scales.

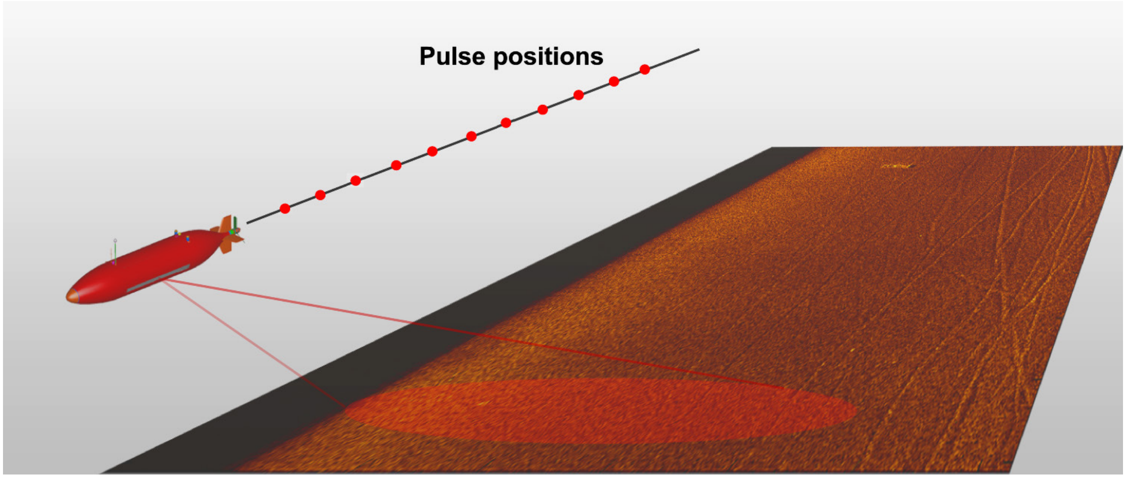

Figure 8-17 SAS principle: by combining multiple executive pings along the AAUV's travel path, a very long receiver array can be synthesized. This results in high-resolution imagery, and an angular resolution which is independent of range. Image credit FFI.

Figure 8-18 shows an example HISAS image of a portion of the seabed acquired during the 2019 nearshore experiment. The leak frame as well as Template A is visible in the image. No CO_2 was released at this time. This image was formed using standard "out of the box" processing in the FOCUS software package. Another example image with a different viewing angle is shown in Figure 8-19. Further image enhancement and dedicated post processing may be performed to enhance objects of interest including gas plumes.

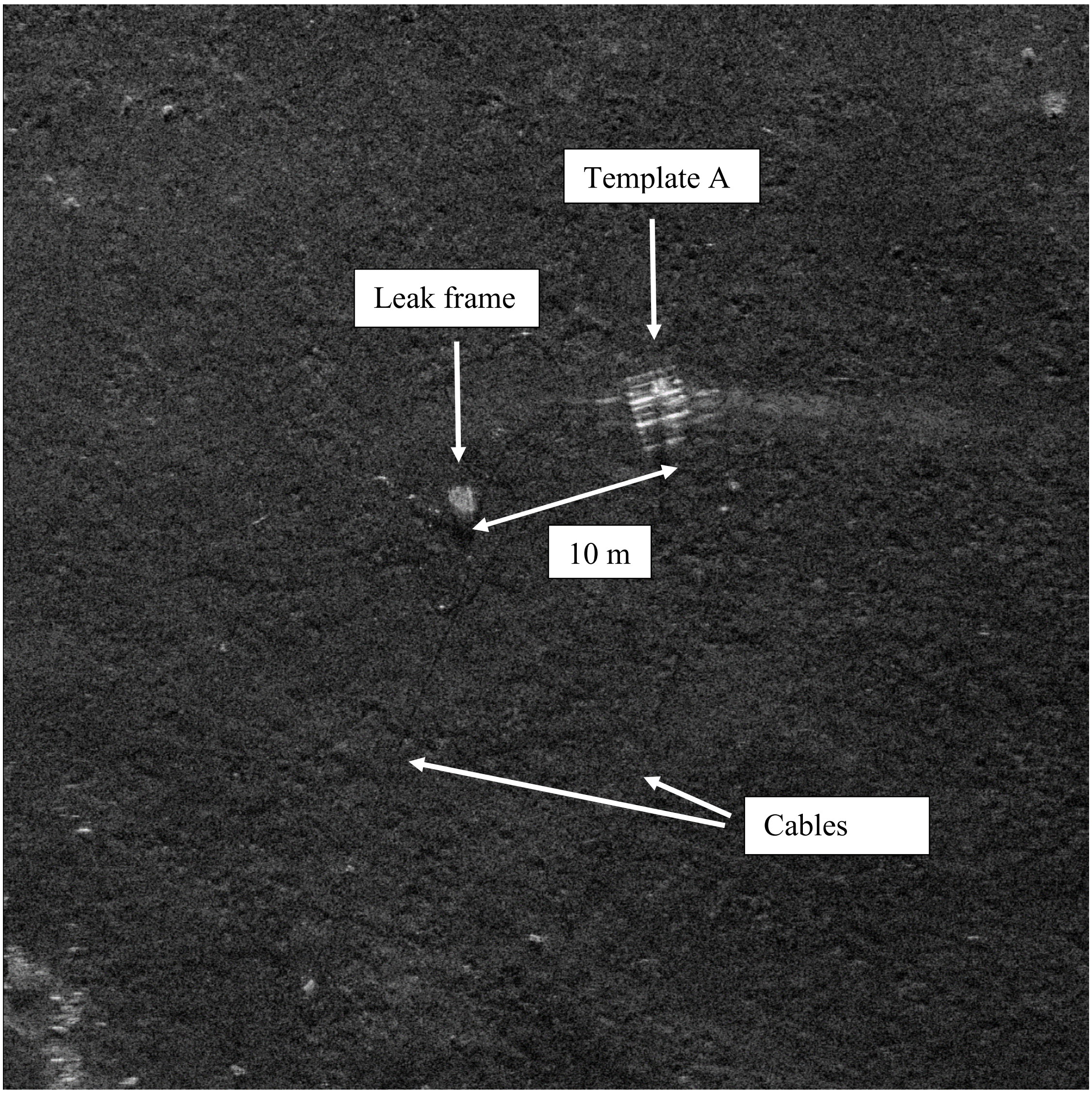

Figure 8-18 HISAS image of the seabed including the leak frame and Template A. This image has a 4 X 4 cm resolution. Notice that cables and hoses on the seabed are visible in the image.

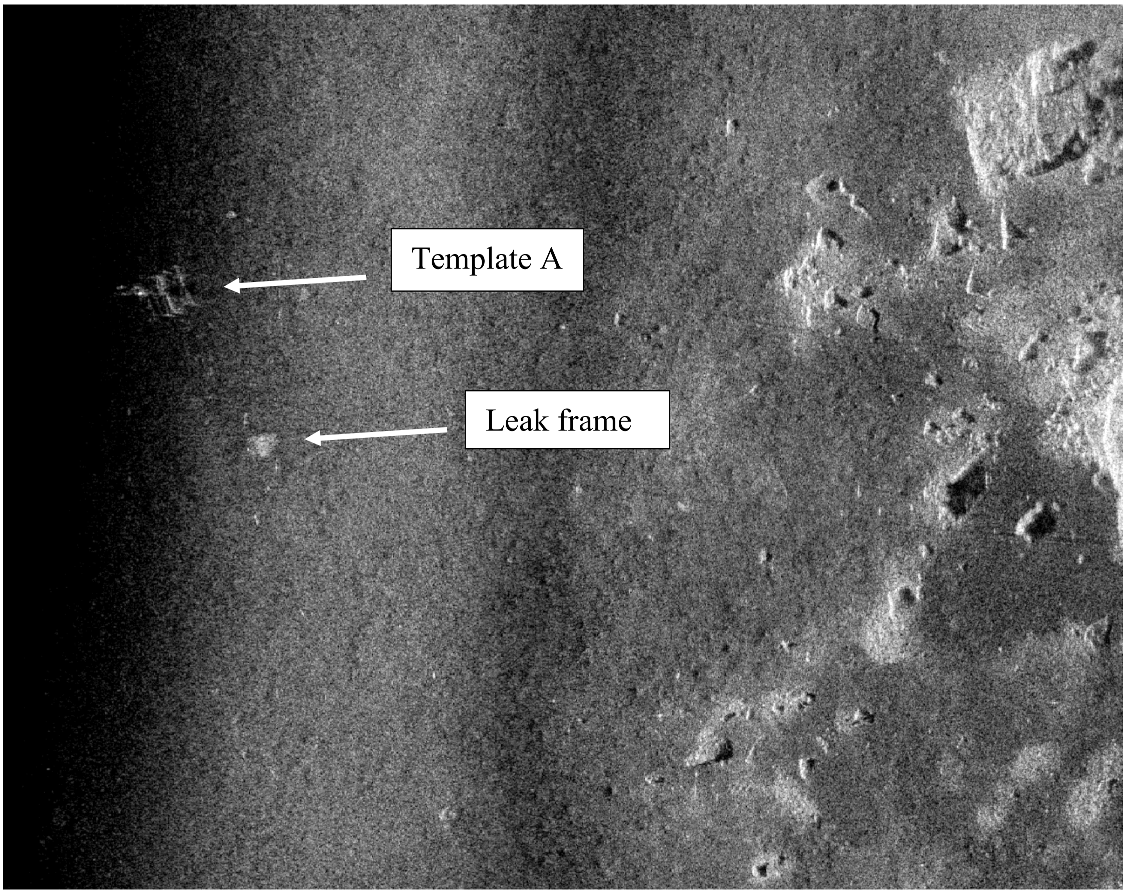

Figure 8-19 HISAS image of the seabed including the leak frame and Template A at close range.

We observe that gaseous CO_2 is nicely documented using the HISAS sonar. The ability to image the bubbles, however, depends on the imaging geometry. Figure 8-20 shows an example image when gaseous CO_2 was released at a relatively high flow rate (~35 l/min), and the AUV was passing at a ground distance of 50 m from the leak frame, at a height of 50 m above the seabed. We clearly observe the gas plume as a long, "plume-like" region of high intensity in the image. The plume is also clearly visible in Figure 8-21 when the AUV passed at the same ground distance, at a height of 30 m above the seabed. Figure 8-22 shows a HISAS image obtained while releasing the same amount of CO_2, but this time the AUV passed at height of only 10 m above the seabed. In this case the CO_2 plume is not visible in the sonar image. This is due to the imaging geometry, as illustrated by Figure 8-23. Taking the sonar field of view into account, we observe that the CO_2 plume is best imaged when the AUV is traveling at a height of 30-50 m above the seabed. When the AUV s traveling near the seabed (10 m), the plume is completely missed when the distance to the plume is larger than 50 m. Based on these observations we conclude that the HISAS is useful for detecting and imaging CO_2 gas plumes, and that the imaging geometry should be considered when planning the AUV travel path.

A feasible methodology to loosen the requirements of the imaging geometry and thus increase the effective coverage rate could be to use change detection methods when surveying a known area. By comparing with previously collected data, we could identify leaks by the change in backscatter intensity even if it is mapped into a single resolution cell due to the imaging geometry.

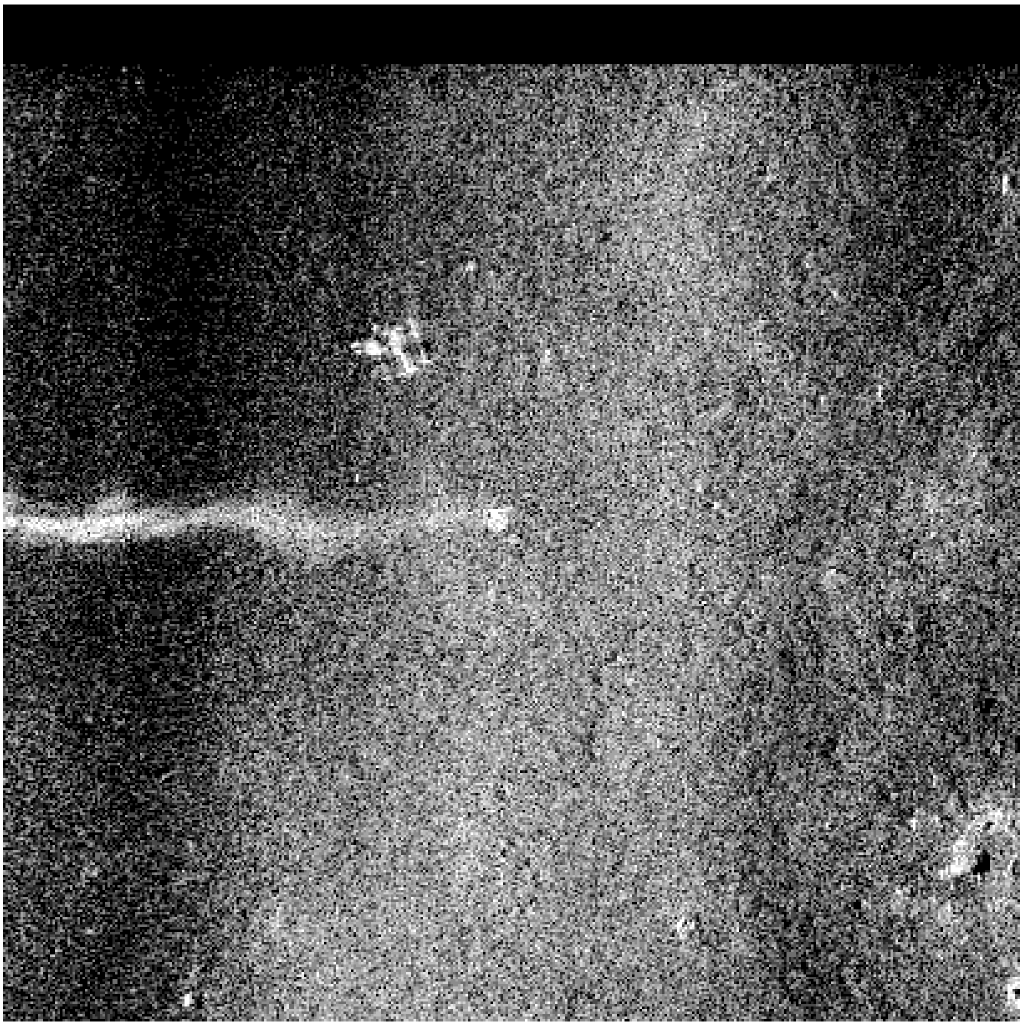

Figure 8-20 Example HISAS image showing the CO_2 gas plume. In this case the AUV travelled 50 m above the seabed.

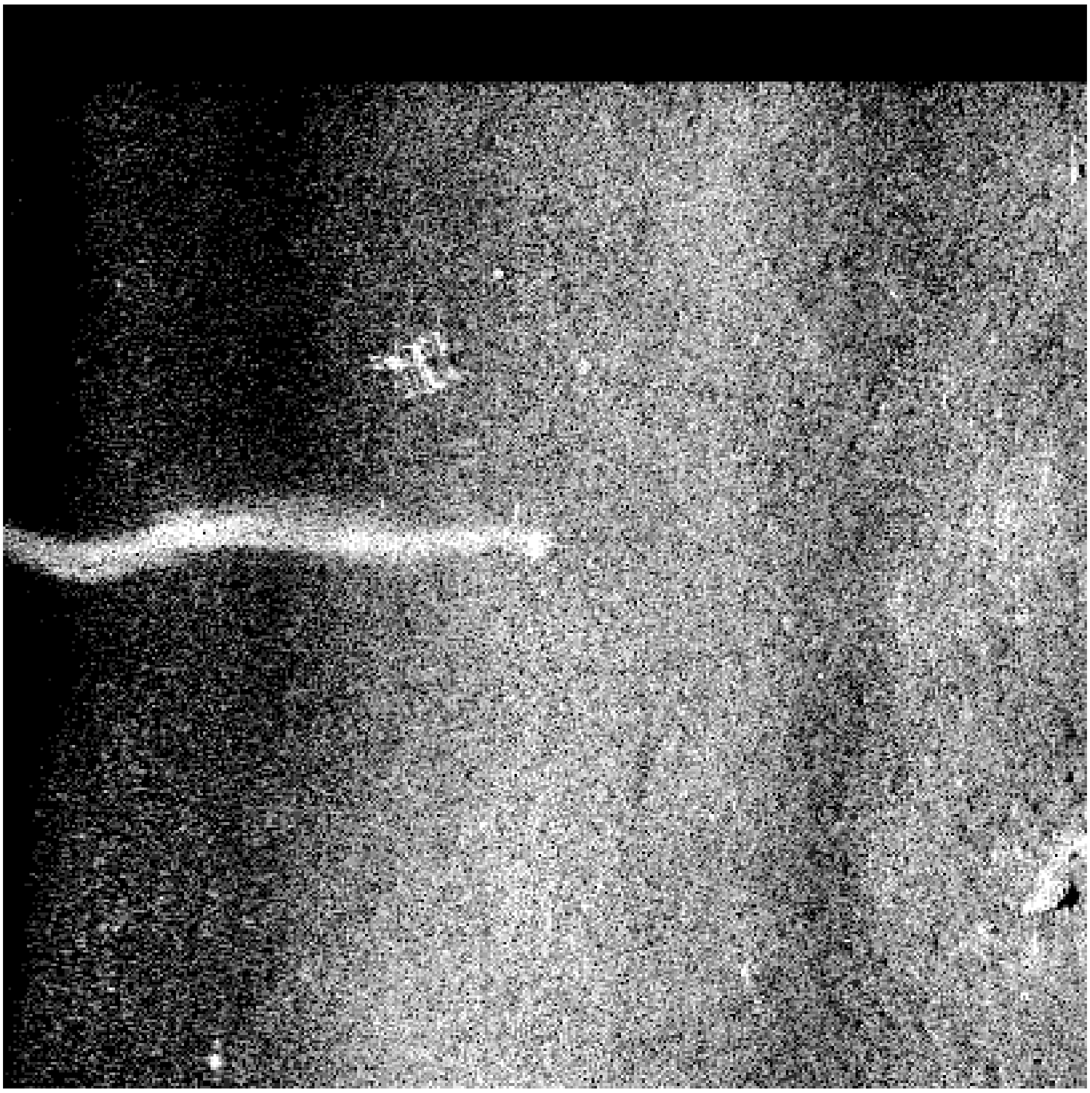

Figure 8-21 HISAS image of the CO_2 gas plume obtained when the AUV was traveling at a height of 30 m above the seabed

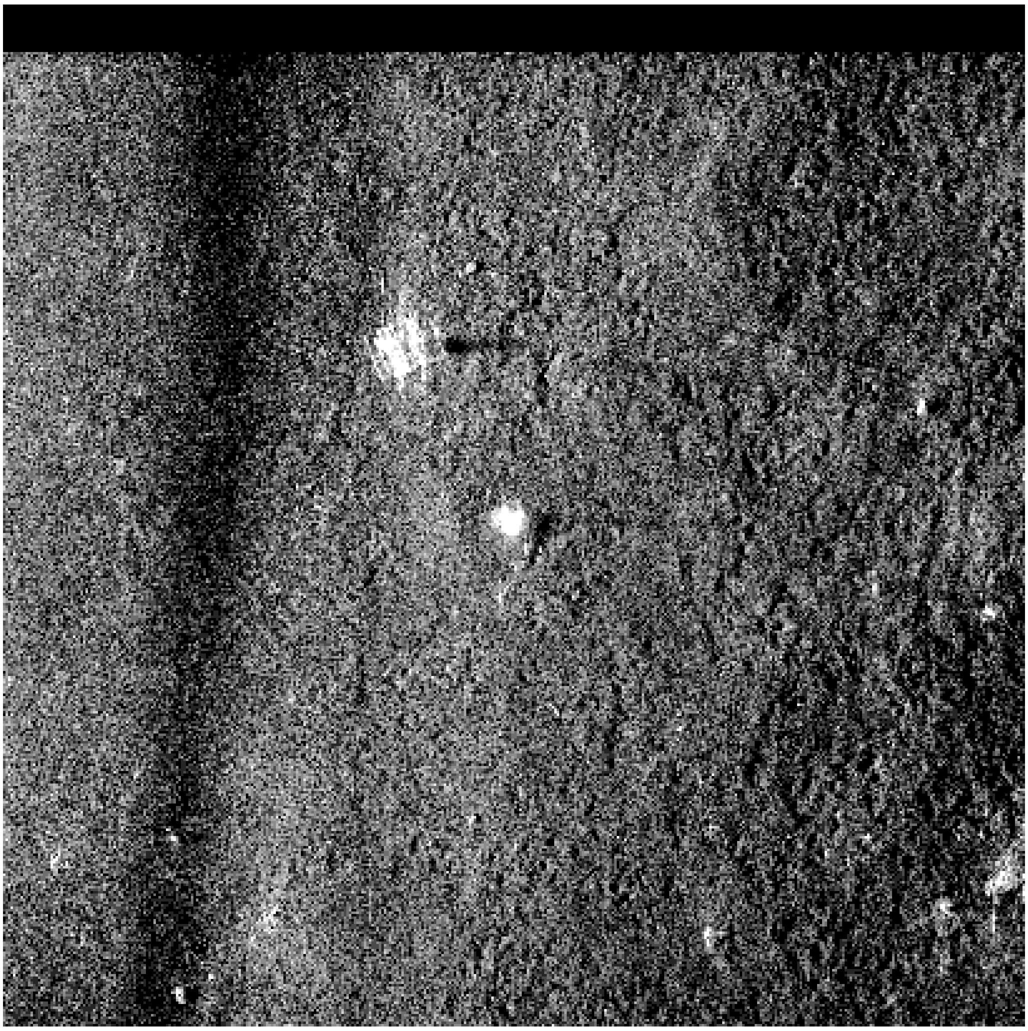

Figure 8-22 HISAS image obtained during a controlled release of gaseous CO_2, at a rate of ~35 l/min. The plume is not clearly visible in the sonar image due to the imaging geometry.

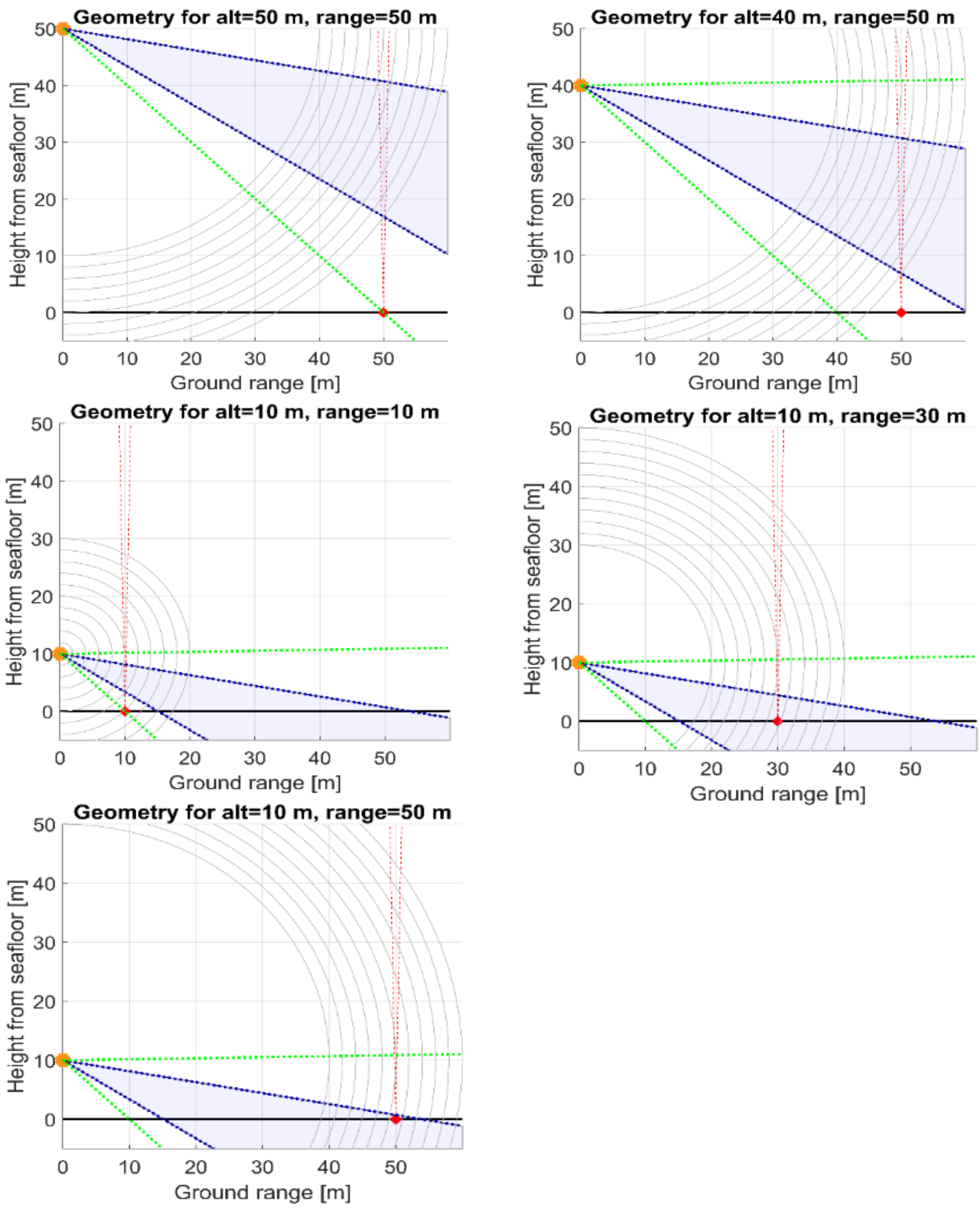

Figure 8-23 Sonar imaging geometry. The sonar's field of view is limited by the vertical opening angle of 23 degrees for the half value indicated by the dotted, blue line and shaded area. The full beam all the way to the first zero value is about 46 degrees, indicated here by the dotted green lines. The orange dot indicates the sonar position, and the red dot indicates the source of the gas seep on the seafloor. A potential CO_2 plume is indicated by the dotted, red lines. A plume is best imaged with a more vertical geometry, e.g. from a height of 40-50 m above the seabed. When traveling at 10 m above the seabed most of the swath has low grazing angles, and much of the plume in the water column is missed and it will not have a large extent in the sonar image. This makes it difficult to distinguish from an object on the seafloor that also has strong backscatter intensity.

9 Response to controlled release experiments – SeaExplorer

In this section we present results from the Pro-Oceanus Mini-CO2 sensor mounted on the SeaExplorer glider. The sampling rate of the sensor was fixed to be 0.5Hz. The first descent profile of a given dive was systematically discarded because the CO_2 sensor has not had time to stabilize, resulting in unrealistically low CO_2 values (similarl to the HUGIN-based measurements). Comparison of pCO_2 and O_2 time-series also highlighted a lag in the sensor response around 240s (4min). Adjusted CO_2 values were thus calculated as follow:

$$[CO_2]_{adjusted}(t) = [CO_2](t + 240) \quad (2)$$

A constant time-lag correction was applied because temperature variations in the survey area were limited to few a degrees.

Figure 9-1 shows that the glider was able to monitor the natural variability of pCO_2 vertical distribution, and strong changes were observed during the glider's mission. Two different situations can be distinguished:

- **Period 1**: Corresponds to the navigation test and the two first days of the glider's mission (from May 11th to May 14th, 2019 AM). During these periods, pCO_2 was generally higher than 400 µatm and constant over depth (in blue, Fig. 1a).
- **Period 2**: Corresponds to the two-last days of the glider's mission (from May 14th, 2019 PM to May 16th, 2019, AM). During this period, pCO_2 was generally lower than 400 µatm and increasing with depth (in red Figure 9-1a).

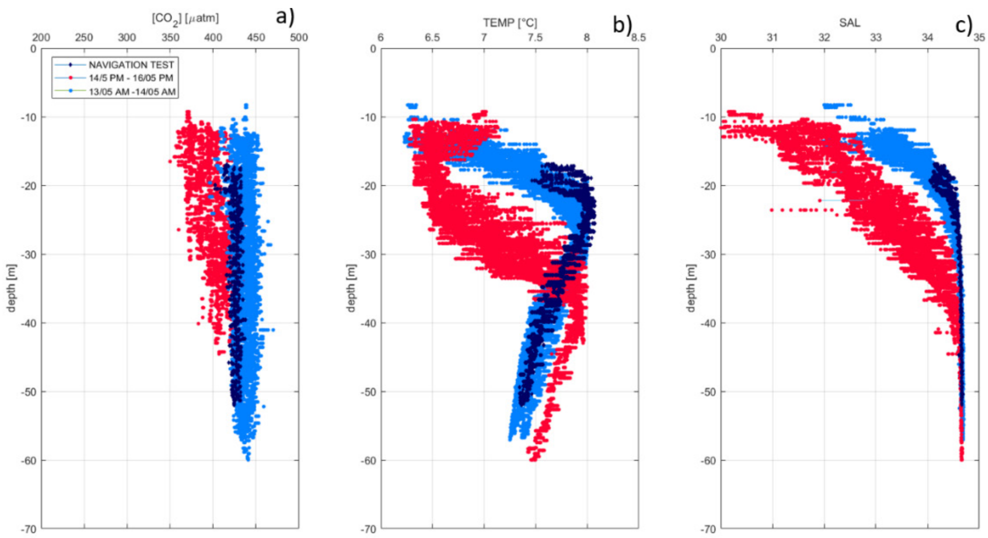

Figure 9-1 a) Adjusted [CO_2] vertical profiles, b) temperature vertical profiles, c) salinity vertical profiles. Dark blue dots correspond to data acquired during the navigation test, red dots to data acquired during period 2 and light blue to data acquired during period 2.

Interestingly, these two situations were associated with very different temperature and salinity vertical distributions corresponding to different water-masses. Main changes are observed in the intermediate layer (10-40m).

No obvious anomalies related to the controlled leak experiment are visible in the data. This agrees with our findings, including the experiments carried out with the HUGIN AUV. A membrane-based CO_2 sensor may not have time to detect a CO_2 plume with limited spatial extent (a few tens of meters) since the glider passes through the plume in a matter of seconds. No direct comparison can be made because of the different travel paths of the AUV and the glider, and the fact different CO_2 sensors were used. ALSEAMAR together with Pro-Oceanus teams are still working on the dataset to assess to which extent a dedicated algorithm can help anomalies detections.

The strong density gradient at this site was also very high, making glider navigation challenging and the data acquisition suboptimal. It should be stressed that such strong density gradients are not expected in most relevant CCS storage sites.

Figure 9-2 AlSeamar personnel preparing to deploy the SeaExplorer at Østøya

Finally, the SeaExplorer is one of several gliders on the market, and this is a field in rapid development. For example, the SeaGlider C2 manufactured by Kongsberg is specifically designed for shallow water operations.

10 Response to controlled release experiments – Simrad Echo R/V

The active acoustic sensors used on the Simrad Echo nicely document the shape, intensity and spatial development of the plume of CO_2 bubbles. We consistently observe CO_2 bubbles rising at least 25 m above the leak point at the seabed, even for small leak rates (0.125 l/min). An important factor is the imaging geometry of the different systems

(Figure 10-1). In some cases, the top of the plume is missed because the vessel is not directly above the plume. This may result in an underestimation of the plume height. In this section we present observations of CO_2 and air release using a single beam echo sounder (SBES), and several different multibeam echo sounders (MBES). More information about the different sensors is available at https://www.simrad.com and https://www.kongsberg.com.

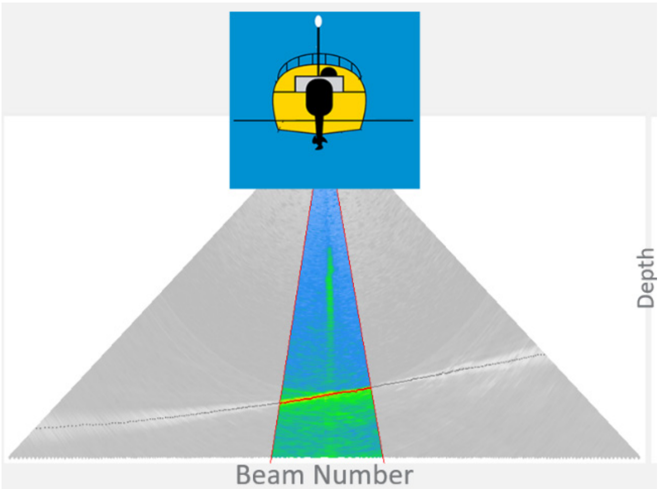

Figure 10-1 Example MBES image of the CO_2 plume, with the centre beam in colour and the outer beams in grey. In this case the plume is located within the centre beam. Note that the beam width is narrow at the top, making it easy to "lose" the plume if it drifts slightly due to currents, or if the vessel is not placed directly above the plume. Different SBES and MBES have different imaging geometries, and this has implications for the ability to detect a bubble plume close to the surface.

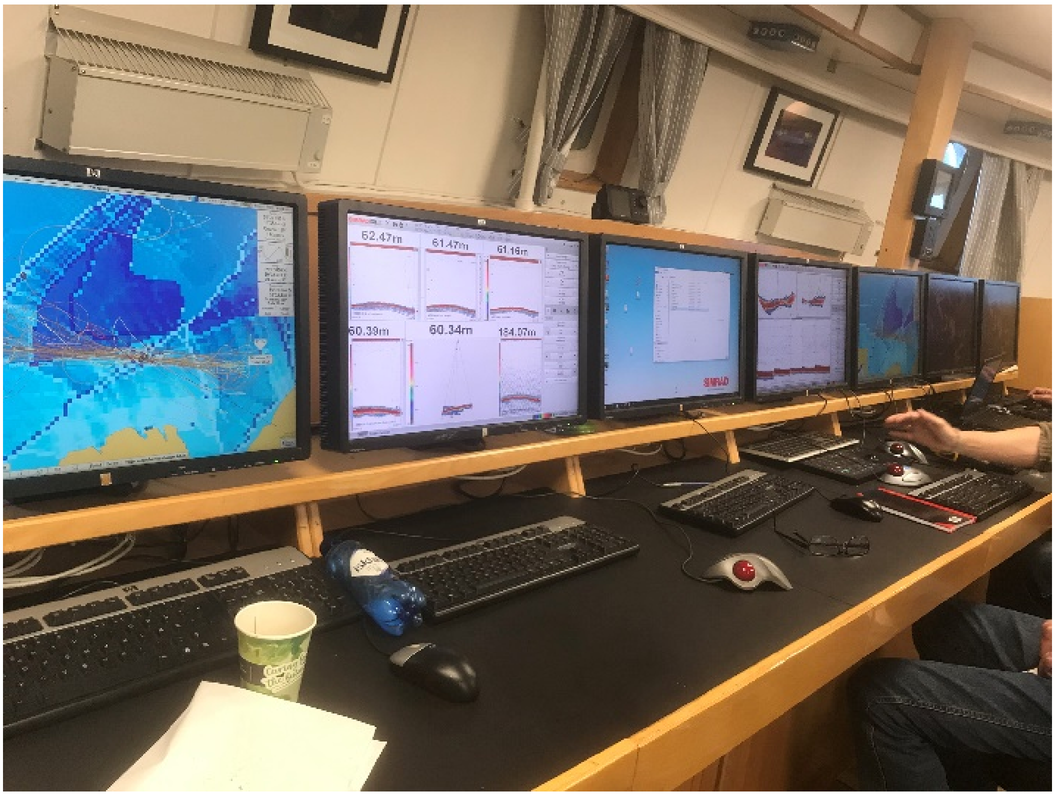

Figure 10-2 Photo from inside the Simrad Echo R/V, where Kongsberg Maritime Subsea personnel are operating several of their echo sounders

During this experiment, we performed controlled releases of CO_2 gas bubbles with varying release rates (0.125 l/min, 0.625 l/min and 1.3 l/min), and air bubbles. The acoustic response to each of these releases was mapped using the above-mentioned acoustic sensors, and the results are presented below.

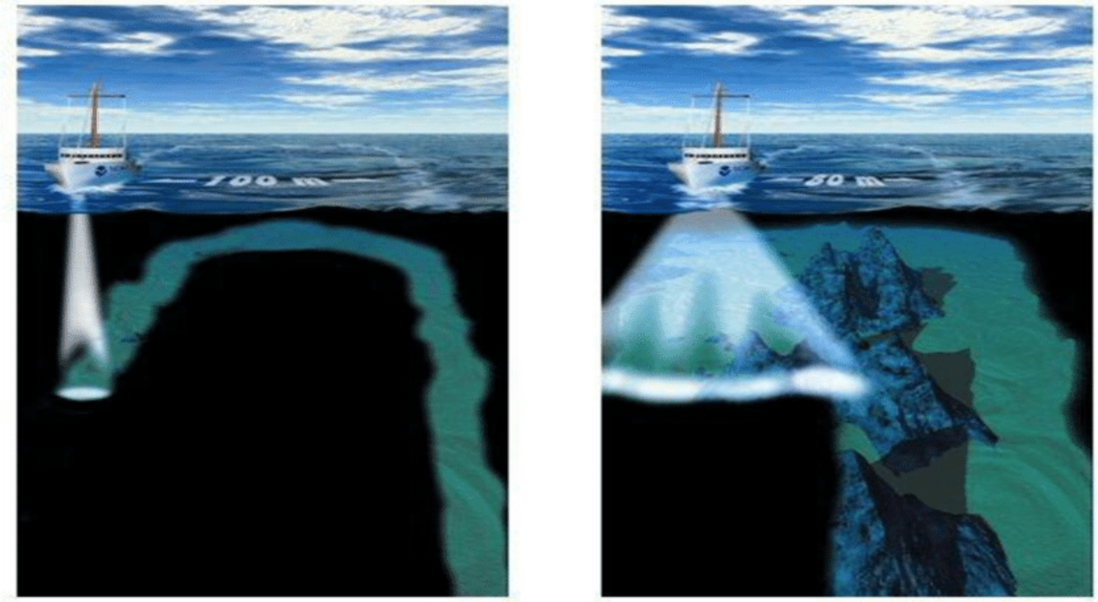

Figure 10-3 Left: a single beam echo sounder (SBES) transmits a single beam and uses the echo to map the seafloor and/or water column. Right: a multibeam echo sounder (MBES) uses multiple beams to achieve a higher area coverage rate. Image courtesy: NOAA Office of Coast Survey.

10.1.1 EK80

The EK80 is a scientific broadband SBES with very high sensitivity. It has proven capabilities when it comes to mapping and characterizing marine gas seeps. The EK80 transceiver unit can be hooked up to multiple transducers operating at different frequency ranges. The operating range depends on the transducer, with low-frequency transducers having a longer range than the high-frequency transducers. Our observations from the stationary platforms as well as when having the EK80 mounted on the hull of the Simrad Echo indicate that it can detect very small bubble releases, or analogously, larger releases at great ranges.

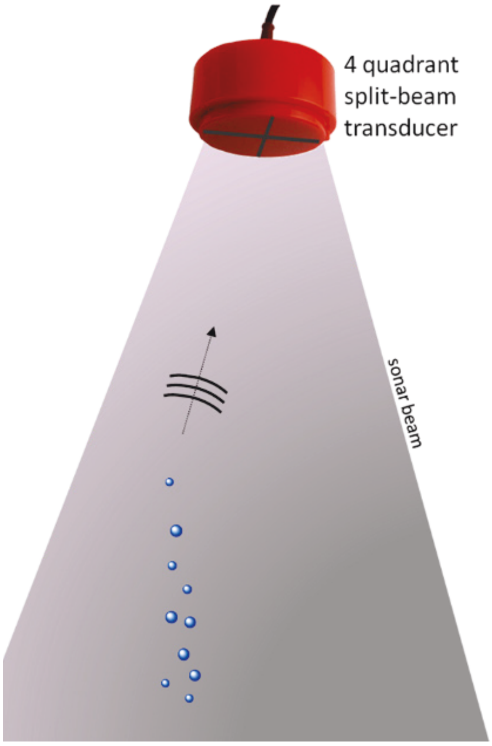

Figure 10-4 The acoustic beam of the EK80 SBES is conically shaped with approximately 7 degrees opening angle. The split beam capability makes it possible to position a target within the acoustic beam and to derive its acoustic properties. This is relevant when quantifying gas seeps acoustically.

A potential challenge when using the EK80 SBES mounted on a vessel, is the limited area coverage rate. The acoustic beam is conically shaped, with an opening angle of approximately 7 degrees (Figure 10-4). As a result, a bubble plume is easily missed, or its height underestimated unless the vessel passes directly above it. An advantage of the EK80 is that it can be calibrated, making it possible to position a target within the acoustic beam. Subsequently, target strengths can be estimated taking into account the calibrated beampattern of the system (i.e., compensating for the fact that a target in the centre of the beam will result in a stronger echo than the same target in the periphery of the beam). This process – beam pattern compensation – is important for acoustic quantification of a CO_2 leak.

The EK80 echogram in Figure 10-5 shows the multi-frequency response of 1.3 l/min CO_2 release. We observe the CO_2 plume at all frequencies, and observed rise heights are in the order of 30 m. Each rectangle represents the acoustic response centred around a frequency of (from left to right) 18 kHz, 38 kHz, 70 kHz, 120 kHz and 200 kHz.

We compare bubble rise heights and acoustic target strength of a plume of CO_2 bubbles and a corresponding plume of air bubbles. As expected, air bubbles rise higher (all the way to the surface) and display higher target strength since they dissolve at a slower rate in seawater than CO_2 bubbles.

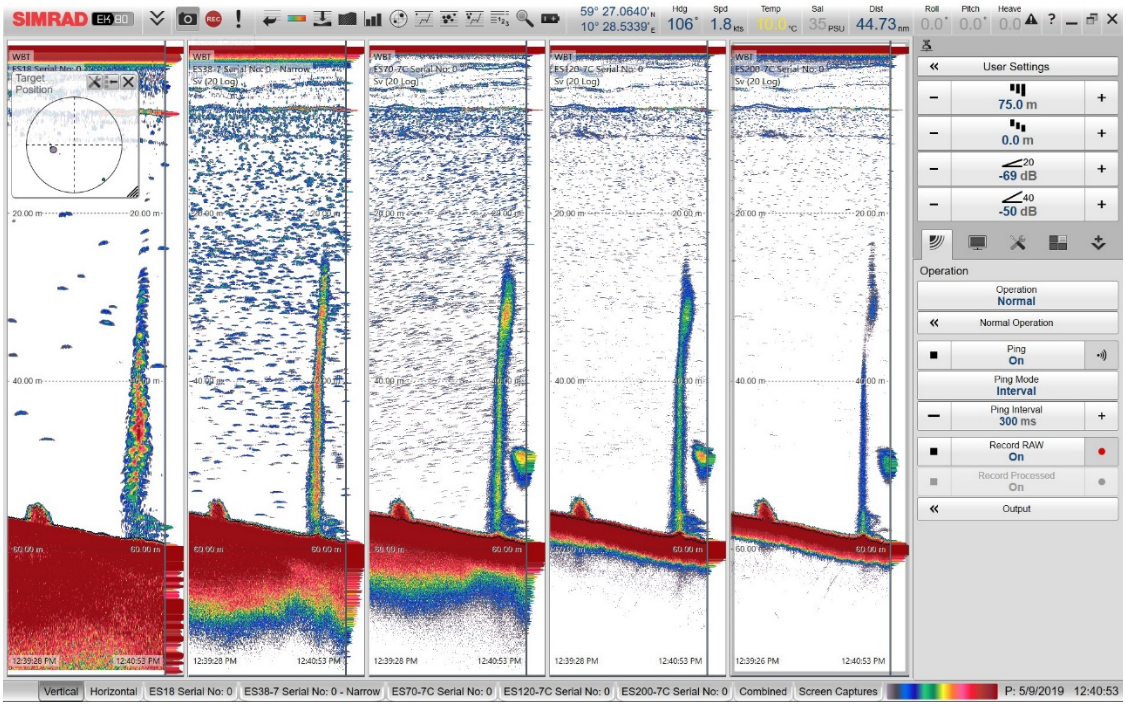

Figure 10-5 EK80 echogram visualized using the accompanying software from Simrad. Each rectangle shows the bubble plume observed using different EK80 transducers, i.e., insonified at different frequencies. Starting from the left these transducers operate at 18 kHz, 38 kHz, 70 kHz, 120 kHz, and 200 kHz. The CO_2 gas plume is visible at all frequencies, as a consistent vertical stripe with high reflectivity.

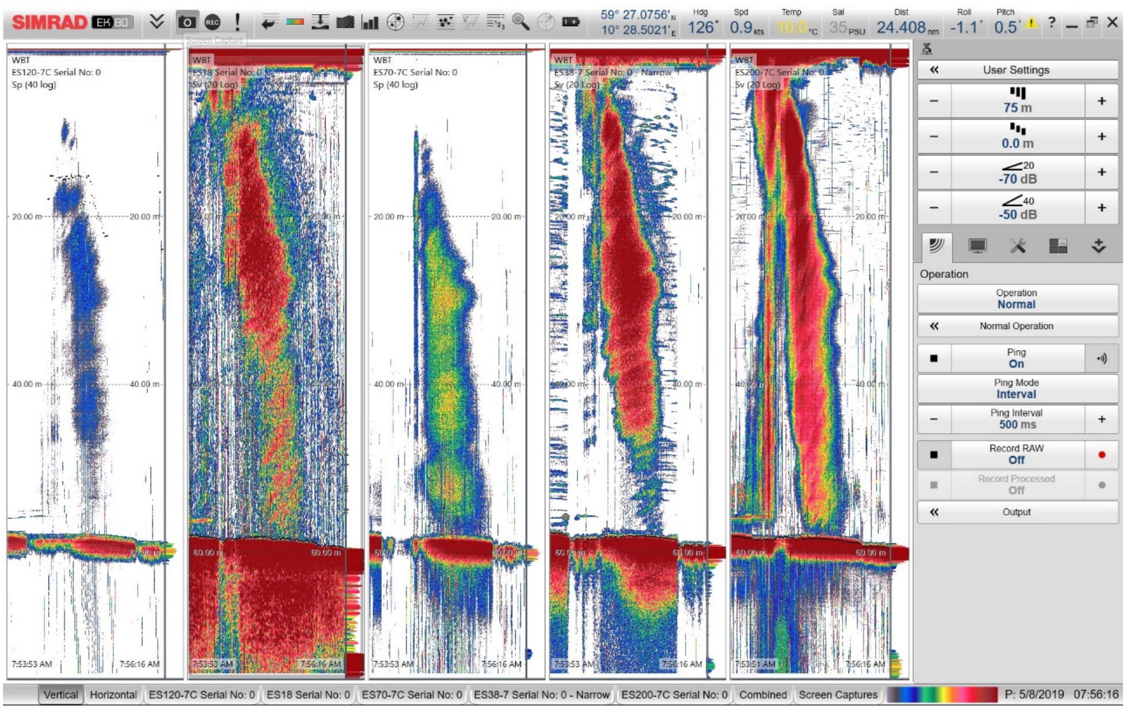

Figure 10-6 EK80 echogram during release of air bubbles. As expected, the air bubbles result in a clear "flare" shape in the echogram, reaching all the way to the surface.

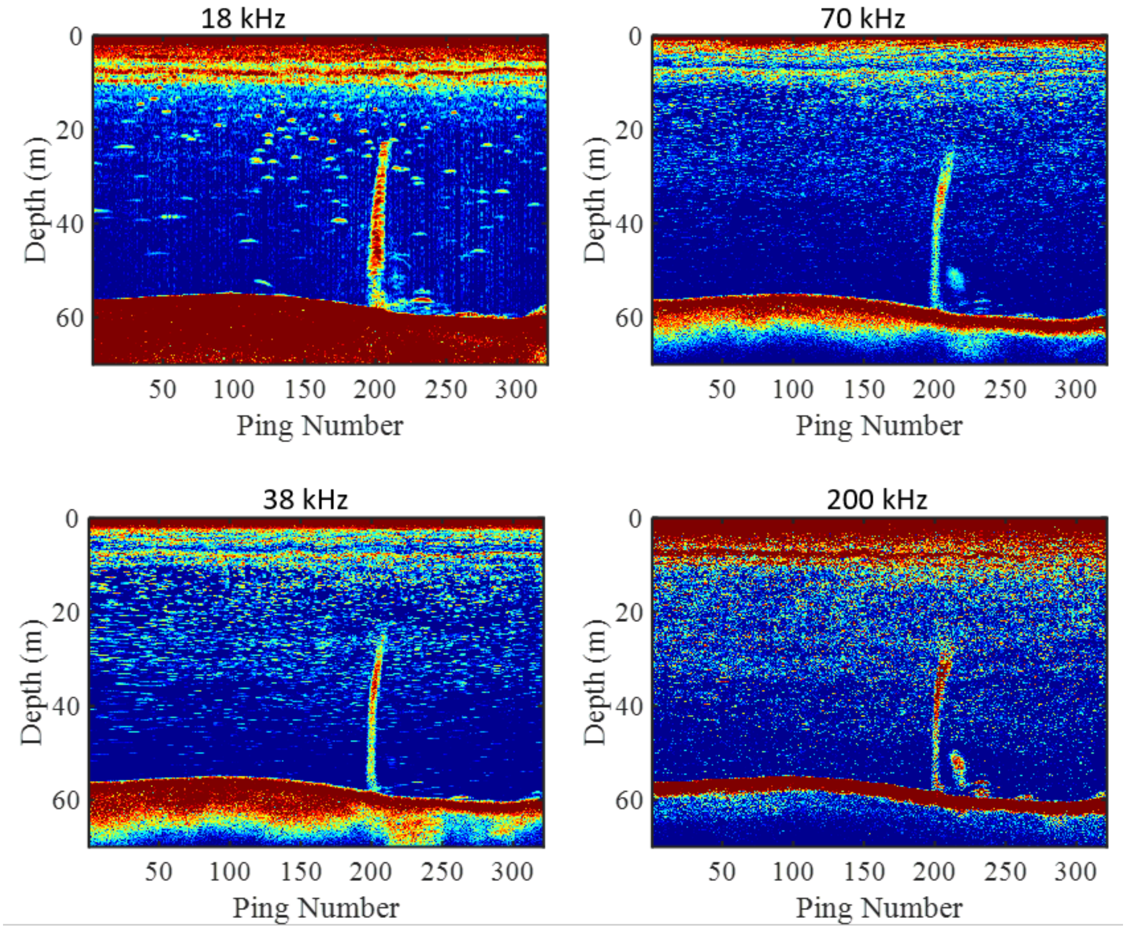

Figure 10-7 EK80 data can also readily be processed using e.g. MATLAB, as in these plots. The release rate is l/min of CO_2 in gas phase. The ability to store raw data and to post process the data makes it possible to develop and test targeted, case-specific processing algorithms. Observed bubble rise heights are at least 30 m above the release point at the seabed.

10.1.2 EM2040

The EM2040 is a wideband multibeam echo sounder (MBES) with a frequency range of 200-400 kHz. It is aimed at high-resolution seafloor mapping in relatively shallow water. The EM2040 is flexible, allowing the user to tailor beamwidths, operating frequencies, and area coverage to their needs. The maximum swath size is 200 degrees.

Figure 10-8 shows the CO_2 plume imaged using the EM2040 MBES. The current release rate is 1.3 l/min, and we observe bubble rise heights around 30 m above the seabed. This image is in "stacked view", processed using the Fledermaus software package.

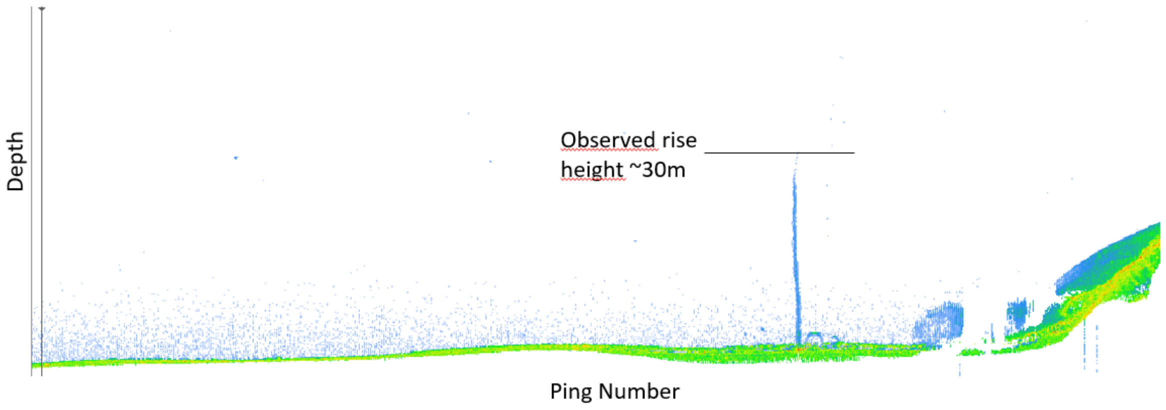

Figure 10-8 Example of a "stacked view" of data from the EM2040 multibeam echo sounder. The data has been processed using the Fledermaus toolbox. The seep is visible with an observed bubble rise height of approximately 30 m. The release rate is 1.3 l/min CO_2 in gas phase.

10.1.3 EM712

The Kongsberg EM712 MBES is a high-resolution echo sounder with an operating frequency range of 40 – 400 kHz. The maximum acquisition depth is 3500 m, with an across-track area coverage of 5.5 times the water depth. Figure 10-9 shows the EM712 data during a single pass above a CO_2 plume with a release rate of 0.625 l/min. The upper plot shows an overview of the local bathymetry, with the field of view of the current ping highlighted. The lower plot shows the current ping in "swath mode", i.e., showing echoes from the 200 degrees field of view.

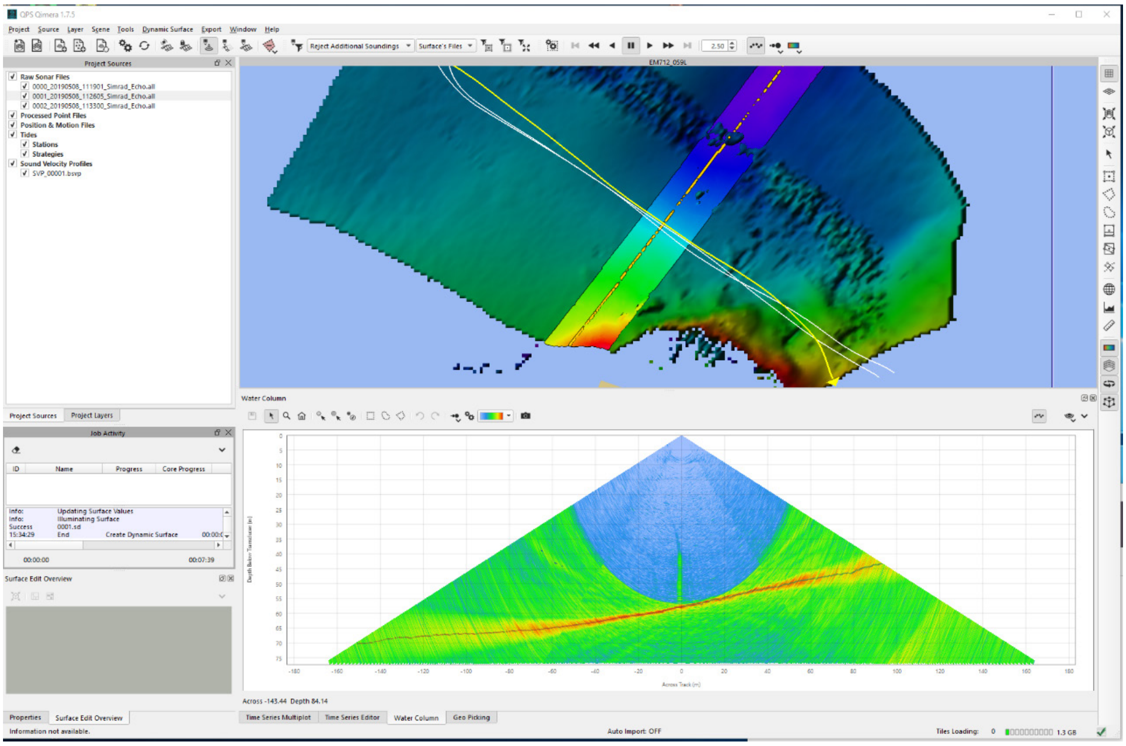

Figure 10-9 Multibeam (EM712) image showing the CO_2 plume. The upper plot shows the local bathymetry, and the field of view for the current ping. The lower plot shows the echoes present from the current ping, spanning a 200-degree sector. The current release rate is 0.625 l/min.

Figure 10-10 and Figure 10-11 show EM712 data in stacked view of a 0.625 l/min of gas phase CO_2, and air bubbles, respectively. As expected, the air bubbles result in stronger echoes reaching all the way to the surface. This is due to the comparably fast dissolution rate of gaseous CO_2 in seawater.

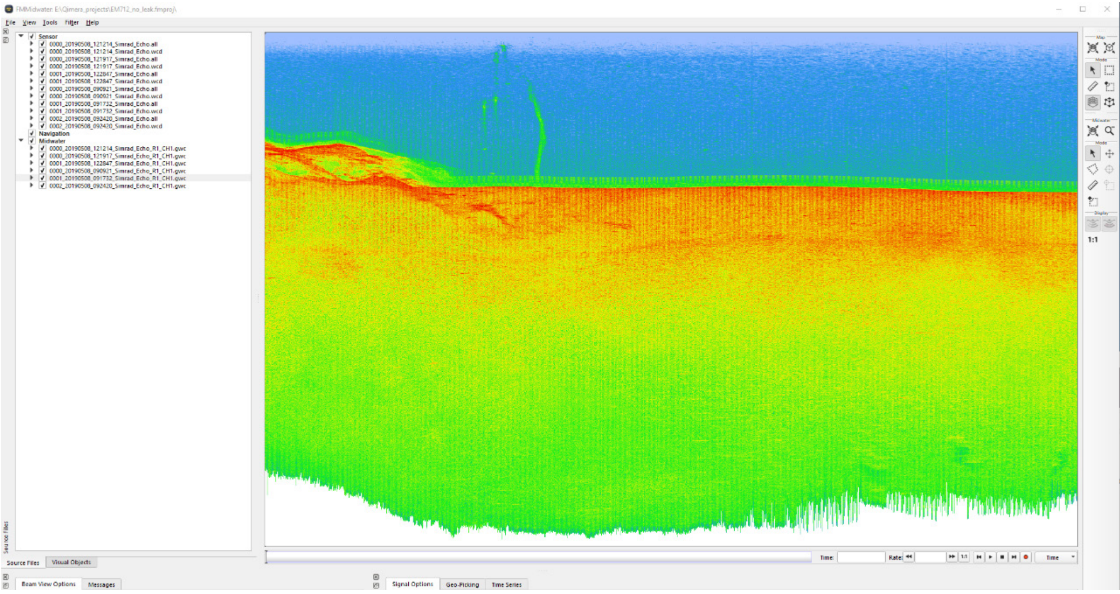

Figure 10-10 This image shows a "stacked view" of the EM712 multibeam data, while releasing 0.625 l/min gaseous CO_2. Again, observed bubble rise heights are approximately 30 m above the release point at the seabed.

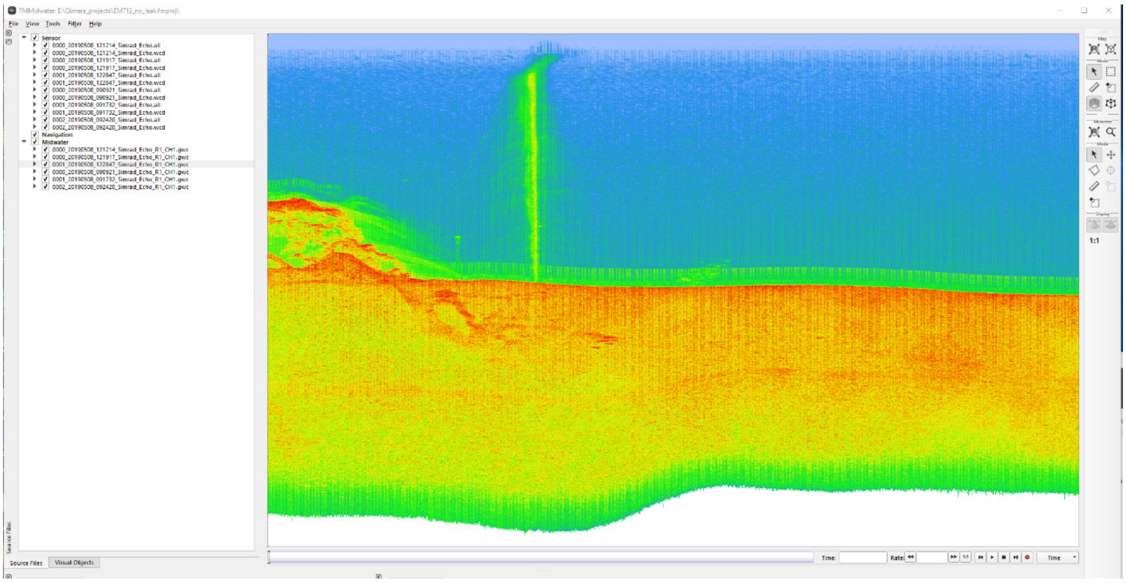

Figure 10-11 When releasing air instead of CO_2, the plume of air bubbles is observed all the way to the surface as expected

10.1.4 ME70 Scientific multibeam echo sounder

The Simrad ME70 is a scientific multibeam echo sounder with a frequency range of 70 – 120 kHz. It can be calibrated, which makes it possible to relate echo strengths directly to target properties (i.e., fish species and abundance or bubble sizes). It transmits multiple beams operating at different frequencies. Typically, the beams are distributed to cover a large area swath, but they may also be pointed in the same direction to evaluate frequency dependant scattering from the same scene. Figure 10-12 shows an example echogram where five beams are pointed in different cross-track directions. The release rate is 1.3 l/min of CO_2 in gas phase, and the bubble plume is visible in all beams, although beams 1 and 3 only capture part of the plume (the upper and the lower part, respectively).

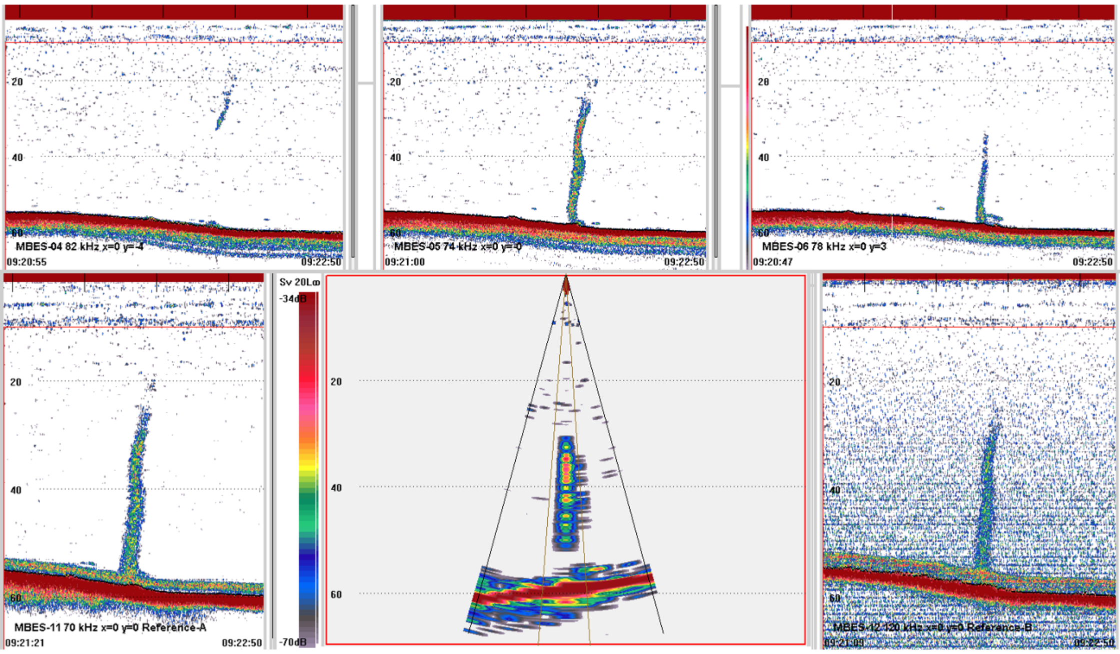

Figure 10-12 Echogram from the ME70, showing the seep at different frequencies but also different spatial beams (i.e., pointed in slightly different directions). A conservative bubble rise height estimate is ~30 m, but from the upper middle and lower left images rise heights as high as 40 m above the seabed (20 m below sea surface) appear likely.

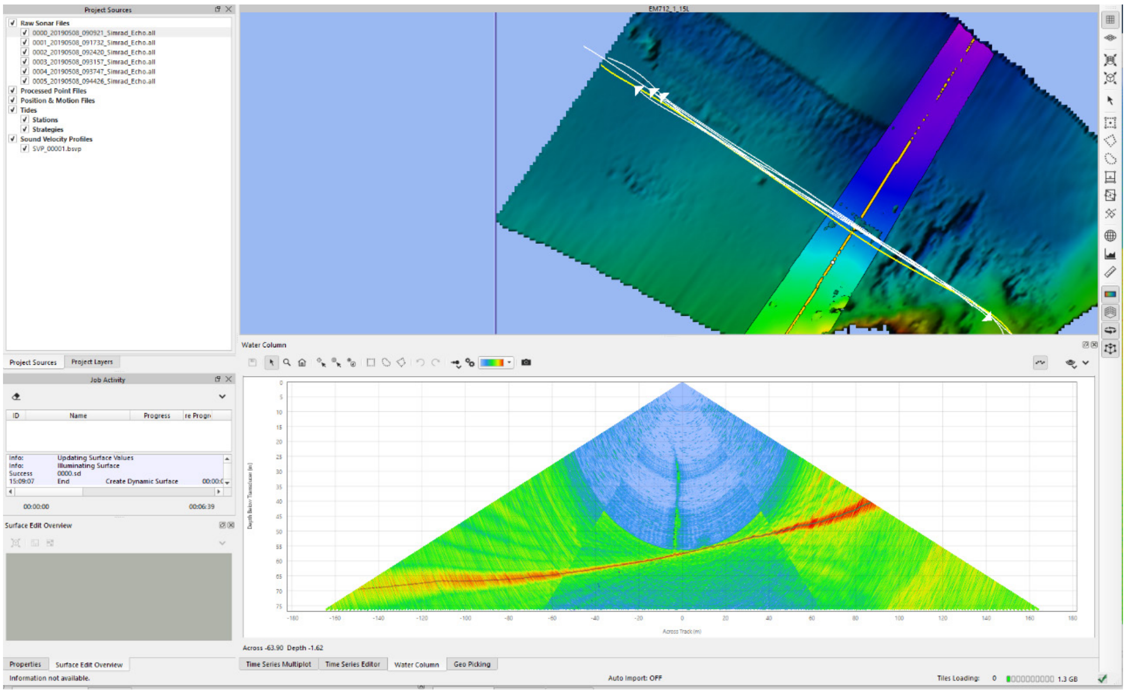

Figure 10-13A different view of the ME70 echogram showing the bathymetry and current swath (upper plot), and the full swath from a single ping when passing above a CO_2 release at 1.3 l/min. Again, bubbles are observable up to 30-35 m above the leak point at the seabed.

10.1.5 SN90 purse seine and trawling sonar

The SN90 is a highly flexible system offering wide coverage both in the horizontal (160 degrees) and vertical (60 degrees) plane. It can be tilted between 0 and 60 degrees, and five separate inspection beams can be adjusted to the operator's needs. This system makes it easy to find and map an object or feature in the entire water column. Using the EK80, EM2040, EM712 and ME70 systems we observed bubble rise heights of approximately 30 m above the sea bed. The SN90 echogram (Figure 10-15) shows bubble rise heights as high as 50 m above the sea bed (10 m below the sea surface). This may be related to the SN90 beampattern and the resulting field of view, indicating that the other systems are not able to capture the top of the plume due to the imaging geometry. Note that the since the plume bends according to ocean currents, it may not stay in a single beam. In Figure 10-15 we observe CO_2 bubbles in inspection beams 1, 2 and 3, but only inspection beam 2 captures the top of the seep.

Figure 10-14 Illustration of the swath coverage offered by the SN90 in both the along-track and across-track directions. The beamwidths and beam angles can be tuned to suit operational needs. Image courtesy: Simrad.com

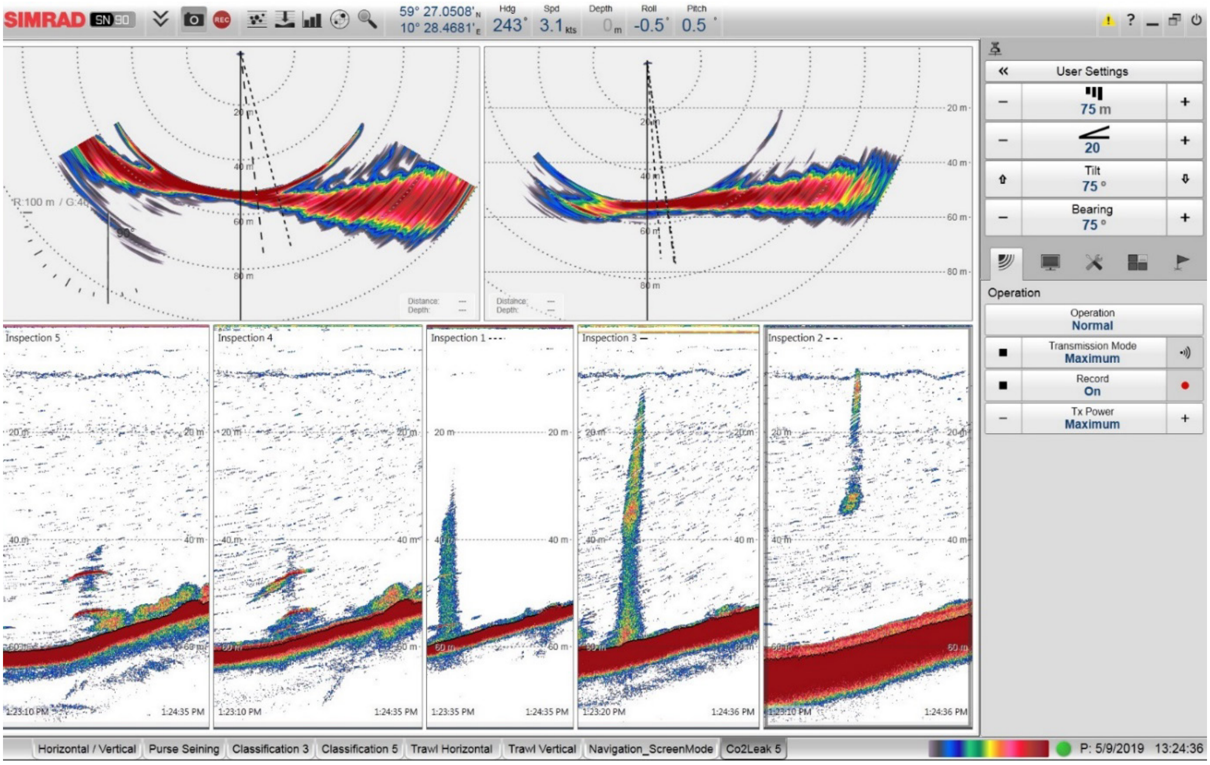

Figure 10-15 Echogram showing the 5 different inspection beams of the SN90. The release rate is 1.3 l/min of CO_2 in gas phase. We observe the plume in inspection beams 1, 2, and 3, but only inspection beam 2 captures the top of the plume reaching as high as 50 m above the seabed.

11 Discussion

11.1 Combining CO_2 and O_2 measurements for robust anomaly detection

Marine environmental GCS monitoring is intended to verify that there is no leakage of CO_2 into the oceans, and to detect and quantify any leakage if it should occur. CO_2 is naturally present in the oceans and the levels of dissolved CO_2 fluctuates according to seasonal and other variations. The increase in dissolved CO_2 related to a potential leak is expected to be spatially confined to a few tens or hundreds of meters, depending on the size of the leak. As large water masses mix, the CO_2 is quickly diluted to background concentrations. Therefore, it is challenging to detect an anomaly based on measurements of CO_2 alone. A better approach is to monitor the relationship between CO_2 and O_2, and to have an anomaly detection algorithm that identifies a deviation from the normal correlation pattern.

This approach is valid in open water conditions including the North Sea, where both CO_2 and O_2 are naturally present. Under anoxic conditions (i.e., water with little or no oxygen content), a different approach should be taken.

11.2 Chemical sensors on an AUV or a glider

AUVs and gliders are both powerful tools for marine environmental monitoring, since they can cover large areas efficiently and carry a range of sensors selected for the task at hand. As technology, both on the sensor and AUV side matures, using different types of AUV's may be the most cost-effective option for marine monitoring on a broad scale including for geological storage of CO_2. The movement of the vessel sets high demands on the response times of the chemical sensors. Most CO_2 sensors on the market are based on a technology where the gas molecules dissolved in seawater pass through a membrane before they can be measured. This process takes some time, in the order of several minutes. As a result, the measured CO_2 concentration is temporally and due to the platform movement also spatially dampened. This sets a higher limit to the size of CO_2 plume that can be detected. As discussed previously, dedicated post processing (RTC) may to a certain degree compensate for the response-time of the membrane-based CO_2 sensor. Our observations indicate that a pH sensor, which has a much faster response time, can successfully act as a proxy for a CO_2 sensor on a moving platform. A strong chemical sensor combination would be an O_2, pH and CO_2 sensor, and the sampling rate should be high.

Another issue to be aware of is the vertical movement of the vessel. Natural levels of CO_2 typically increase with increasing water depth, while O_2 levels decrease correspondingly. The natural vertical variability in CO_2 may be larger than the expected increase caused by a CO_2 leak. A potential pre-processing step may include removing natural trends in CO_2 versus depth to identify comparably small anomalies related to a secondary source of CO_2. This applies especially to underwater glider platforms as these, unlike AUVs that can travel at a constant water depth, always combine vertical with horizontal movement.

11.3 Observed CO_2 bubble rise heights and implications for marine monitoring

CO_2 is known to quickly dissolve in seawater, effectively limiting the bubble rise heights. This has direct consequences for the applicability of active acoustic sensors for marine environmental monitoring, and for modelling the spatial footprint and concentration of a CO_2 plume. Our observations confirm that compared to CO_2, air bubbles rise higher and appear more clearly in data from single- and multibeam echosounders mounted on the hull of the Simrad Echo R/V. However, we also observe that the CO_2 bubbles rise as high as 30-50 m above the leak point at the seabed. This implies that for many leak scenarios, active acoustic sensors can be mounted on an AUV, a glider, or on a surface vessel for effective monitoring of CO_2 bubbles in the water column.

The CO_2 bubble rise height is strongly dependent on the initial bubble size distribution. In the experiments carried out here we observe what we believe are realistic bubble sizes, with predominant bubble diameters in the range 1 to 6 mm. The bubble sizes are determined from visual inspection of video recordings, and laboratory experiments with similar orifice sizes but a different release pressure. We assume that these are similar (but not necessarily identical) to those released during the nearshore controlled release experiments.

It should be noted that there may be other factors affecting the CO_2 bubble rise height, including interaction between bubbles within a plume, flux rate, release pressure, and ocean currents and stratification. In the QICS experiment bubbles were only observed up to 5-8 m above the seabed, indicating that the bubble rise height may vary depending on the leak scenario.

11.4 Where to place a stationary sensor template

Optimal placement of a sensor template depends on local environmental conditions, the relevant and realistic leakage scenarios and on the sensors selected for monitoring. If the template is used for contingency monitoring of a spatially confined high-risk area (hot-spot), the maximum distance that the sensor template can be placed is limited by the sensor with the shortest detection range. While active and passive acoustic sensors are both remote sensors able to detect CO_2 bubbles at a distance, detection ranges for different acoustic sensors range from ~10 m up to hundreds of meters. Chemical sensors are point sensors and need to be in physical contact with the affected seawater to detect an anomaly. Hence, the detection range is not related so much to the sensor sensitivity but to the spatial footprint of the CO_2 plume. This again is affected by the size of the leak, ocean currents, and local water chemistry. Our observations agree with model predictions indicating a spatial footprint of a few tens of meters, potentially a few hundreds of meters for a large or continuous CO_2 leak. While the sensitivity of the chemical sensor may slightly affect the detection range (a more sensitive instrument can detect a more diluted CO_2 plume), this effect is small compared to the spatial footprint of a plume and eventual heterogeneities in it.

Based on these considerations, a suitable placement of a sensor template carrying a dedicated "sensor package" including an EK80 echo sounder and/or an M3 multibeam sonar, a passive hydrophone, a CO_2, pH, O_2 and ocean current sensor, would be 10-30m downstream of the high-risk location. It is worth noting that because of the general difference in range of active acoustic and chemical sensors, it will in some cases make sense to place these on separate templates to maximise coverage of the acoustic sensors. This would apply to scenarios with multiple hotspots, or where there is a risk of a distributed leakage, e.g. along a geological fault.

12 Summary and the way forward

Technologies for adequate marine environmental GCS monitoring are available on the market. However, more development is needed on the software side to arrive at robust algorithms for automatic detection of anomalies. Development of these solutions can take place parallel to large scale GCS deployment.

Our observations indicate that there is a predictable relationship between the levels of dissolved CO_2 and O_2 in the water, related to natural ocean processes. Existing chemical sensors (CO_2, O_2 and pH) can capture these natural variations, and algorithms for detecting deviations from these can be developed. Based on these observations we recommend further analysis into automatic data processing techniques aimed at anomaly detection.

Active acoustic sensors are excellent tools for detecting even modest amounts of bubbles in the water column. There are a range of systems available on the market, ranging from sonars for detailed mapping of the seabed to scientific echo sounders aimed at detecting and characterizing gas plumes in the water column. Which system to choose depends on the monitoring task. An important finding in the 2019 nearshore controlled release experiment was that CO_2 bubbles may rise 30-50 m above the seabed, depending on their initial size and the surrounding water chemistry. This has direct applications for monitoring and the usefulness of active acoustic sensors on R/Vs and AUVs.

We have confirmed that mobile sensor platforms (AUV's) are useful for detecting leakages. For monitoring of large areas, it would be beneficial to implement some knowledge of the physical environment, including a plume model, into the navigation system. This would enable the AUV to recognize a potential plume and make an autonomous decision to examine a subset of the area in more detail.

Finally, there would be added benefit from more integration of data from different sensor technologies, e.g. integration of acoustic and chemical measurements. This is particularly useful for an operator to get the "whole picture" to evaluate whether a potential anomaly should result in any actions such as contingency monitoring.

13 References

1. Institute, G. C. *Global Status of CCS: 2015*; Global CCS Institute: Melbourne, 2015.
2. Jenkins, C.; Chadwick, A.; Hovorka, S. D., The state of the art in monitoring and verification—Ten years on. *International Journal of Greenhouse Gas Control* **2015,** *40*, 312-349.
3. CO_2CRC *The process of developing a* CO_2 *test injection; experience to date and best practices*; IEAGHG, 2013.
4. Schacht, U.; Jenkins, C., Soil gas monitoring of the Otway Project demonstration site in SE Victoria, Australia. *International Journal of Greenhouse Gas Control* **2014,** *24*, 14-29.
5. Arts, R.; Eiken, O.; Chadwick, A.; Zweigel, P.; van der Meer, L.; Zinszner, B., Monitoring of CO_2 injected at Sleipner using time-lapse seismic data. *Energy* **2004,** *29*, (9), 1383-1392.
6. Myers, M. B.; Roberts, J. J.; White, C.; Stalker, L., An experimental investigation into quantifying CO_2 leakage in aqueous environments using chemical tracers. *Chemical Geology* **2019,** *511*, 91-99.
7. Uchimoto, K.; Nishimura, M.; Kita, J.; Xue, Z., Detecting CO_2 leakage at offshore storage sites using the covariance between the partial pressure of CO_2 and the saturation of dissolved oxygen in seawater. *International Journal of Greenhouse Gas Control* **2018,** *72*, 130-137.
8. Maeda, Y.; Shitashima, K.; Sakamoto, A., Mapping observations using AUV and numerical simulations of leaked CO_2 diffusion in sub-seabed CO_2 release experiment at Ardmucknish Bay. *International Journal of Greenhouse Gas Control* **2015,** *38*, 143-152.
9. Shitashima, K.; Maeda, Y.; Sakamoto, A., Detection and monitoring of leaked CO_2 through sediment, water column and atmosphere in a sub-seabed CCS experiment. *International Journal of Greenhouse Gas Control* **2015,** *38*, 135-142.
10. Atamanchuk, D.; Tengberg, A.; Aleynik, D.; Fietzek, P.; Shitashima, K.; Lichtschlag, A.; Hall, P. O. J.; Stahl, H., Detection of CO_2 leakage from a simulated sub-seabed storage site using three different types of pCO_2 sensors. *International Journal of Greenhouse Gas Control* **2015,** *38*, 121-134.
11. Ohtaki, E.; Yamashita, E.; Fujiwara, F., Carbon dioxide in surface seawaters of the Seto Inland Sea, Japan. *Journal of Oceanography* **1993,** *49*, (3), 295-303.
12. Uchimoto, K.; Kita, J.; Xue, Z., A Novel Method to Detect CO_2 Leak in Offshore Storage: Focusing on Relationship Between Dissolved Oxygen and Partial Pressure of CO_2 in the Sea. *Energy Procedia* **2017,** *114*, 3771-3777.

13. Blackford, J.; Artioli, Y.; Clark, J.; de Mora, L., Monitoring of offshore geological carbon storage integrity: Implications of natural variability in the marine system and the assessment of anomaly detection criteria. *International Journal of Greenhouse Gas Control* **2017,** *64*, 99-112.
14. Bickle, M. J., Geological carbon storage. *Nature Geoscience* **2009,** *2*, 815.
15. Gade, H. G., Horizontal and vertical exchanges and diffusion in the water masses of the oslo fjord. *Helgoländer wissenschaftliche Meeresuntersuchungen* **1968,** *17*, (1), 462-475.
16. Ohsumi, T.; Nakashiki, N.; Shitashima, K.; Hirama, K., Density change of water due to dissolution of carbon dioxide and near-field behavior of CO_2 from a source on deep-sea floor. *Energy Convers. Manage.* **1992,** *33*, (5), 685-690.
17. Kampman, N.; Bickle, M. J.; Maskell, A.; Chapman, H. J.; Evans, J. P.; Purser, G.; Zhou, Z.; Schaller, M. F.; Gattacceca, J. C.; Bertier, P.; Chen, F.; Turchyn, A. V.; Assayag, N.; Rochelle, C.; Ballentine, C. J.; Busch, A., Drilling and sampling a natural CO_2 reservoir: Implications for fluid flow and CO_2-fluid–rock reactions during CO_2 migration through the overburden. *Chemical Geology* **2014,** *369*, 51-82.
18. Atamanchuk, D. T., A.; Aleynik, D.; Fietzek, P.; Shitashima, K.; Lichtschlag, A.; Hall, P. O. J.; Stahl, H, Detection of CO_2 leakage from a simulated sub-seabed storage site using three different types of pCO_2 sensors. *International Journal of Greenhouse Gas Control* **2015,** *38*, 121-134.
19. Fietzek, P. F., B.; Steinhoff, T.; Körtzinger, A., In situ Quality Assessment of a Novel Underwater pCO_2 Sensor Based on Membrane Equilibration and NDIR Spectrometry. *Journal of Atmospheric and Oceanic Technology* **2014,** *31*, (1), 181-196.
20. A. E. A. Blomberg, T. O. S., R. E. Hansen, R. B. Pedersen and A. Austeng, Automatic Detection of Marine Gas Seeps Using an Interferometric Sidescan Sonar. *IEEE Journal of Oceanic Engineering* **2017,** *42*, (3), 590-602.
21. Hansen, R. E., *Introduction to synthetic aperture sonar*. INTECH Open Access Publisher: 2011.

Appendix A

SENSORS AND DATA SHEETS

Contents

A1 Kongsberg Mesotech M3 sonar

The Kongsberg Mesotech M3 is a compact and flexible 2-dimensional multibeam sonar with imaging and profiling capabilities. It operates at high frequencies (500 kHz), resulting in high resolution (detailed) imagery. Designed to get an overview of the subsea surroundings, it offers a wide field-of-view (120-140 degrees, split into 240 beams). The high frequencies also result in a limited operating range (~150 m), since the amplitude of relatively high frequencies are dampened more than lower frequencies.

A2 Simrad EK80 broadband echo sounder

The Simrad EK80 is a wideband split-beam echo sounder with high sensitivity and dynamic range. It is considered a highly relevant sonar for environmental monitoring purposes, due to its sensitivity, as well as wideband capabilities which are useful for classifying seeps and estimating bubble sizes. The wideband capabilities as well as the split-beam configuration (four separate quadrants/channels) enables advanced post-processing for optimized seep detection and monitoring. Furthermore, the EK80 is a calibrated system which makes it possible to estimate bubble flux (provided an estimated of the bubble size distribution). Operating frequencies range from 10 to 500 kHz, depending on system configuration. In the 2018 nearshore test, we used two transducers; one operating at 50-90 kHz and one at 250-450 kHz. The operating range is long, typically several hundred meters depending on the choice of transducer (lower frequencies result in longer operating range).

The Simrad EK80 is known to be sensitive to small leaks. Analogously, very large detection distances are achieved (hundreds of meters) for larger leaks. It is well suited for most platforms, including surface vessels, AUV's, landers, and recently also demonstrated on the Kongsberg SeaExplorer. The EK80 is a split-beam system, i.e. it transmits a single beam with a 7-degree beamwidth, and has the capability to split the receive beam into sectors for better positioning of a target and, after beampattern compensation, improved quantification of the target strength. This technology is powerful both for detecting leaks, and monitoring a known seepage over time in order to understand the dynamics of the leak. The limited beamwidth (7 or 11 degrees depending on selected hardware) limits the area coverage rate.

A3 Ocean Sonics icListen

The Ocean Sonics icListen is a highly sensitive passive hydrophone operating at a broad frequency range. We used the icListen HF, with a frequency range of 10 Hz to 200 kHz. This hydrophone is calibrated, making it possible to relate the measured signal to quantitative estimates of flux. In order to do so, an estimate of the bubble size distribution is required.

A4 Contros HydroC CO_2

The Contros HydroC CO_2 sensor developed by Kongsberg Maritime is a membrane sensor with optical detection for measurement of the partial pressure of CO_2 in water. The measuring principle is illustrated in Figure A4.1. The dissolved gas diffuses from the seawater through a membrane into an internal gas circuit. The CO_2 concentration is then measuerd using non-dispersive infrared spectrometry.

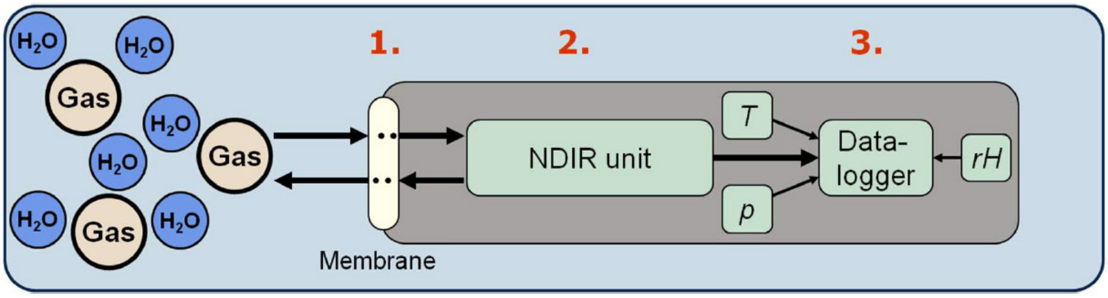

Figure A4.1 Measurement principle of the Contros HydroC sensor. This image is copied from the data sheet attached in Appendix A.

The important mechanisms and measurement/function principles of the HydroC sensor is illustrated in Figure A4.1 and summarized in the data sheet:

1. Dissolved gases and water vapour pass the hydrophobic membrane and form an internal headspace Equilibration of all dissolved partial pressures
2. CO_2-gas concentration measured by non-dispersive infrared spectrometry (NDIR) within a gas circuit
3. pCO_2 data along with temperature, pressure and pH are either transmitted by cable or saved on an internal data logger.

A5 Franatech CO_2

The Franatech CO_2 sensor consists of a metal oxide semi-conductor mounted in a detector chamber. A semi-permeable membrane protects the detector chamber from the water, see Figure A5.1 . The membrane allows for gas permeation, so that there is an equilibrium between the amount of CO_2 in the water and in the detector chamber. The amount of CO_2 in the detector chamber is then measured by the electrical conductivity of the semi-conductor. This conductivity increases proportionally to the concentration of CO_2 in the detector chamber. Eventual temperature effects are corrected for in the internal electronics, and the computed CO_2 concentration in ppm is transmitted by cable.

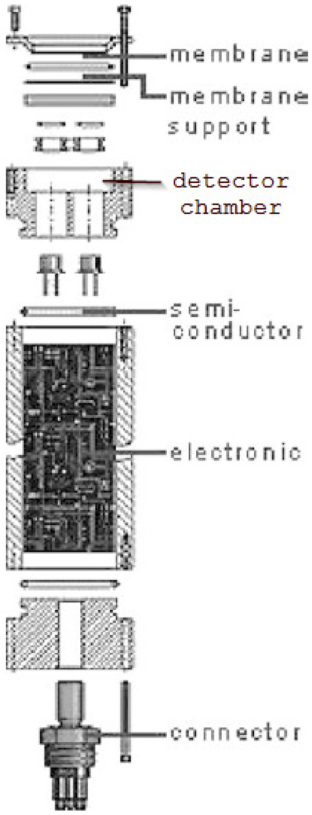

Figure A5.1 Typical arrangement of a semi-conductor gas sensor for underwater measurements. Modified from Garcia and Masson (2004)

A6 Contros HydroFlash O2

The HydroFlash sensor developed by Kongsberg Maritime is used to measure the O_2 concentration in water. The sensor is optical, with a membrane through which dissolved O_2 diffuses. A fluorescent dye is embedded in the membrane, which is affected by the O_2 content through fluorescence quenching. Hence, the more O_2 in the water, the weaker is the measured fluorescence signal. Figure A6.1 is copied from the HydroFlash data sheet and illustrates the functional principle of the sensor.

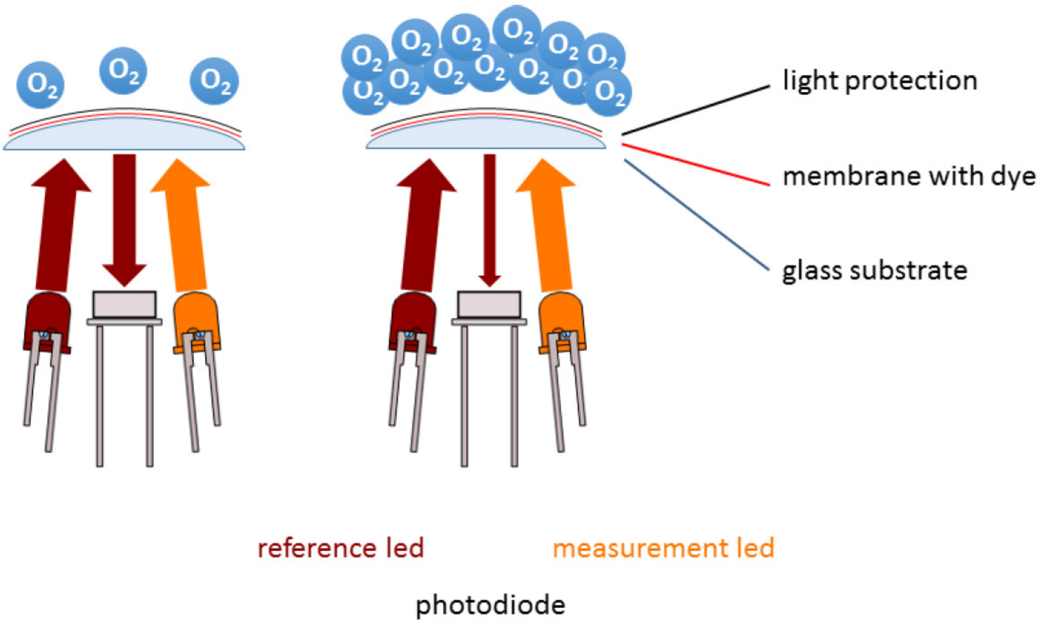

Figure A6.1 Functional principle of the Contros HydroFlash sensor for dissolved oxygen. This image was copied from the data sheet attached in Appendix A.

A7 Idronaut Sondes/multisensors

The Idronaut multisensor is compact sondes equipped with a range of sensors. The sondes may be powered by cable or internal battery. In addition to pH, these sondes are equipped with a wide range of sensors including dissolved O_2, turbidity, temperature, conductivity, salinity, nitrates, and more. Several of these are relevant to environmental monitoring of geologically stored carbon, in particular pH, O_2, and salinity.

A8 EM2040 multibeam echo sounder

The EM2040 is a wideband multibeam echo sounder (MBES) with a frequency range of 200-400 kHz. It is aimed at high-resolution seafloor mapping in relatively shallow water. The EM2040 is flexible, allowing the user to tailor beamwidths, operating frequencies, and area coverage to their needs. The maximum swath size is 200 degrees.

A9 EM712 multibeam echo sounder

The Kongsberg EM712 MBES is a high-resolution echo sounder with an operating frequency range of 40 – 400 kHz. The maximum acquisition depth is 3500 m, with an across-track area coverage of 5.5 times the water depth.

A10 ME70 scientific multibeam echo sounder

The Simrad ME70 is a scientific multibeam echo sounder with a frequency range of 70 – 120 kHz. It can be calibrated, which makes it possible to relate echo strengths directly to target properties (i.e., fish species and abundance or bubble sizes). It transmits multiple beams operating at different frequencies. Typically, the beams are distributed to cover a large area swath, but they may also be pointed in the same direction to evaluate frequency dependant scattering from the same scene.

A11 SN90 purse seine and trawling sonar

The SN90 is a highly flexible system offering wide coverage both in the horizontal (160 degrees) and vertical (60 degrees) plane. It can be tilted between 0 and 60 degrees, and five separate inspection beams can be adjusted to the operator's needs. This system makes it easy to find and map an object or feature in the entire water column. For further information on usage and technical information, see https://www.kongsberg.com/maritime/products/commercial-fisheries/fish-finding-sonars/sn90/

A12 Data sheets

M3 SONAR® - 500M

KONGSBERG

P/N 922-20010000

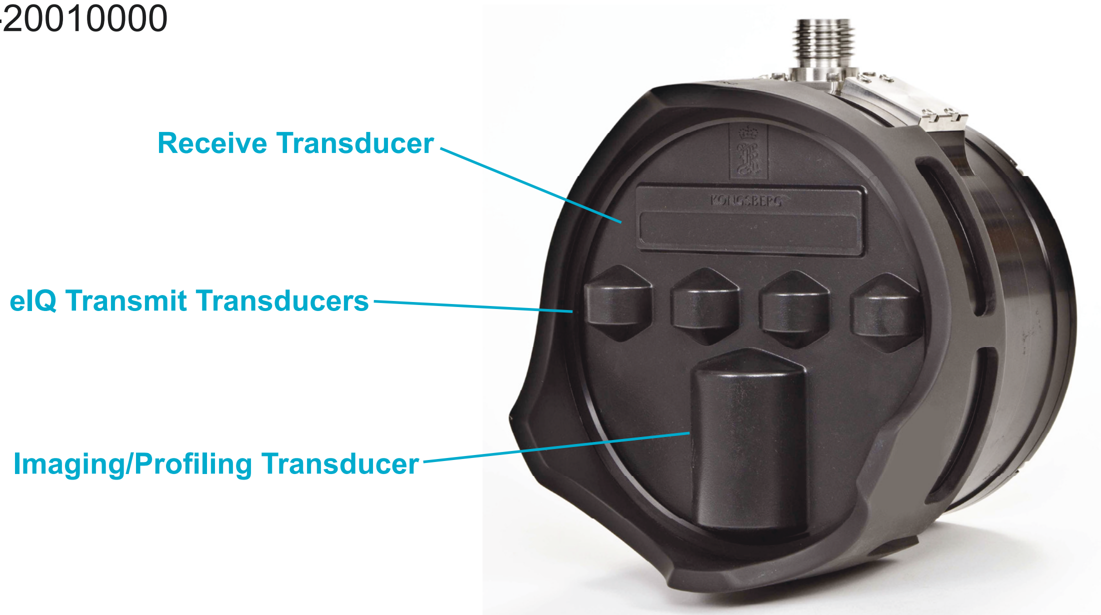

October 2016

THE MULTIMODE MULTIBEAM FOR MULTIPLE APPLICATIONS

- **Imaging and profiling capabilities**
- **GeoTIFF output for image mosaics**
- **Multiple true-zoom windows**
- **CHIRP and Doppler modes of operations**
- **User-friendly interface**
- **Significant time savings**
- **Integrated tilt and pan/tilt control**

The Kongsberg Mesotech M3 Sonar® is a multibeam system with both imaging and profiling capabilites. The M3 Sonar® provides high-resolution and easy to interpret images by combining the rapid refresh rate of a conventional multibeam sonar with image quality comparable to a single-beam sonar.

Detection of small objects out to 150 meters combined with a 120° to 140° field of view allows the operator to see the complete underwater picture in real-time.

APPLICATIONS

- Marine Engineering
- Shallow Water Bathymetric Surveying
- Site Inspection
- Environmental Monitoring
- Site Clearance
- Defense and Security

INSTALLATION OPTIONS

- Pole mount on a surface vessel
- Suitable for a wide range of vehicles from large work-class ROVs to small observation class ROVs
- Tripod mounted

M3 SOFTWARE

The M3 Software was developed specifically for the M3 Sonar® to manage communications with the head and operate all beam-forming and imaging processing.

Four Pre-Defined Operating Modes:

1. **Imaging:** long range navigation with high speed update rate
2. **Enhanced Image Quality (eIQ):** greatest image quality (0.95° angular resolution) from a short range with a slower update
3. **ROV Navigation:** selects eIQ or imaging based on range
4. **Profiling:** narrow 3° beam used to generate a 3D point cloud

TECHNICAL SPECIFICATION

Sonar Specifications

Range:	0.2m to 150m
Range Resolution:	1cm
Frequency:	500 kHz
Pulse Types:	CW, CHIRP
Modes:	Variable Vertical Beamwidth, eIQ

Imaging Mode

Horizontal Field of View:	120°
Vertical Beamwidth:	3°, 7°, 15°, 30°
Angular Resolution:	1.6°
Update Rate:	up to 40 Hz

eIQ Imaging Mode

Horizontal Field of View:	140°
Vertical Beamwidth:	30°
Angular Resolution:	0.95°
Update Rate:	up to 10 Hz

Profiling Mode

Horizontal Field of View:	120°
Vertical Beamwidth:	3°
Number of Beams:	256
Update Rate:	up to 40 Hz

Interface Specifications

Communication:	Ethernet
Data Rates:	10/100/1000 Mbps
Input Voltage:	12 to 36 VDC
Input Power:	22W (avg.), peak power < 60W, mode dependant
Operating System:	Windows 7 Professional SP1 or Windows XP Professional SP3

Environmental Specifications

Temperature

Operation:	-2°C to +38°C
Storage:	-40°C to +55°C

Shock and Vibration

Shock Qualified:	+/-50gs, 3 Axes, 6 shocks per axis
Vibration Qualified:	4g, 30Hz 3 Axes, 2 hours per axis. No resonance below 800Hz

Mechanical Specifications

Dimensions:	*(see diagram below)*
Weight in Air:	4.6kg
Weight in Water:	1.7kg
Depth Rating:	500m
Connector Type:	SEA CON®
Connector Model:	MINK-10-FCRL
Materials:	Hard Anodized Aluminum, Stainless Steel 316, Elastomeric Polyurethane

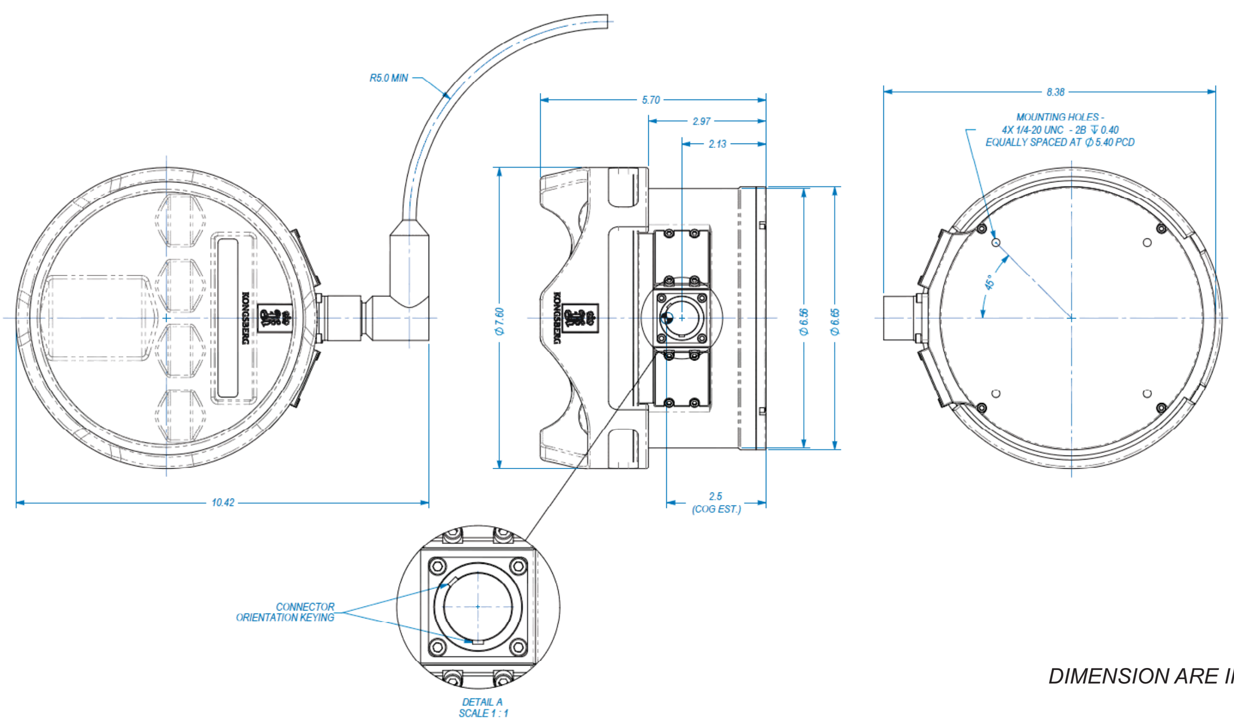

DIMENSION ARE IN INCHES

Specifications subject to change without any further notice.

922-20017901-1.4

www.kongsbergmesotech.com

E-mail: km.sales.vancouver@kongsberg.com
Telephone: +1 604 464 8144
Toll-free: +1 888 464 1598

KONGSBERG

Simrad WBAT

Wideband Autonomous Transceiver

WBAT is a “cutting edge” subsea innovation rising from a need to monitor marine life and detect oil and gas leaks at virtually any corner of the world.

Description

The Simrad WBAT system is at the forefront of monitoring marine life capable of being submerged to a maximum depth of 1500 meters and prolonged periods of up to 15 months.

When deployed, the WBAT is self-contained and will record data with the acoustic settings at the given time intervals.

Between data recording events the WBAT will be in “deep sleep”, conserving energy and extending battery life.

The WBAT Transceiver comprises a rugged cylinder providing all necessary transmitter and receiver electronics, a battery and the necessary interface and control circuitry.

Key features

- Autonomous all-in-one echo sounder
- Advanced mission control
- Internal battery and data storage
- More than 1 year deployment
- Depth rated to 1500 m
- Frequencies from 30 to 500 kHz
- Connects two split-beam or four single-beam transducers
- Chirp and CW pulse forms
- Standardized Simrad® EK80 raw data format
- Built in calibration tool
- Wide range of transducers available

Typical applications

- Ocean observatories
- Fish migration studies
- Long-term biological studies
- Improved fish stock assessment
- Water column profiling
- Instrumentation on ROVs and AUVs

WBAT mounted on Conductivity-Temperature-Depth sensor unit.

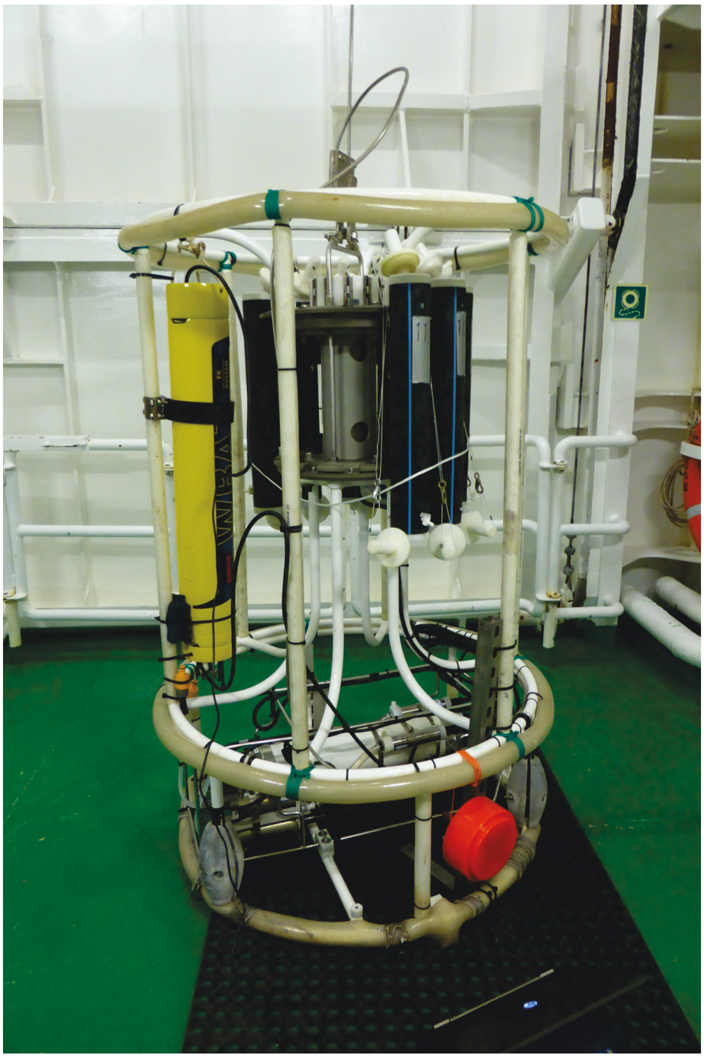

Mission Planning

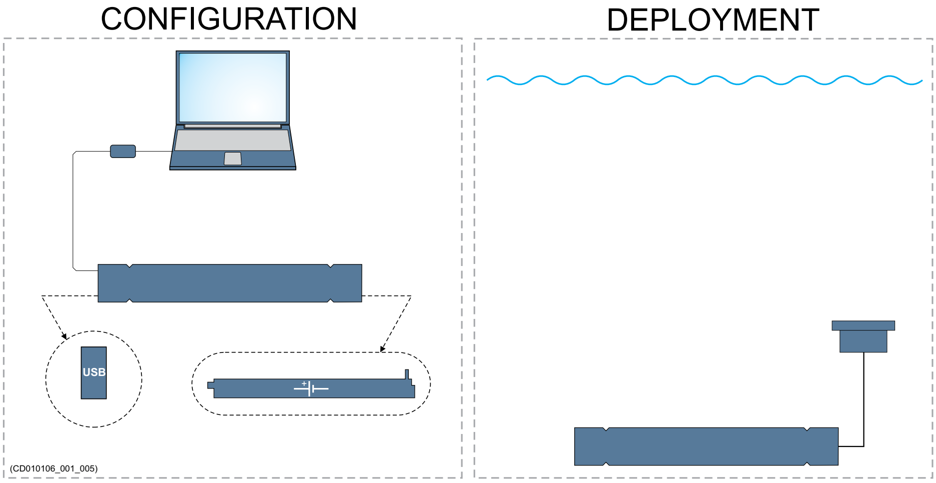

A WBAT system consists of an autonomous transceiver, one or more transducers and Mission Plan software.

Regardless if the data is collected from the ship sounders, a profiling probe, or from other platforms; the echo sounders use the same data format.

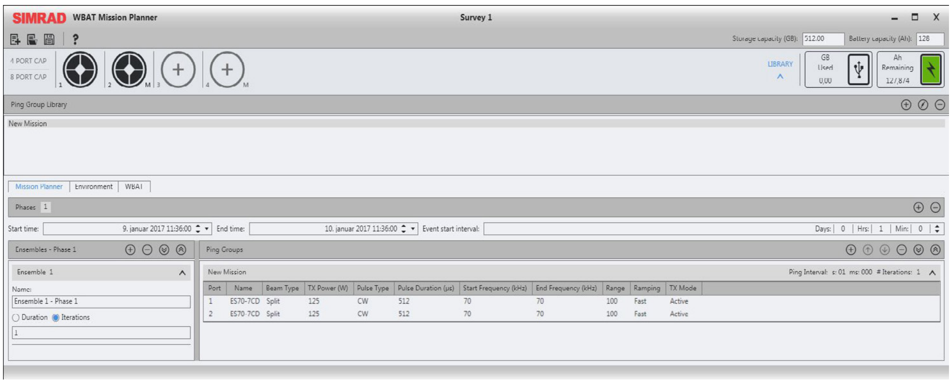

Mission Planner user interface

An advanced mission control software gives the operator a full spectre of parameters to chose from. Once uploaded into the transceiver the unit will record the data based on the acoustic settings.

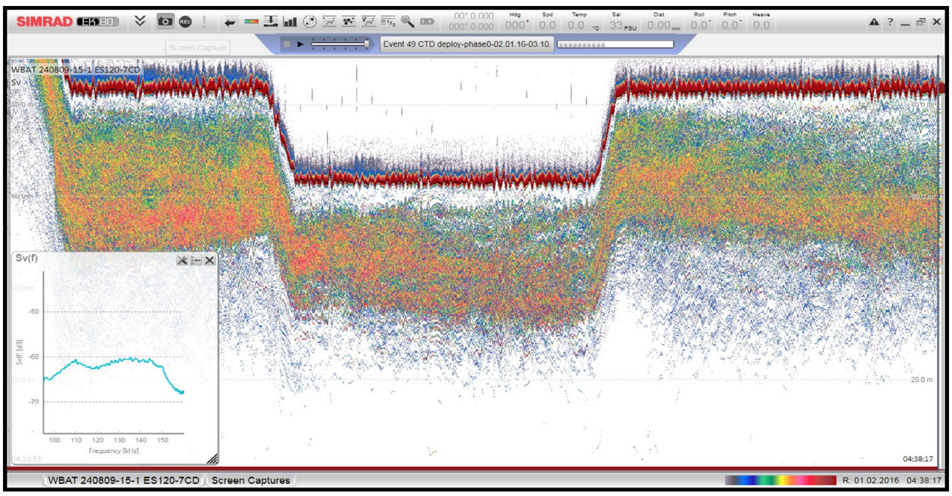

EK80 echogram playback of krill from Antarctica. (Screen capture kindly provided by British Antarctic Survey, UK)

The data from the system can be viewed and calibrated with the EK80 software as the RAW data format used by these products are identical.

Technical specifications

- Physical dimensions: 100 x 16.6 cm
- Weight in air/water: 25/12 kg
- Operational frequency: 30-500 kHz
- Max Transmit power: 250 W per channel with 70Ω load at 38 kHz
- No. of channels: Four independent channels
- Pulse types: CW, FM, Active, Passive
- Pulse lengths: 128 µs to 2 ms
- Transducer types: Single and/or split-beam
- Multiplexing: Built in multiplexer on each channel
- DC voltage: 14 V (internal battery)
- Battery capacity: 128 Ah
- Current consumption active: 350 mA
- Current consumption inactive: 1.5 mA
- Control: Pre-planned mission
- External interface: RS-422
- Depth rating Transceiver: 1500 meters
- Data format: Same as EK80
- EK 80 SW: Replay, calibration
- Calibration: Calibration tool built into the mission planner. Data calibration in EK80 or 3rd party processing software.
- License required: No

WBAT assembled with transducer mount

WBAT testing onboard NOAA/Saildrone platform San Francisco Bay, CA.

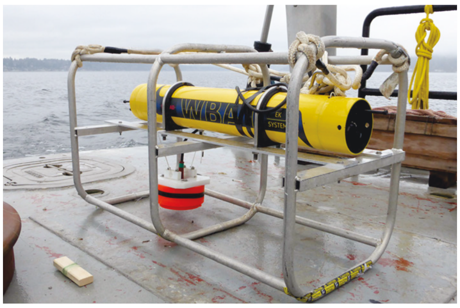

WBAT calibration on Lake Washington Seattle, WA.

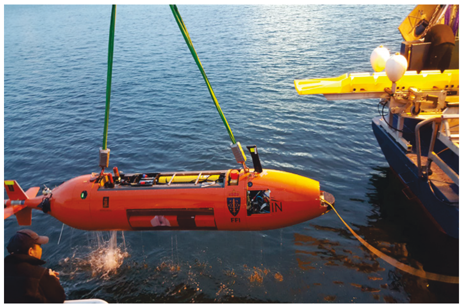

WBAT mounted on HUGIN Oslofjord, Norway

418953 / Rev. B / January 2017

Simrad

Kongsberg Maritime AS
Strandpromenaden 50
P.O.Box 111
N-3191 Horten, Norway

Telephone: +47 33 03 40 00
Telefax: +47 33 04 29 87
www.simrad.com
simrad.sales@simrad.com

SIMRAD

Simrad ES70-7C
Split beam echo sounder transducer

Introduction

The **Simrad ES70-7C** is a split-beam composite transducer with a large bandwidth. This provides a fine range resolution, which is important for single fish detection and target strength measurement. The transducer has four quadrants.

Order number

KSV-203678

Technical specifications

The following specifications are valid when all four quadrants are wired in parallel.

- Resonant frequency: 70 kHz
- Circular beamwidth: 7 deg
- Directivity:
  D: 650
  DI = 10 log D: 28 dB
- Equivalent two-way beam angle:
  Ψ: 0.009
  10 log Ψ: -21 dB
- Side lobes: Less than -23 dB
- Back radiation: Less than -40 dB
- Nominal impedance: 19 ohm
- Transmitting response:
  185 dB re 1μPa per V
- Receiving sensitivity, open circuit: -190 dB re 1V per μPa
- Electro-acoustic efficiency: 0.75
- Max. pulse power input: 1000 W
- Max. continuous input: 10 W
- Max. transducer depth: 20 m
- Cable length: 20 m
- Cable diameter: 10.6 mm
- Weight without cable: 6.4 kg
- Storage temperature: -20° to 70°C

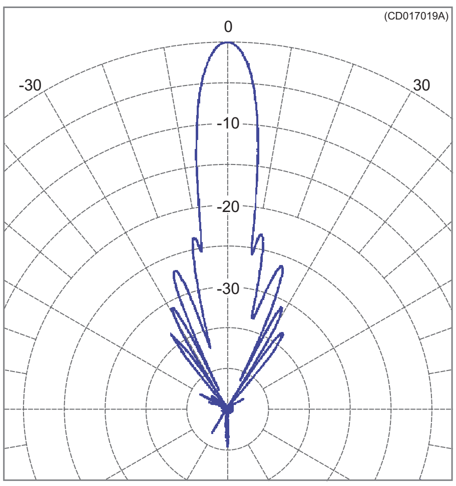

Beam pattern

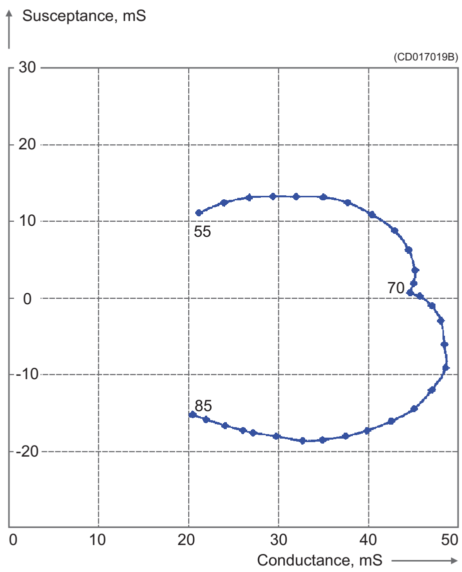

Admittance

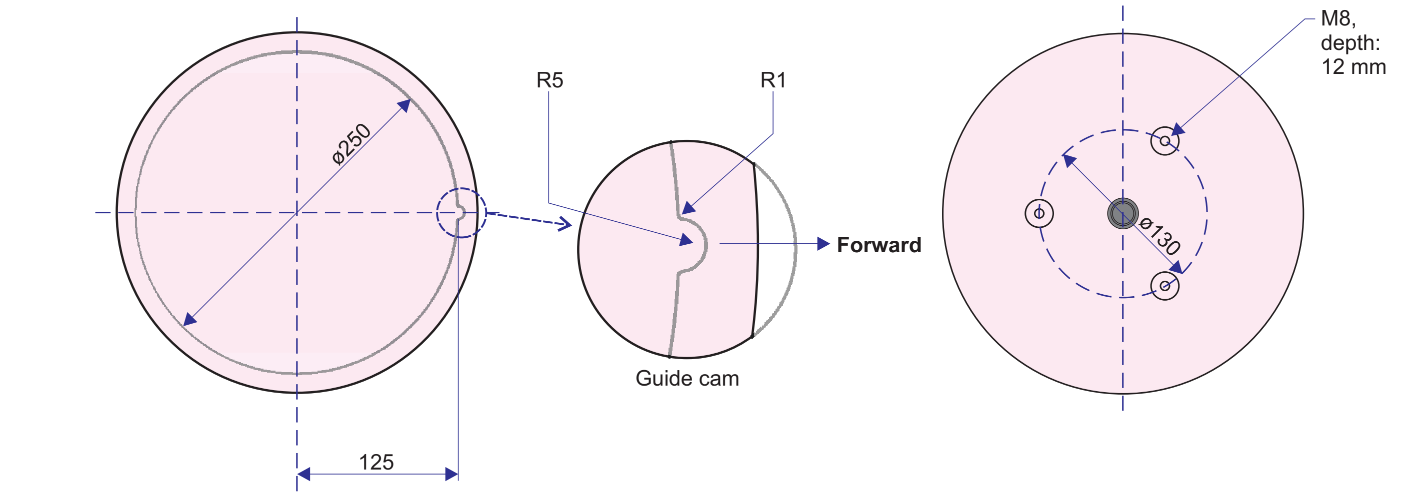

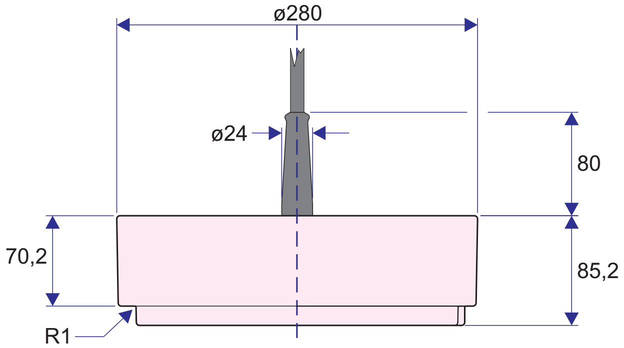

Outline dimensions

All dimensions in mm

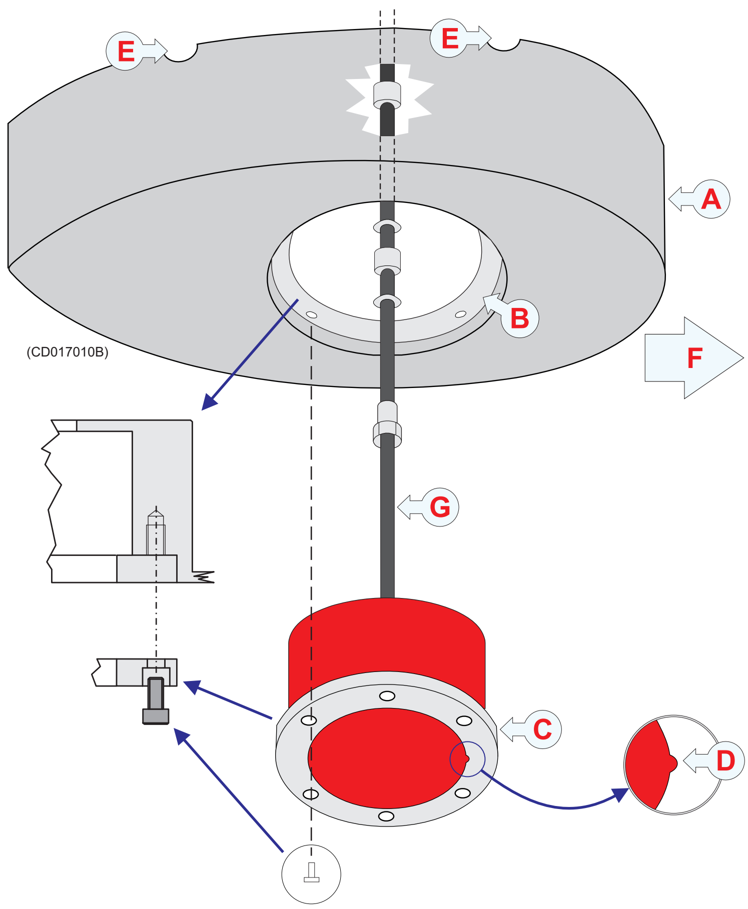

Installation principle

(A) = Steel blister, must be manufactured by the shipyard
(B) = Mounting ring, can be supplied by Simrad
(C) = Clamping ring, can be supplied by Simrad
(D) = Guide to indicate “Forward”
(E) = Air outlet
(F) = Forward
(G) = Transducer cable

Refer to the *Simrad ES70-7C Installation manual* for more information.

855-164385 / Rev.C / November 2006

Simrad Horten AS
Strandpromenaden 50
P.O.Box 111
N-3191 Horten,
Norway

Telephone: +47 33 03 40 00
Telefax: +47 33 04 29 87
www.simrad.com
simrad.sales@simrad.com

SIMRAD
A KONGSBERG Company

Simrad ES200-7C
Split beam echo sounder transducer

Introduction

The Simrad ES200-7C is a split-beam composite transducer with a large bandwidth. This provides a fine range resolution, which is important for single fish detection and target strength measurement. The transducer has four quadrants.

Order number

KSV-203003

Technical specifications

The following specifications are valid when all four quadrants are wired in parallel.

- Resonant frequency: 200 kHz
- Circular beamwidth: 7 deg
- Directivity:
  D: 650
  DI = 10 log D: 28 dB
- Equivalent two-way beam angle:
  Ψ: 0.009
  10 log Ψ: -20.5 dB
- Side lobes: Less than -23 dB
- Back radiation: Less than -40 dB
- Nominal impedance: 19Ω
  (Each quadrant: 75Ω)
- Transmitting response:
  185 dB re 1μPa per V
- Receiving sensitivity, open circuit: -190 dB re 1V per μPa
- Electro-acoustic efficiency: 0.75
- Max. pulse power input: 1000 W
- Max. continuous input: 10 W
- Max. transducer depth: 20 m
- Cable length: 20 m
- Cable diameter: 10.6 mm
- Weight: 1.1 kg
- Storage temperature: -20° to 70°C

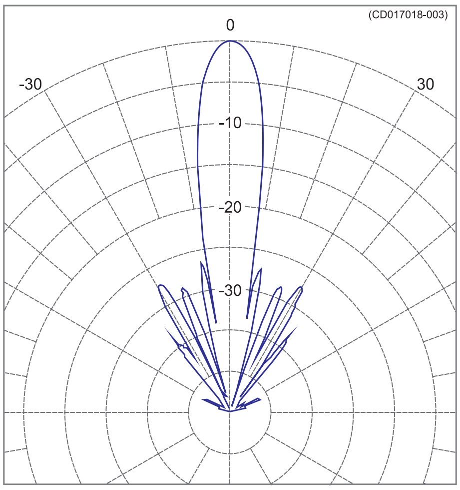

Beam pattern

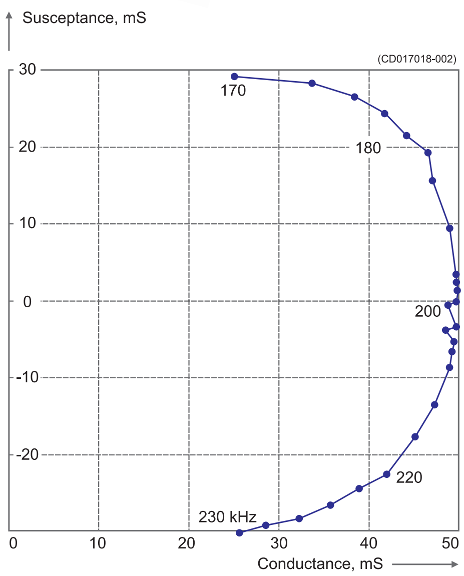

Admittance

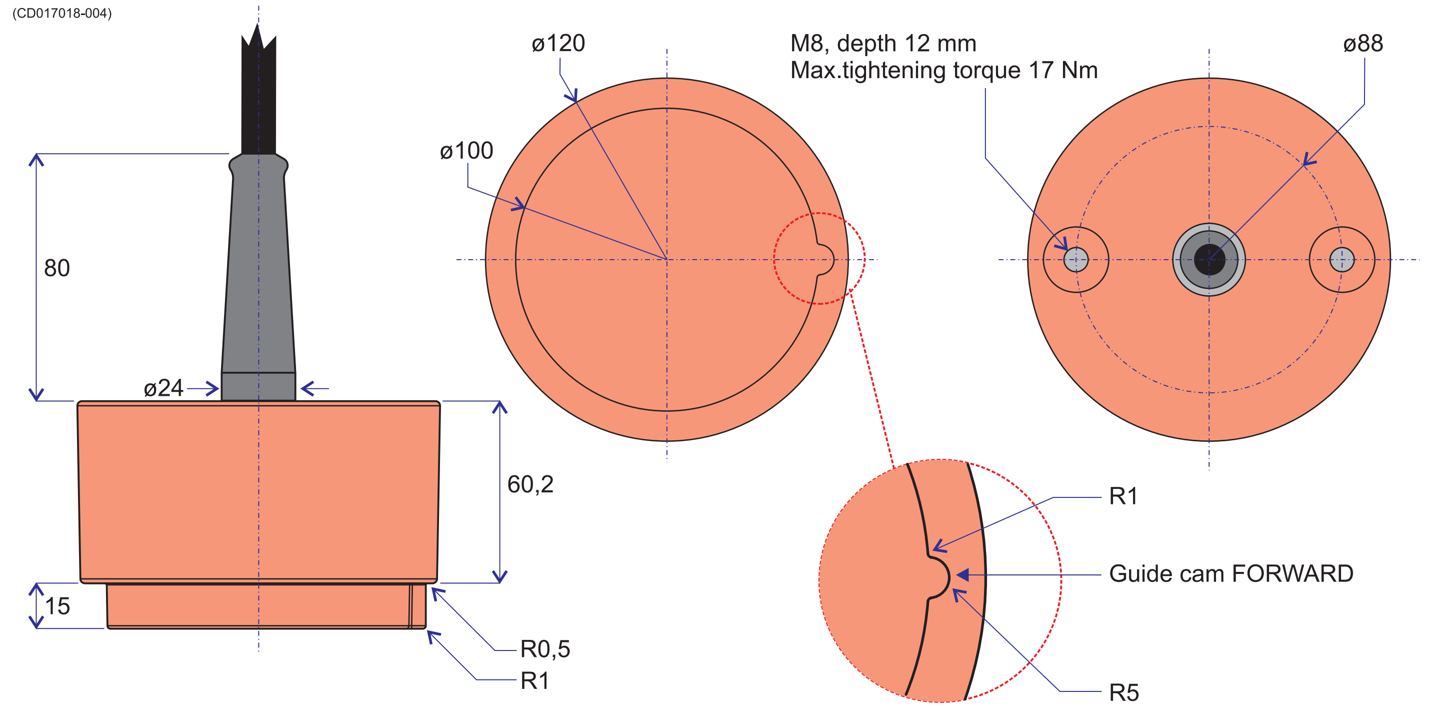

Outline dimensions

All dimensions in mm

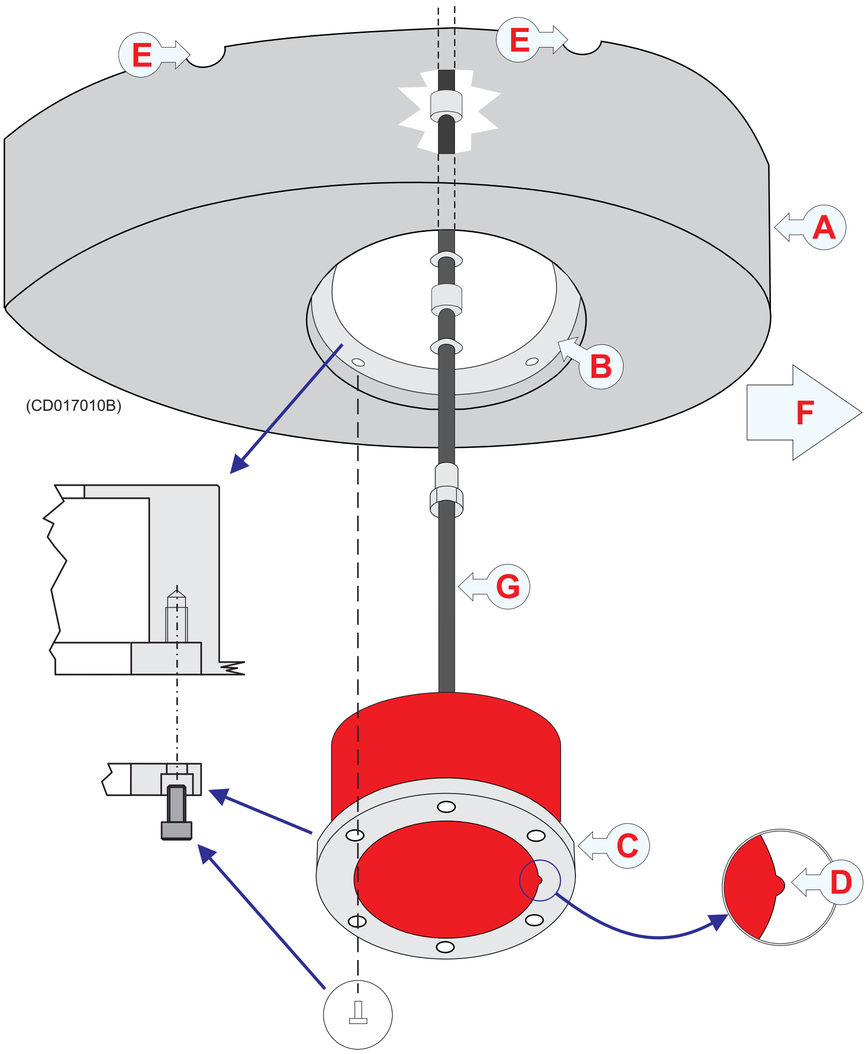

Installation principle

A Steel blister, must be manufactured by the shipyard
B Mounting ring
C Clamping ring
D Guide to indicate “Forward”
E Air outlet
F Forward
G Transducer cable

For more information regarding installation, refer to the *Simrad ES200-7C Installation manual*.

855-204465 / Rev.E / January 2009

Simrad
Kongsberg Maritime AS
Strandpromenaden 50
P.O.Box 111
N-3191 Horten, Norway

Telephone: +47 33 03 40 00
Telefax: +47 33 04 29 87
www.simrad.com
simrad.sales@simrad.com

SIMRAD

icListen Specification

The new standard in broadband digital marine acoustics

The icListen Smart Hydrophone is a compact, all-in-one instrument that logs calibrated waveforms, spectral or event data in standard formats and can be use to stream real-time data. Use the icListen as a digital hydrophone, acoustic data logger, or both at once.

This compact instrument includes rechargeable batteries, large memory and 24 bit data acquisition system. The icListen detects real-time events and can log or transmit just the event data in real-time.

icListen Self-Noise

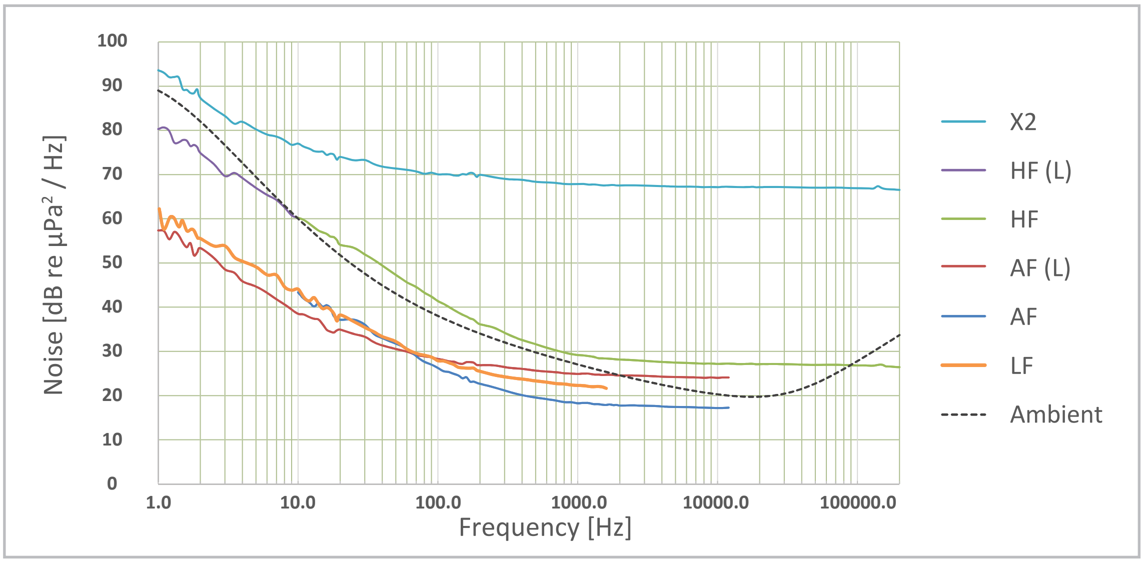

Instrument access methods

- **Stream/Collect** waveform and spectrum (FFT) data.
- Use **Lucy PC software** to view and process data or enquire and set up instrument.

HF and AF

- Use the **Web Browser** to view instrument status download logged data, configure instrument settings and put to sleep.
- Use **FTP** to manage files on the instrument copy and delete stored data files, and install firmware upgrades.
- Ethernet Interface

Ocean Sonics
The Smart Hydrophone Company

icListen Models
HF, AF, LF

200m icListen HF

Engineered Plastic

3500m icListen HF

Titanium

Hill House
11 Lornevale Rd., Great Village
Nova Scotia, Canada B0M 1L0
+ 1 902 655 3000

OceanSonics.com

	LF	AF(L)	AF	HF(L)	HF	X2	UNITS
SIGNAL PERFORMANCE							
Low Frequency Cutoff	1	1	10	1	10	1	Hz
+/- 3 dB bandwidth	1.6	4	4	100		100	kHz
+/- 6 dB bandwidth	6.4	12.8		200		200	kHz
Sigma Delta Modulator Rate	1.024	16.384		16.384		16.384	MHz
Maximum Data Rate	4 / 16[A]	32		512		512	ksps
Minimum Data Rate	0.25	1		1		1	ksps
Resolution	24	16 or 24		16 or 24		16 or 24	bits
Minimum Self Noise	22	24	18	27		67	dB re μPa^2/Hz
Peak Input Level (μPa)	176	172	165	175		215	dB re μPa
Peak Input Level (Volts)	5	6		6		6	dBV
Voltage Sensitivity	-171	-166	-159	-169		-209	dBV re μPa
Digital Sensitivity, 24-bit, Ref.[B]	-2	2	8	-1		-41	dBSR
Digital Sensitivity, 24-bit, count^2 / μPa^2	-32	-28	-22	-31		-71	dB
Digital Sensitivity, 16-bit, Ref.[B]	-	8	14	5		-35	dBSR
Digital Sensitivity, 16-bit, count^2 / μPa^2	-	-76	-70	-79		-119	dB
Dynamic range, 1.0 Hz BW	154	148	147	148		148	dB
Full bandwidth Dynamic Range	122	107	106	95		95	dB
SOFTWARE / INTERFACE							
Communications Interface	RS-422	Ethernet		Ethernet		Ethernet	
Lucy Software Support	Yes	Yes		Yes		Yes	
Collect Data Protocol	Serial	TCP		TCP		TCP	
Streaming Data Protocol	-	TCP / UDP		TCP / UDP		TCP / UDP	
Web Server (HTTP)	-	TCP		TCP		TCP	
FTP, SFTP and SSH Console	-	TCP		TCP		TCP	
Maximum Internal Data Storage	32	128		128		128	GB
POWER							
Internal Battery Life[C]	30	10		10		10	Hours
Metalic Lithium Equivalent Content	420	780		780		780	mg
Recommended Supply Voltage	12 - 36	18 - 36		18 - 36		18 - 36	V
Supply Voltage Limits	9 - 48	15 - 48		15 - 48		15 - 48	V
External Power (min, no networking)	-	1.8		1.8		1.8	W
External Power (typical)	0.14	2.1		2.1		2.1	W
External Power (charging)	1	3.8		3.8		3.8	W
MECHANICAL							
Mass (Titanium Case)	977	958		958		958	gm
Mass (Plastic Case)	461	442		442		442	gm
Volume (Displacement)	360	320		320		320	cm^3
Overal Length, including connector	267	267		267		267	mm
Sensor Element Length	65	65		65		65	mm
Body (Can) Length	165	165		165		165	mm
Element Diameter	38	22		22		22	mm
Body Diameter	48	48		48		48	mm
Notes:	A. No internal logging above 4 ksps. B. dBSR is the ratio of Sensitivity in dB to a reference sensitivity. (see our white paper on Digital Hydrophone Sensitivity.) C. Initial battery life. Battery life will decrease by about 20% per year.						

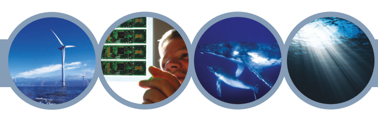

CONTROS HydroC CO_2

KONGSBERG

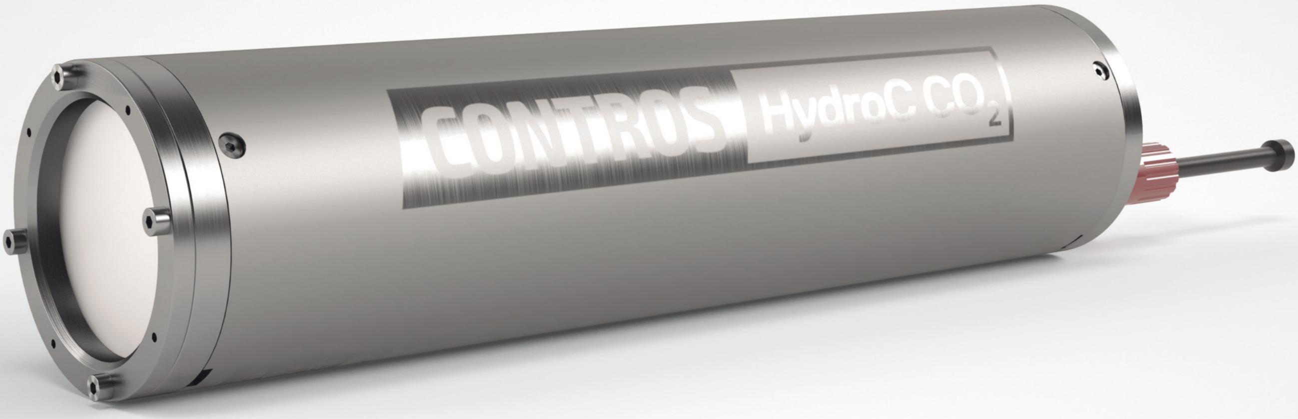

HIGHLY ACCURATE UNDERWATER pCO_2 SENSOR

The CONTROS HydroC® CO_2 sensor is a unique and versatile underwater carbon dioxide sensor for in-situ and online measurements of dissolved CO_2. The CONTROS HydroC® CO_2 is designed to be used on different platforms following different deployment schemes. Examples are moving platform installations, such as ROV/ AUV, long term deployments on seabed observatories, buoys and moorings as well as profiling applications using water sampling rosettes.

Individual 'in-situ' calibration

All sensors are individually calibrated in a water tank which simulates the deployment temperature. A sophisticated reference detector is used to verify the pCO_2 concentrations in the calibration tank. The reference sensor is recalibrated with secondary standards on a daily basis. This process ensures that the CONTROS HydroC® CO_2 sensors achieve unmatched short and long term accuracy.

Operating principle

Dissolved CO_2 molecules diffuse through a custom made thin film composite membrane into the internal gas circuit leading to a detector chamber, where the partial pressure of CO_2 is determined by means of IR absorption spectrometry. Concentration dependent IR light intensities are converted into the output signal from calibration coefficients stored in firmware and data from additional sensors within the gas circuit.

Accessories

A wide range of available accessories ensures that each of the CONTROS HydroC® CO_2 sensors can be adapted to meet customers' requirements. The optional pumps with the different flow heads are the most popular options that ensure very fast response times. An anti-fouling head is used under conditions with significant biofouling pressure. The internal data logger can be used in conjunction with the HydroCs flexible power management features and the CONTROS HydroB® battery packs to conduct unattended long-term deployments.

405881 rev B / September 2016

FEATURES

- High accuracy
- Very robust, depth rating up to 6,000 m (profiling)
- Very fast response time
- User-friendly
- Versatile – easy integration into almost every oceanographic measurement system and platform
- Long-term deployment capability
- ‘Plug & Play’ principle; all required cables, connectors and software are included

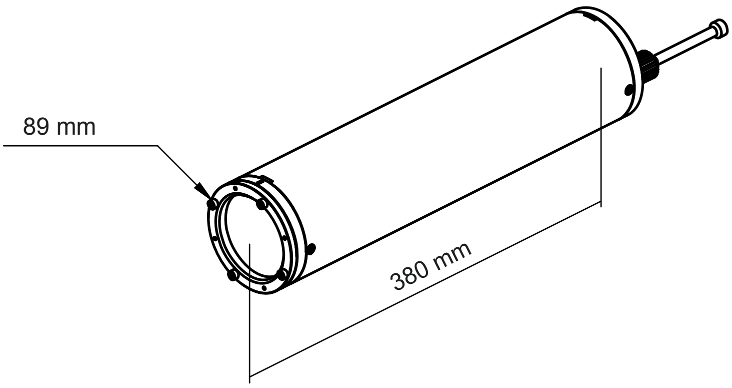

TECHNICAL SPECIFICATIONS

CONTROS HydroC CO_2

• Detector	High-precision optical analyzing NDIR system
• Measuring range	Standard calibration is 200 - 1,000 µatm (other ranges on request)
• Weight	2.2 kg in water, 4.5 kg in air
• Dimensions	89 x 380 mm (without connector)
• Depth rating	2,000 to 6,000 m (profiling) versions available
• Temperature range	Standard range is -2°C to +35°C (other ranges on request)
• Response time	t_{63} ~ 60 s (with SBE-5T)
• Resolution	< 1 µatm
• Initial accuracy	±0.5 % of reading
• Connector	SubConn MCBH8-M titanium 8-pin (other connectors on request)
• Supply voltage	11 V - 30 V
• Power consumption	Sensor approx. 300 mA @ 12 V + approx. 8 W with SBE-5T ext. pump (approx. values for standard configuration at 20°C ambient temperature)
• Data interface	RS-232C
• Data format	ASCII

SOFTWARE

CONTROS DETECT® incl. real-time data visualization, setting of sensor parameters (e.g. measuring intervals, internal data logger settings, sleep mode function) supported by a mission planning tool; data download from internal logger

HARDWARE REQUIREMENTS

Win 7 32 Bit, 200 MB free disk space,
Dual Core CPU with 2GB RAM

OPTIONS

- Available temperature ranges for reduced power consumption
  -2°C to +30°C
  -2°C to +20°C
  -2°C to +8°C
- Measuring range up to 6,000 µatm
- Analog output: 0 V - 5 V
- RS-485 data interface
- Internal data logger
- External battery packs
- ROV and AUV installation packages
- Profiling and mooring frames
- CO_2 flow through sensor for underway (FerryBox) and lab applications
- External pump (SBE-5T or SBE-5M)
- Easy deployment together with a CONTROS HydroFlash® O_2

405881 rev B / September 2016

Specifications subject to change without any further notice.

KONGSBERG MARITIME
Switchboard: +47 815 73 700
Customer support: +47 33 03 24 07
E-mail sales: km.sales@km.kongsberg.com
E-mail support: km.support@kongsberg.com

FRANATECH

Dissolved CO_2 Sensor

APPLICATION

- Process control in aquaculture
- Long-term monitoring in hydroelectricity reservoirs
- Survey of coastal waters

FEATURES

- Maintenance limited to a few minutes a month
- No recalibration
- Plug-and-play
- Continuous monitoring
- Reliable and accurate values from 1 - 50 mg / l

SPECIFICATIONS

- Weight sensor alone: 2.3 kg
- Range: 0 - 50 mg / l
- Operation temperature:
  +2°C to +40°C
- Storage temperature:
  -10°C to +50°C,
  <85% humidity
- Water tight: IP68 5bar
- Output: 4 - 20mA
- Power supply:
  110 / 230 VAC (50 / 60 Hz)
- Current drain: 200mA

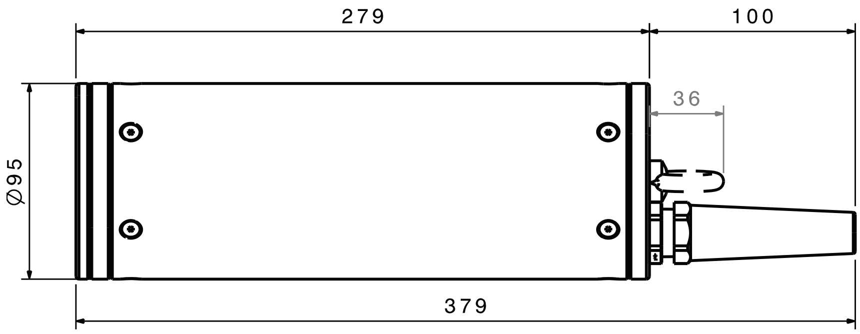

Dimensions in mm

AUDITED NORM COMPLIANCE FOR OPERATION IN INDUSTRIAL INSTALLATION

- CE compliant
- Electromagnetic compatibility
  EN50270:2006 (Type I Class B, Type II), EN61000-3-2:2006, EN61000-3-3:1995+A1:2001+A2:2005
- Shock and Vibration
  IEC 60068-2-6, DIN EN22248

FRANATECH

FRANATECH AS
OSLO, NORWAY
PHONE: +47 - 900 - 21 49 2

FRANATECH GMBH
LÜNEBURG, GERMANY
PHONE: +49 - 4131 - 7 89 28 0

INFO@FRANATECH.COM
WWW.FRANATECH.COM

CONTROS HydroFlash

ACCURATE, FAST AND VERSATILE OXYGEN OPTODE

The CONTROS HydroFlash® O_2 optode is a versatile shallow and deep-water oxygen sensor which can be used for autonomous deployments as well as integrated into sensor systems. The CONTROS HydroFlash® O_2 is designed for a wide variety of deployment schemes and platforms including but not limited to AUVs, gliders, floats, water sampling rosettes, buoys, and moorings.

Individual 'in-situ' calibration

The optode head has a unique design featuring an anti-fouling head, a fast response temperature probe and a curved glass substrate coated with the sensing membrane. All sensors are individually calibrated in a water tank over a wide range of temperatures and oxygen concentrations. An established laboratory method ('Winkler test') is used to ensure the quality of the calibration.

Operating principle

The advanced, optical sensor is based on the principle of fluorescence quenching. Dissolved oxygen (O_2) molecules diffuse into a membrane in which a fluorescent dye is embedded. Oxygen is capable of quenching this fluorescence by transferring the excitation energy from the dye to the O_2 molecule. The sensor repeatedly excites the dye in the membrane and measures the intensity and phase shift of the fluorescence light. The more O_2 is present in the water, the smaller is the measured fluorescence signal and the higher is the phase shift.

Accessories

KONGSBERG provides a dedicated power solution for the CONTROS HydroFlash® O_2 optode, the CONTROS HydroB® Flash. Its simple yet efficient "plug-and-play" design allows for autonomous deployments of up to three months.

FEATURES

- Highly efficient fluorescent dye embedded on a curved, solid substrate to enhance light yield
- Very fast response time (t_{63} < 3 s) combined with high stability and accuracy
- Versatile - easy integration into almost every oceanographic measurement system and platform
- Robust - can be used in water depths up to 6000 meters
- Titanium housing with small dimensions
- Very low power consumption
- Programmable sleep mode extends battery lifetime during autonomous deployment
- Comprehensive software for programming, data download and visualization included
- Non-consumptive O_2 measurement

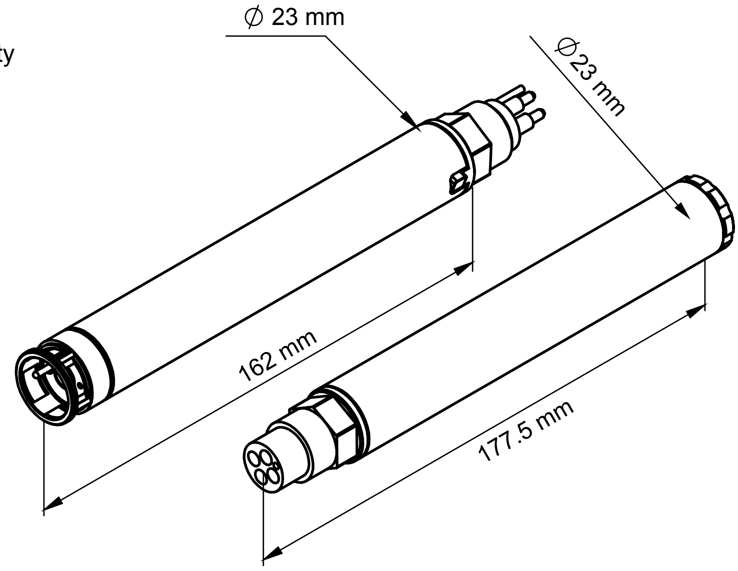

TECHNICAL SPECIFICATIONS

CONTROS HydroFlash O_2

• Measuring range	0 - 300 mbar pO_2
• Weight	0.11 kg in water 0.17 kg in air
• Dimensions	23 x 162 mm (without connector) 23 x 197 mm (with connector)
• Operational depth	up to 6000 m
• Temperature range	5°C - 35°C
• Response time	t_{63} < 3 s
• Resolution	< 0.1 %
• Initial accuracy	±1 %
• Memory	2 million sets of data
• Connector	SubConn MCBH-4M Titanium 4-pin (other connectors on request)
• Supply voltage	6 V - 32 V
• Data interface	RS-232C
• Data format	ASCII

SOFTWARE

CONTROS DETECT® incl. real time data visualization, setting of sensor parameters (e.g. measuring intervals, internal data logger settings, sleep mode function) supported by a mission planning tool and data download from internal logger

HARDWARE REQUIREMENTS

Win 7 32 Bit, 200 MB free disk space,
Dual Core CPU with 2GB RAM

OPTIONS

- Flow head
- Autonomous deployment with CONTROS HydroB® Flash (attachable battery) possible
- Easy deployments together with CO_2 and CH_4 sensors
- ROV and AUV installation packages
- Profiling and mooring frames

Specifications subject to change without any further notice.

405884 / Rev. B / June 2017

KONGSBERG MARITIME
Switchboard: +47 815 73 700
Customer support: +47 33 03 24 07
E-mail sales: km.sales@km.kongsberg.com
E-mail support: km.support@kongsberg.com

IDRONAUT

OCEAN SEVEN 311 pH probe

Specifically designed to simplify the monitoring of pH in fresh and saline waters. A temperature sensor is included to automatically compensate the pH readings. High quality long life IDRONAUT pH and reference (AgCl or NaCl) sensors. Digital interface (RS232 or RS485) and simple protocol for easy integration with third party CTD, AUV, ROV and SAV.

Features

- AgCl/NaCl long life reference sensor
- Internal logging and scheduling
- Integrated temperature sensor
- Internal battery pack *(max. working temperature < 60 °C)*
- Calibrated using a single buffer
- Galvanic insulation 10^{-15} Ω
- Differential pH preamplifier, 10^{-14} Ω input impedance

Applications

- ✓ Ocean acidification research
- ✓ Coral reef physiology and sensitivity analyses
- ✓ Near-shore biological research
- ✓ Environmental monitoring
- ✓ Volcanic went monitoring
- ✓ Brine monitoring
- ✓ ROV-AUV-SAV

www.idronaut.it idronaut@idronaut.it +39 039 879656

Sensor

Parameter	Range	Accuracy	Resolution	Time constant
pH	**0..14 pH**	**0.01 pH**	**0.001 pH**	**3 s**
Temperature	**-5.. +35°C**	**0.005 °C**	**0.0001 °C**	**50 ms**

Environmental

Operating temperature:	-5 to 35 °C
Storage temperature:	-2 to 35 °C
Salinity range:	0 to 350 PSU
Depth range:	up to 700 bar

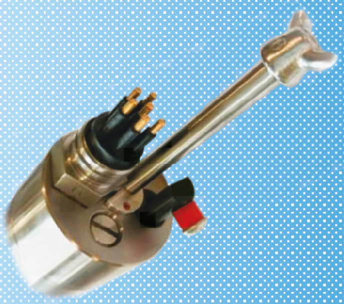

Electrical

Supply voltage	**external:**	6 to 18 VDC
	battery:	2.9 to 3.6 VDC
Power consumption	**sampling:**	200 mW
	sleep:	0.01 mA
Batteries:		1x 3.6V AA Lithium
or		2x 1.5V AA Alkaline
Storage:		4 GB
Communication:		RS232C – RS485
Sampling rate:		8 Hz

Operating modes

- Continuous mode, sampling up to 8 Hz
- Timed mode, interval from 5 sec. up to 1day
- Polled mode, responds to data logger via simple proprietary protocol.

Physical characteristics

Housing	1000 dbar AISI / POM	1000 dbar AISI/POM AUV	2000 dbar POM	7000 dar Titanium	7000 dar Titanium AUV
Diameter	48 mm	48 mm	75 mm	48 mm	48 mm
Length	562 mm	435 mm	580 mm	562 mm	435 mm
Weight in water	0.65 Kg	0.6 Kg	0.5 Kg	1.1 Kg	0.9 Kg
Weight in air	1.1 Kg	0.9 Kg	2.2 Kg	1.8 Kg	1.5 Kg

EM® 2040 MKII

KONGSBERG

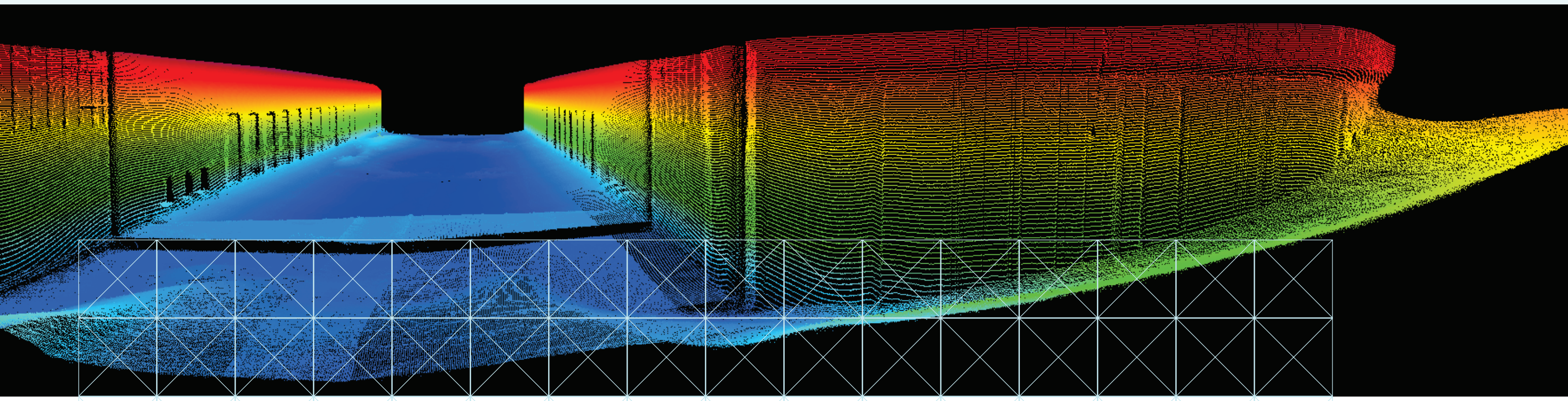

MULTIBEAM ECHO SOUNDER

The EM 2040 MKII is a true wide band high resolution shallow water multibeam echo sounder, an ideal tool for any high resolution mapping and inspection application. With the release of the EM 2040 MKII series Kongsberg Maritime has upgraded the hardware and software to increase the swath and improve the data quality of our EM 2040 series.

Key facts

The operating frequency range of the EM 2040 MKII is 200 to 400 kHz. The operator can on the fly choose the best operating frequency for the application: 300 kHz for near bottom, 200 kHz for deeper waters and 400 kHz for very high resolution inspection. Due to the large operating bandwidth, the system has an output sample rate up to 60 kHz. The system can effectively operate with very short pulse lengths, the shortest pulse being 14 microseconds giving a raw range resolution (CT/2) of 10.5 mm.

By utilizing both CW and FM chirp pulses, the system can achieve long range capability with a high resolution giving the system a maximum depth range in cold ocean water of 600 m at 200 kHz and a swath width up to 900m.

The angular coverage for the 200 and 300 kHz is up to 170°, with coverage up to 7.5 times water depth on a flat bottom. For a dual transducer system, 200° angular coverage or 10 times the water depth is achieved on a flat bottom.

As an option the EM 2040 MKII can be delivered with dual swath capability, allowing a sufficient sounding density to meet survey coverage standards along track while maintaining a high vessel speed.

Components

The EM 2040 MKII is a modular system, fully prepared for upgrading to cater for more demanding applicatons. The basic system has four units: a transmit transducer, a receive transducer, a processing unit and a hydrographic workstation.

The EM 2040 MKII receiver is 0.7° and is delivered with a 0.4° or 0.7° transmitter(s). The transmit fan is divided into three sectors pinging simultaneously at separate frequencies ensuring a strong and beneficial dampening of multibounce interference.

A single transmitter with dual receiver setup fully exploits the unique angular coverage of our three-sector transmitter for full 200° angular coverage per ping. The specialised dual transmitter and receiver setup is ideal where mounting requires a large separation of receivers, where mounting the transmitter at the keel is not an option or for ROV pipeline surveying and free span detection. This configuration transmits on a single sector per transmitter with selectable frequency in steps of 10 kHz from 200 to 400 kHz.

The standard depth rating of the EM 2040 MKII transducers is 6000 m, making it ideal for operation on subsea vehicles such as ROVs or AUVs.

443810 /B August 2019

FEATURES

- High resolution
- Wide frequency range
- FM chirp
- Roll, pitch and yaw stabilisation
- Nearfield focusing - both on transmit and receive
- Short pulse lengths, large bandwidth
- Seabed image
- Depth rated to 6000 m
- Easy to install
- Water column logging
- Water column display
- Extra detections
- Dual swath
- Dual RX
- Dual TX

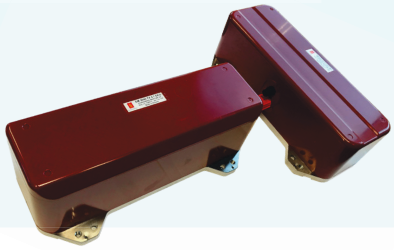

TECHNICAL SPECIFICATIONS

Frequency range	200 to 400 kHz
Max ping rate	50 Hz
Swath coverage sector	Up to 170° (single receiver) / 200° (dual receiver)
Beam patterns	Equiangular, equidistant high density and ultra high density
No. of beams per ping	512 (Single RX)/1024 (Single RX, Dual Swath)/1600 (Dual RX, Dual Swath)
Roll stabilised beams	± 15°
Pitch stabilised beams	± 10°
Yaw stabilised beams	± 10°

Coverage example for EM 2040 with bottom type rock (BS = - 10 dB), NL = 45 dB, FM mode

Operating mode	Cold ocean water			Cold fresh water		
EM 2040-04:	**Max depth**	**Max coverage single RX**	**Max coverage dual RX**	**Max depth**	**Max coverage single RX**	**Max coverage dual RX**
200 kHz	635 m	920 m	980 m	1360 m	1990 m	2110 m
300 kHz	480 m	670 m	760 m	740 m	1100 m	1270 m
400 kHz	315 m	410 m	430 m	430 m	570 m	610 m
EM 2040-07:						
200 kHz	600 m	880 m	930 m	1300 m	1870 m	2000 m
300 kHz	465 m	640 m	725 m	700 m	1050 m	1200 m
400 kHz	300 m	385 m	410 m	375 m	540 m	570 m

Pulse lengths	200 kHz mode		300 kHz mode		400 kHz mode	
	CW	**FM**	**CW**	**FM**	**CW**	**FM**
Normal mode	38, 108 & 324 µs	3 & 12 ms	38, 108 & 324 µs	2 & 6 ms	27, 54 & 108 µs	N/A
Single sector mode	19, 38 & 81 µs	1.5 ms	19, 38 & 81 µs	1.5 ms	14, 27 & 54 µs	N/A
	200 - 400 kHz CW in 10 kHz step			**200 - 400 kHz FM in 10 kHz step**		
Dual TX model	14, 27, 54, 135, 324 & 918 µs			3 & 12 ms		

Max no. of beams per ping	Single swath	Dual swath
Single RX	512	1024
Dual RX	800	1600

	Beamwidth			Physical dimensions (excluding connectors and mounting arrangements)	
	200 kHz	**300 kHz**	**400 kHz**	**Dimensions**	**Weight**
TX EM 2040-04	0.7°	0.5°	0.4°	727 x 142 x 150 mm (LxWxH)	45 kg
TX EM 2040-07	1.5°	1°	0.7°	407 x 142 x 150 mm (LxWxH)	23 kg
RX	1.5°	1°	0.7°	407 x 142 x 136 mm (LxWxH)	22 kg
Processing Unit (2U for 19" rack)*				482.5 x 424 x 88.6 mm (WxDxH)	10.5 kg
Portable Processing Unit (IP67)				370 x 390 x 101 mm (WxDxH)	10.5 kg

Laptop, HWS and monitor can be delivered on request.

Specifications subject to change without any further notice.
EM® is a registered trademark of Kongsberg Maritime AS in Norway and other countries.
Front page: Curtesy of Port of London.

KONGSBERG MARITIME
Switchboard: +47 815 73 700
Global support 24/7: +47 33 03 24 07
E-mail sales: km.sales@km.kongsberg.com
E-mail support: km.support@kongsberg.com
km.kongsberg.com

KONGSBERG

EM® 712

KONGSBERG

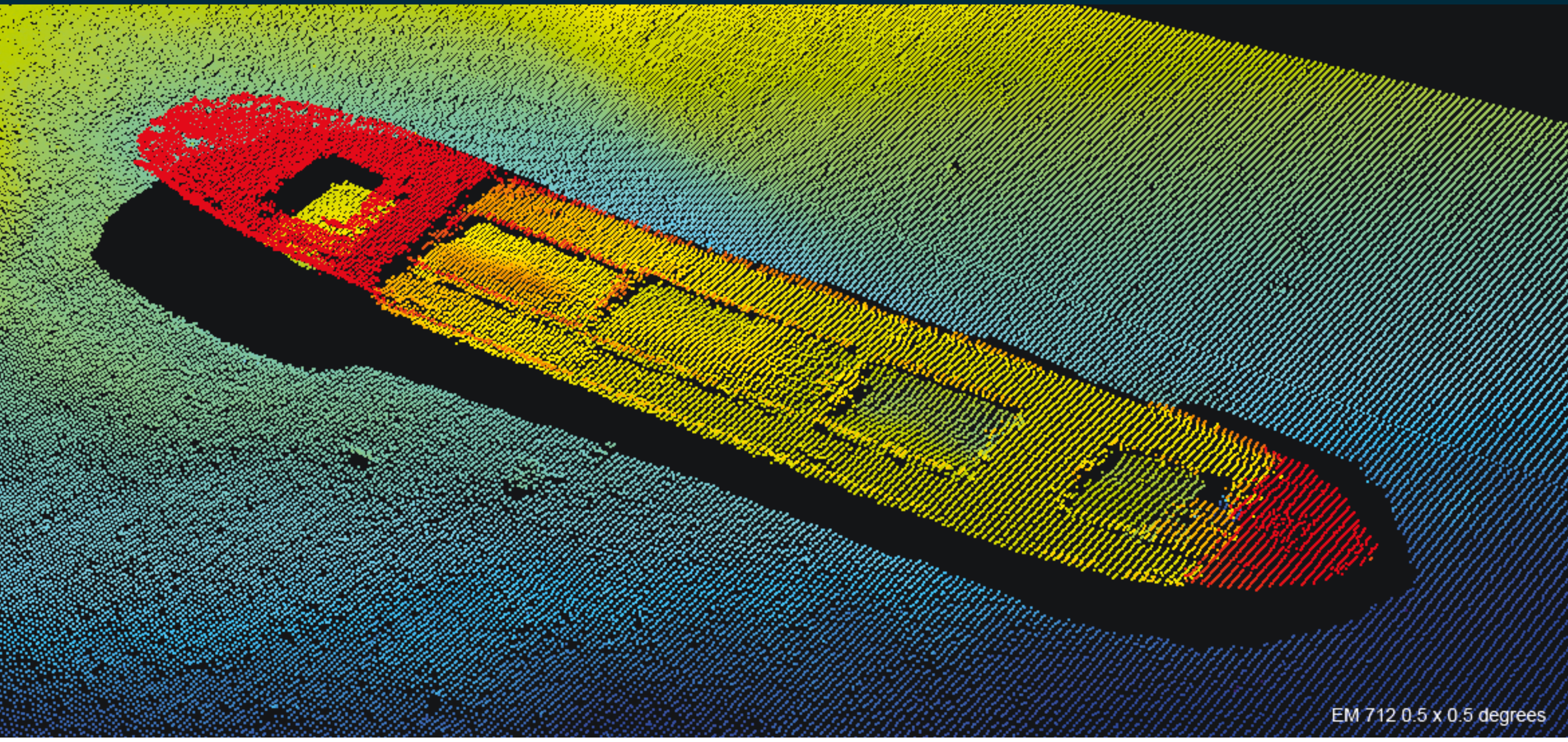

MULTIBEAM ECHO SOUNDER

The EM 712 multibeam echo sounder is a high to very high resolution seabed mapping system capable of meeting all relevant survey standards. The minimum acquisition depth is from less than 3 m below its transducers, to a maximum of approximately 3500 m, somewhat dependant upon array size. Across track coverage (swath width) is up to 5.5 times water depth, with a maximum of more than 3500 m.

Echo sounder models
There are three basic versions of the EM 712 system, with different range performances:
- EM 712 - Full performance version.
- EM 712S - CW pulse forms only.
- EM 712RD - Short CW pulse only.

Choice of beamwidths
The transmit and receive beamwidth depends upon the chosen transducer configuration with 0.5, 1 and 2 degrees available as standard.

Innovative acoustic principles
The EM 712 operates at sonar frequencies in the 40 to 100 kHz range. The transmit fan is divided into three sectors to maximize range capability, but also to suppress interference from multiples of strong bottom echoes.
The sectors are transmitted sequentially within each ping, and uses distinct frequencies or waveforms.
EM 712S and EM 712RD both use CW pulses of different lengths. The full performance version, EM 712, supports even longer, compressible waveforms (FM sweep).

Fully stabilized and focused beams
The system applies beam focusing to both transmit and receive beams in order to obtain the maximum resolution even inside the acoustic near-field.
During transmission, focusing is applied individually to each transmit sector with a focus point on the range defined by the previous ping, to retain the angular resolution in the near field. Dynamic focusing is applied to all receive beams. The transmit beams are electronically stabilised for roll, pitch and yaw, while the receive beams are stabilised for roll movements.

Transducers
The active elements of the EM 712 transducers are based upon composite ceramics, a design which has several advantages, in particular increased bandwidth and tighter performance tolerances. Normal transducer mounting is flush with the hull, in a blister or in a gondola. The 1x2 degrees and 2x2 degrees versions can be mounted on a pole for portable deployment.

Electronics
The EM 712 electonics consist of Transmitter Unit, Receiver unit, Prosessing unit and Work station. The EM 712 electronics system is a true wideband design. The transmitter circuits are fully programmable to support any frequency or pulse form. The use of FM sweep as a pulse form allows for more energy per pulse and thus increased range performance, without any sacrifice of range resolution. Filters, correlators and beamformers are fully digital implementations, and the beam forming method is by time delays, to allow for the wide frequency band of the system.

FEATURES

- High resolution
- Wide frequency range
- FM chirp
- Roll, pitch and yaw stabilisation
- Near-field focusing
- Water column display
- Seabed image
- Dual swath
- Modular design

Options:
- Water column logging
- Extra detections

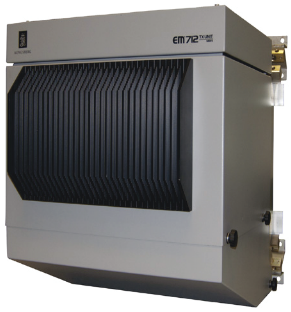


TECHNICAL SPECIFICATIONS

Frequency range	40 to 100 kHz
Max ping rate	30 Hz
Swath coverage sector	Up to 140 degrees
Min depth	3 m below transducer

Max depth (approximate values)	EM 712 0.5 x 0.5 degrees	EM 712S 1 x 2 degrees	EM 712 RD
	3600 m	1800 m	600 m
CW transmit pulses	0.2 to 2 ms	0.2 to 2 ms	0.2 ms
FM sweep pulse	Yes	No	No

Roll stabilised beams	Yes, ±15 degrees
Pitch stabilised beams	Yes, ±10 degrees
Yaw stabilised beams	Yes, ±10 degrees
Sounding patterns	Equiangular
	Equidistant

Transducer choices	0.5 x 0.5 deg.	0.5 x 1 deg.	1 x 1 deg.	1 x 2 deg.	2 x 2 deg.
Availability	Not EM 712 RD	Not EM 712 RD	Not EM 712 RD	All models	All models
TX dimensions (L x W x H)	1940 x 224 x 118 mm	1940 x 224 x 118 mm	970 x 224 x 118 mm	970 x 224 x 118 mm	490 x 224 x 118 mm
RX dimensions (L x W x H)	1940 x 224 x 118 mm	970 x 224 x 118 mm	970 x 224 x 118 mm	490 x 224 x 118 mm	490 x 224 x 118 mm
Max no. of soundings per ping (Dual swath mode)	1600	800	800	400	400

Transmitter Unit dimensions (W x H x D) and weight	600 x 380 x 600 mm	71 kg (for 0.5 degrees TX array)
Receiver Unit dimensions (W x H x D) and weight	250 x 350 x 260 mm	11 kg

		0.5 x 0.5 deg.	0.5 x 1 deg.	1 x 1 deg.	1 x 2 deg.	2 x 2 deg.
Max coverage	winter*	3600	3400	3200	3000	2800
Max coverage	summer*	4200	3900	3650	3450	3250
Max depth	winter*	3400	3250	3100	2900	2700
Max depth	summer*	3600	3400	3300	3150	3000

* Estimated depth and coverage for EM 712, based on BS= -20 dB, NL= 35 dB, f = 40 kHz

387595/B February 2017

KONGSBERG MARITIME
Switchboard: +47 815 73 700
Global support 24/7: +47 33 03 24 07
E-mail sales: km.sales@km.kongsberg.com
E-mail support: km.support@kongsberg.com

km.kongsberg.com

KONGSBERG

SIMRAD ME70 TECHNICAL SPECIFICATION

Please note that we are engaged in continuous development of our products. For this reason we reserve the right to alter technical specifications without prior notice.

TYPE OF SYSTEM

- Scientific multibeam echo sounder

FREQUENCY RANGE

- 70 to 120 kHz

BEAMS

- Organisation: Fan
- Total number of beams: Maximum 45 beams in fan plus two reference beams
- Number of split beams: Maximum 45 split beams in fan plus two reference beams

BEAM OPENING ANGLES

- Alongship: Selectable 2° to 20°
- Athwartship: Selectable 2° to 20°
- Opening angles depend on beam steering and frequency.

OPERATING SECTORS

- Athwartship: 60° (Maximum 140° with reduced sidelobe suppression)
- Athwartship sector centre angle: ±45°
- Alongship sector centre angle: ±5°

MOTION COMPENSATION

- Roll: ±10°
- Pitch: ±5°
- Heave

SIDELOBE AND BEAM INTERLEAKAGE

- Alongship: Less than -35 dB
- Athwartship: Less than -35 dB
- Adjustable depending on beamwidth and frequency configuration.

TRANSMISSION

- FM with pulse duration 128 to 5120 µs
- CW with pulse duration 64 to 5120 µs
- Source level: > 225 dB (depending on beam opening and frequency)

RECEIVING

- Receiver dynamic range: 150 dB (instantaneous)

CALIBRATION

- Calibration software included

- Target: Tungsten sphere

TRANSDUCER

- Number of elements: 800
- Technology: Ceramic polymer composite
- Housing: Circular
- Housing diameter: 700 mm

TRANSCEIVER UNIT

- Individual Tx channels: 800
- Individual Rx channels: 800
- Communication: 2 x 1 Gb Ethernet
- Physical dimensions:
  - Height: 1921 mm
  - Depth: 900 mm
  - Width: 600 mm

POWER SUPPLY UNITS

- Quantity: Three cabinets
- Physical dimensions:
  - Height: 812 mm
  - Depth: 418 mm
  - Width: 600 mm

PROCESSOR UNIT

- Type: Simrad ME70 Processor Unit
- Operating system: Microsoft® Windows 7

OPTIONAL SYSTEMS

- Element data logger
- Bathymetric processing system

CURRENT PROFILER

Aquadopp Profiler 600 kHz

Up to 40 m current profiling range; easy to operate and deploy

The Aquadopp Profiler is a highly versatile Acoustic Doppler Current Profiler (ADCP) available in four profiling range options, from < 1 m to > 85 m. Designed for simple yet powerful operation, this current profiler is packed with features used by engineers and researchers to enable accurate and effective hydrodynamic data collection in a variety of environmental conditions.

CURRENT PROFILER

Aquadopp Profiler 600 kHz

NORTEK

Highlights

- Up to 40 m current profiling range
- Ideal for mean current measurements
- Easy to operate and deploy

Applications

- Mean flow measurements with high focus on ease of use and simplicity
- Measurements in flow regimes with strong variations in flow speeds
- Studies of tidal currents
- Measurements of combinations of waves and currents
- Suitable for wave buoys

CURRENT PROFILER

Aquadopp Profiler 600 kHz

Technical specifications

⟶ Water velocity measurements	
Maximum profiling range	30-40 m
Cell size	1-4 m
Minimum blanking	0.50 m
Maximum number of cells	128
Measurement cell position	N/A
Default position (along beam)	N/A
Velocity range	±10 m/s
Accuracy	±1% of measured value ±0.5 cm/s
Velocity precision	Consult instrument software
Maximum sampling rate (output)	1 Hz
Internal sampling rate	4 Hz
⟶ Echo intensity (along slanted beams)	
Sampling	Same as velocity
Resolution	0.45 dB
Dynamic range	90 dB
Transducer acoustic frequency	600 kHz
Number of beams	3
Beam width	3.0°
⟶ HR option	
Maximum profiling range	N/A
Cell size	N/A
Minimum blanking	N/A
Maximum number of cells	N/A
Range/Velocity limitations	N/A

Aquadopp Profiler 600 kHz

→ HR option	
Accuracy	N/A
Max. sampling rate	N/A
→ Z-Cell option	
Cell zero acoustic frequency	N/A
Maximum profiling range	N/A
Number of beams	N/A
→ Sensors	
Temperature:	Thermistor embedded in head
Temp. range	-4 to +40 °C
Temp. accuracy/resolution	0.1 °C/0.01 °C
Temp. time response	10 min
Compass:	Magnetometer
Accuracy/resolution	2°/0.1° for tilt < 20°
Tilt:	Liquid level
Accuracy/resolution	0.2°/0.1°
Maximum tilt	30°
Up or Down	Automatic detect
Pressure:	Piezoresistive
Range	0-100 m (inquire for options)
Accuracy/precision	0.5% FS / 0.005% of full scale
→ Analog inputs	
No. of channels	2
Supply voltage to analog output devices	Three options selectable through firmware commands:1) Battery voltage/500 mA, 2) +5 V/250 mA, 3) +12 V/100 mA
Voltage input	0-5 V
Resolution	16-bit A/D

CURRENT PROFILER

Aquadopp Profiler 600 kHz

→ Data recording	
Capacity	9 MB, can add 4/16 GB

CURRENT PROFILER

Aquadopp Profiler 600 kHz

⟶ Data recording	
Data record	9*Ncells + 32 bytes
Diagnostics record	N/A
Wave record	Nsamples * 24 + 60 bytes
Mode	Stop when full (default) or wrap mode
⟶ Real-time clock	
Accuracy	±1 min/year
Backup in absence of power	4 weeks
⟶ Data communications	
I/O	RS-232 or RS-422
Communication baud rate	300-115200 Bd
Recorder download baud rate	600/1200 kBd for both RS-232 and RS-422
User control	Handled via "Aquadopp" software, ActiveX®function calls, or direct commands with binary or ASCII data output
⟶ Connectors	
Bulkhead (Impulse)	MCBH-8-FS
Cable	PMCIL-8-MP on 10m polyurethane cable
⟶ Software	
Functions	Deployment planning, instrument configuration, data retrieval and conversion (for Windows®)
⟶ Power	
DC input	9-15 V DC
Maximum peak current	3 A
Avg. power consumption	0.06 W
Sleep current	< 100 µA
Transmit power	0.3-20 W, 3 adjustable levels
⟶ Batteries	
Battery capacity	1) 50 Wh (alkaline or Li-ion), 2) 165 Wh (lithium), 3) Single or dual

CURRENT PROFILER

Aquadopp Profiler 600 kHz

→ Batteries	
New battery voltage	13.5 V DC (alkaline)
→ Environmental	
Operating temperature	-5 to +40 °C
Storage temperature	-20 to +60 °C
Shock and vibration	IEC 721-3-6
EMC approval	IEC 61000
Depth rating	300 m
→ Materials	
Standard model	POM and polyurethane plastics with titanium fasteners
→ Dimensions	
Maximum diameter	100 mm
Maximum length	~550 mm (single battery), +110 mm (double battery) depending on head configuration
→ Weight	
Weight in air	2.9 kg
Weight in water	0.4 kg
→ Options	

1) Alkaline, lithium or Li-ion external batteries, 2) Inquire for different head configurations

Kontroll- og referanseside/ Review and reference page

Dokumentinformasjon/*Document information*		
Dokumenttittel/*Document title* D3 - Nearshore evaluation report 2019		**Dokumentnr./*Document no.*** 20180127-03-R1
Dokumenttype/*Type of document* Rapport / Report	**Oppdragsgiver/*Client*** Gassnova	**Dato/*Date*** 2019-11-26
Rettigheter til dokumentet iht kontrakt/ *Proprietary rights to the document according to contract* NGI		**Rev.nr.&dato/*Rev.no.&date*** 2 / 2021-02-01
Distribusjon/*Distribution* BEGRENSET: Distribueres til oppdragsgiver og er tilgjengelig for NGIs ansatte / LIMITED: Distributed to client and available for NGI employees		
Emneord/*Keywords*		

Stedfesting/*Geographical information*	
Land, fylke/*Country* Norge	**Havområde/*Offshore area*** Oslofjorden
Kommune/*Municipality*	**Feltnavn/*Field name***
Sted/*Location* Horten	**Sted/*Location***
Kartblad/*Map*	**Felt, blokknr./*Field, Block No.***
UTM-koordinater/*UTM-coordinates* **Zone: East: North:**	**Koordinater/*Coordinates*** **Projection, datum: East: North:**

Dokumentkontroll/*Document control*
Kvalitetssikring i henhold til/*Quality assurance according to NS-EN ISO9001*

Rev/ *Rev.*	**Revisjonsgrunnlag/*Reason for revision***	**Egenkontroll av/ *Self review by:***	**Sidemanns-kontroll av/ *Colleague review by:***	**Uavhengig kontroll av/ *Independent review by:***	**Tverrfaglig kontroll av/ *Interdisciplinary review by:***
0	Original document	2019-11-24 AEB	2019-11-26 IKW		
1	Additional input regarding chemical sensors	2020-01-16 AEB	2020-01-17 IKW		
2	Minor revisions in Section 3.2. and 9 after input froma Alseamar	2021-01-25 AEB			

Dokument godkjent for utsendelse/ *Document approved for release*	**Dato/*Date*** 1 February 2021	**Prosjektleder/*Project Manager*** AEB

OSLO
TRONDHEIM
HOUSTON
PERTH

NORWEGIAN GEOTECHNICAL INSTITUTE
NGI.NO

Main office
PO Box 3930 Ullevaal St.
NO-0806 Oslo
Norway

Trondheim office
PO Box 5687 Torgarden
NO-7485 Trondheim
Norway

T (+47)22 02 30 00
F (+47)22 23 04 48
NGI@ngi.no

BIC NO. DNBANOKK
IBAN NO26 5096 0501 281
ORGANISATION NO.
958 254 318MVA

ISO 9001/14001
CERTIFIED BY BSI
FS 32989/EMS 612006